

LOCAL EFFICIENCY MEASUREMENTS OF
AUTOMOTIVE AIR FILTERS USING
LASER DOPPLER VELOCIMETRY

By

BALASUBRAMANIAN NATARAJAN

Bachelor of Engineering

The Institution of Engineers

Calcutta, India

1990

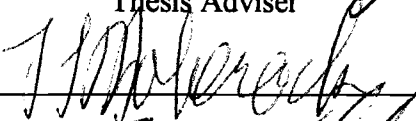
Submitted to the faculty of the
Graduate College of the
Oklahoma State University
in partial fulfillment of
the requirements for
the Degree of
MASTER OF SCIENCE
December, 1995

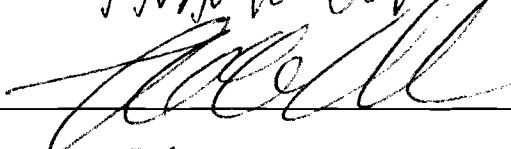
LOCAL EFFICIENCY MEASUREMENTS OF
AUTOMOTIVE AIR FILTERS USING
LASER DOPPLER VELOCIMETRY

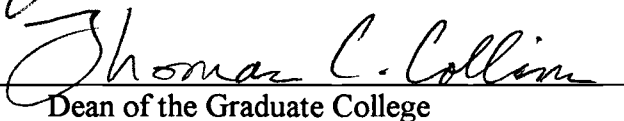
Thesis Approved:



Thesis Adviser







Dean of the Graduate College

ACKNOWLEDGEMENTS

I would like to take this opportunity to thank the individuals who have assisted me in successfully completing this project and other requirements for my Masters Degree. First of all, I am grateful to the almighty God without whose wish nothing is possible.

I wish to express my sincere gratitude to my major adviser Dr. R. L. Dougherty, for his invaluable guidance, encouragement and constant help. I am grateful to the other committee members, Dr. F. W. Chambers and Dr. L. L. Hoberock for their valuable suggestions and guidance.

A sincere appreciation is extended to my colleagues, Faqiu Liang, Jeff Williams, Sachin Anand, Rob Duran, C. Tebbutt, Y. Tian, and G. Liu for their understanding, help, and cooperation. A special thanks to my friend Abhijit for his encouragement.

The financial support provided by Purolator Products, Inc., and the Oklahoma Center for the Advancement of Science and Technology (OCAST) is greatly appreciated. I would like to thank Dr. G. Ferrell at Purolator Products, Inc., for his suggestions and help. A special thanks to James Davis and his North Lab Workshop personnel for their help and valuable suggestions.

I wish to extend my deepest regards to my parents and brothers whose love and encouragement has always shown me the right path.

TABLE OF CONTENTS

Chapter	Page
I. INTRODUCTION.....	1
II. LITERATURE REVIEW.....	5
2.1 Filter Testing Methods	5
2.1.1 SAE J726 Standard	5
2.1.2 Continuous Aerosol Monitoring System	7
2.1.3 ASTM Standard for Testing Flat Filter Media	9
2.1.4 Other Testing Methods	12
2.1.5 Aerosolization.....	16
2.1.6 Electrostatic Effects	20
2.2 Laser Doppler Velocimetry	22
2.2.1 Basic Principles	22
2.2.2 Laser Doppler Signals and Particles	26
2.3 Filtration Models	30
2.4 Automotive Filter Media	32
2.4 Present Work	36
III. EXPERIMENTAL PROCEDURE	38
3.1 Experimental Setup	38
3.2 Test Housing and Flow Setup	46
IV. RESULTS AND DISCUSSION	55
4.1 Flow Directions	55
4.2 SAE J726 Housing Results	57
4.3 Results of the Small Angle Diffuser Housing	62
4.3.1 One Micron Particles	62
4.3.2 Five Micron Particles	67
4.4 Reliability of the Test Results	70
4.5 Results of the New Diffuser Housing with Modified Setup	73
4.6 Filtration Efficiency Modeling	85
4.7 Stokes Number Analysis	90
4.8 Data Reproducibility Measurements	95

Chapter	Page
4.9 Flow Visualization	100
V. SUMMARY AND RECOMMENDATIONS	105
5.1 Summary of Results.....	105
5.2 Recommendations for Future Work	108
REFERENCES	111
APPENDIXES	115
APPENDIX A - LIST OF EQUIPMENT	116
APPENDIX B - DSA PARAMETERS	118
APPENDIX C - VERTICAL TRAVERSE.....	122
APPENDIX D - SMOKE GENERATOR.....	128
APPENDIX E - OTHER RESULTS	132

LIST OF TABLES

Table		Page
4.1	Modifications to the Experimental Setup.....	73
4.2	Pressure Drop Measurements.....	82
4.3	Elemental Areas Covered by the Measurement Points.....	86
4.4	Overall Efficiency for Different Values of Packing Density and Fiber Dia....	90
4.5	Overall Efficiency Parameters As a Function of Particle Diameter.....	91

LIST OF FIGURES

Figure	Page
2.1 Sketch of Test Housing and Overall Testing Apparatus as Per SAE J726 Standard (SAE, 1987).....	6
2.2 Schematic Diagram of the Universal Test Stand for Air Filter Media Testing (Jaroszcyk, 1987).....	8
2.3 Schematic Diagram of Air Filter Media Test Method (ASTM F 1215-1989)....	10
2.4 Air Filtration Test Stand Used by Davis (1994).....	11
2.5 Collection Efficiency for Three Particle Sizes (Davis, 1994).....	12
2.6 Filtration Efficiency of 20/66 Paper Versus Flow Velocity of Aerosol for Different Sizes of Particles (Baczewski and Jaroszcyk, 1981).....	14
2.7 Filtration Efficiency of 20/66 Paper Versus Accumulated Dust Load. (w = Average Flow Velocity) (Baczewski and Jaroszcyk, 1981).....	15
2.8 The Dilution Ratio, y , for a Singlet Ratio, $R=0.95$, Versus the Sphere Diameter for Various Values of Volume Median Diameter (Raabe, 1968).....	19
2.9 Schematic Sketch of a Typical Dual-Beam LDV System.....	24
2.10 The Probe Volume and the Fringe Pattern (Liang, 1994).....	25
2.11 Gaussian Intensity Distribution in the Probe Volume (Liang, 1994).....	25
2.12 Doppler Signals Generated for Four Different Situations in a Steady, Uniform Flow (George, 1975).....	27
2.13 LDA Signals Recorded with the Biomation Transient Recorder (Durst and Eliasson, 1975).....	28

Figure	Page
2.14 Burst Analysis of a Doppler Signal in the Presence of Another Disturbing Particle Away from the Middle of the Measuring Volume (Ruck and Pavlovski, 1993).....	29
2.15 SEM Pictures of the Top Surface and Cross-section of Wet-laid Automotive Filter Papers (Rodman and Lessman, 1988).....	34
2.16 Top Surface Photograph of Purolator A13192 Clean Flat Filter Media (440 x)	34
2.17 Top Surface Photograph of Purolator A13192 Pleated Filter Media Loaded with Dust to 10 Inches of H ₂ O Pressure Drop (440 x).....	35
2.18 Top Surface Photograph of Purolator A13192 Pleated Filter Media Loaded with Dust to 10 Inches of H ₂ O Pressure Drop (440 x).....	35
2.19 Photograph Showing the Scale Engraving Used for Comparison (Smallest Division = 10 μm).....	36
3.1 Schematic of LDV System (Modified from Liang, 1994).....	39
3.2 Sample Velocity Histogram.....	41
3.3 Probe Volume Location and Geometry	42
3.4 Swept Volume Technique for Particle Counting.....	44
3.5 Sketch of the SAE J726 Housing	47
3.6 Sketch of the New Diffuser Housing	49
3.7 Experimental Setup for the New Housing.....	50
3.8 Measurement Grid in Two Dimensions.....	52
4.1 The Two Components of Velocity Measurements.....	56
4.2 Old and New Mixing Chambers.....	57
4.3 Axial Velocity Upstream (SAE, 204 m ³ /hr, 0.966 μm Particles).....	59
4.4 Number Density Upstream (SAE, 204 m ³ /hr, 0.966 μm Particles).....	59
4.5 Axial Velocity Downstream (SAE, 204 m ³ /hr, 0.966 μm Particles).....	59

Figure	Page
4.6 Number Density Downstream (SAE, 204 m ³ /hr, 0.966 μm Particles).....	59
4.7 Transverse Velocity Upstream (SAE, 204 m ³ /hr, 0.966 μm Particles).....	61
4.8 Transverse Velocity Downstream (SAE, 204 m ³ /hr, 0.966 μm Particles).....	61
4.9 Local Efficiencies over Filter Face (SAE, 204 m ³ /hr, 0.966 μm Particles)	61
4.10 Overall Efficiency vs. Flow Rate (SAE, 0.966 μm Particles).....	61
4.11 Axial Velocity Upstream (Diffuser, 204 m ³ /hr, 0.966 μm Particles).....	63
4.12 Number Density Upstream (Diffuser, 204 m ³ /hr, 0.966 μm Particles).....	63
4.13 Axial Velocity Downstream (Diffuser, 204 m ³ /hr, 0.966 μm Particles)	63
4.14 Number Density Downstream (Diffuser, 204 m ³ /hr, 0.966 μm Particles).....	63
4.15 Transverse Velocity Upstream (Diffuser, 204 m ³ /hr, 0.966 μm Particles)	65
4.16 Transverse Velocity Downstream (Diffuser, 204 m ³ /hr, 0.966 μm Particles) ...	65
4.17 Local Efficiencies over Filter Face (Diffuser, 204 m ³ /hr, 0.966 μm Particles) ..	65
4.18 Overall Efficiency vs. Flow Rate (Diffuser, 0.966 μm Particles).....	65
4.19 Axial Velocity Upstream (Diffuser, 204 m ³ /hr, 5.3 μm Particles)	68
4.20 Number Density Upstream (Diffuser, 204 m ³ /hr, 5.3 μm Particles).....	68
4.21 2D Axial Velocity Upstream (Diffuser, 204 m ³ /hr, 5.3 μm Particles)	68
4.22 2D Number Density Upstream (Diffuser, 204 m ³ /hr, 5.3 μm Particles).....	68
4.23 Axial Velocity Downstream (Diffuser, 204 m ³ /hr, 5.3 μm Particles)	69
4.24 Number Density Downstream (Diffuser, 204 m ³ /hr, 5.3 μm Particles).....	69
4.25 Local Efficiencies over Filter Face (Diffuser, 204 m ³ /hr, 5.3 μm Particles)	69
4.26 Overall Efficiency vs. Flow Rate (Diffuser, 5.3 μm Particles).....	69

Figure	Page
4.27 Axial Velocity Upstream (Diffuser, 204 m ³ /hr, 0.966 μm Particles, Feb. 95) ...	75
4.28 Number Density Upstream (Diffuser, 204 m ³ /hr, 0.966 μm Particles, Feb. 95).....	75
4.29 2D Axial Velocity Upstream (Diffuser, 204 m ³ /hr, 0.966 μm Particles, Feb. 95).....	76
4.30 2D Number Density Upstream (Diffuser, 204 m ³ /hr, 0.966 μm Particles, Feb. 95).....	76
4.31 Axial Velocity Downstream (Diffuser, 204 m ³ /hr, 0.966 μm Particles, Feb. 95)	77
4.32 Number Density Downstream (Diffuser, 204 m ³ /hr, 0.966 μm Particles, Feb. 95).....	77
4.33 Transverse Velocity Upstream (Diffuser, 204 m ³ /hr, 0.966 μm Particles, Feb. 95)	78
4.34 Transverse Velocity Downstream (Diffuser, 204 m ³ /hr, 0.966 μm Particles, Feb. 95)	78
4.35 Local Efficiencies over Filter Face (Diffuser, 204 m ³ /hr, 5.3 μm Particles, Feb. 95)	79
4.36 2D Local Efficiencies over Filter Face (Diffuser, 204 m ³ /hr, 5.3 μm Particles, Feb. 95)	80
4.37 Overall Efficiency vs. Flow Rate (diffuser, 0.966 μm Particles, Feb. 95).....	80
4.38 Axial Velocity Upstream (0.5 μm Particles, 204 m ³ /hr, Feb. 95).....	83
4.39 Number Density Upstream (0.5 μm Particles, 204 m ³ /hr, Feb. 95).....	83
4.40 Axial Velocity Downstream (0.5 μm Particles, 204 m ³ /hr, Feb. 95).....	84
4.41 Number Density Downstream (0.5 μm Particles, 204 m ³ /hr, Feb. 95).....	84
4.42 Local Efficiencies (0.5 μm Particles, Feb. 95).....	85

Figure	Page
4.43 Elemental Efficiencies over the Filter (Diffuser, 204 m ³ /hr, 0.966 μm Particles, Duran’s Model with c = 0.345, and D _f = 51.78 μm, and Velocities from Fig. 4.27).....	88
4.44 Comparison of Measured and Calculated Overall Efficiencies as a Function of Flow Rate.....	88
4.45 Elemental Efficiencies over the Filter (Diffuser, 204 m ³ /hr, 0.966 μm Particles, Duran’s Model with c = 0.49, and D _f = 51.78 μm, and Velocities from Fig. 4.27).....	89
4.46 Comparison of Sabnis’ Model to Flagan and Seinfeld’s Exact Solution and Other Isolated Collision Efficiency Models (Duran, 1995).....	93
4.47 Measured Filtration Efficiencies as a Function of Stokes Number.....	93
4.48 Comparison of Measured Overall Efficiencies with Theoretical Model.....	94
4.49 Measurement Grid for Repeatability Tests.....	95
4.50 Data Repeatability Upstream of Filter at Nine Locations in a Grid (10-1-94)...	96
4.51 Data Repeatability Upstream of Filter at Nine Locations in a Grid (10-2-94)...	96
4.52 Data Repeatability with Time at Center of the Housing Without Filter.....	98
4.53 Dependence of Number Density on Laser Power.....	99
4.54 Setup for Flow Visualization Using Water Mist.....	102
4.55 Flow Visualization Using Water Mist Upstream of the Filter.....	102
4.56 Flow Visualization Using Water Mist Near the Filter Exit.....	103
4.57 Flow Visualization Using Water Mist Far from the Filter Exit.....	103
B-1 Variable Setup Page from DSA Software.....	118
C-1 The Vertical Traverse	123
D-2 Wiring Diagram for Vertical Traverse Automation.....	126
D-1 Schematic of the Smoke Generator (Wang, 1990).....	129

Figure	Page
E-1 Axial Velocity Upstream (Diffuser, 68 m ³ /hr, 0.966 μm Particles, July 94)...	134
E-2 Number Density Upstream (Diffuser, 68 m ³ /hr, 0.966 μm Particles, July 94)	134
E-3 Axial Velocity Downstream (Diffuser, 68 m ³ /hr, 0.966 μm Particles, July 94).....	134
E-4 Number Density Downstream (Diffuser, 68 m ³ /hr, 0.966 μm Particles, July 94).....	134
E-5 Local Efficiencies over Filter Face (Diffuser, 68 m ³ /hr, 0.966 μm Particles, July 94).....	135
E-6 Axial Velocity Upstream (Diffuser, 170 m ³ /hr, 0.966 μm Particles, July 94).	135
E-7 Number Density Upstream (Diffuser, 170 m ³ /hr, 0.966 μm Particles, July 94).....	135
E-8 Axial Velocity Downstream (Diffuser, 170 m ³ /hr, 0.966 μm Particles, July 94).....	135
E-9 Number Density Downstream (Diffuser, 170 m ³ /hr, 0.966 μm Particles, July 94).....	136
E-10 Local Efficiencies over Filter Face (Diffuser, 170 m ³ /hr, 0.966 μm Particles, July 94).....	136
E-11 Axial Velocity Upstream (Diffuser, 204 m ³ /hr, 0.966 μm Particles, July 94).	136
E-12 Number Density Upstream (Diffuser, 204 m ³ /hr, 0.966 μm Particles, July 94).....	136
E-13 Axial Velocity Downstream (Diffuser, 204 m ³ /hr, 0.966 μm Particles, July 94).....	137
E-14 Number Density Downstream (Diffuser, 204 m ³ /hr, 0.966 μm Particles, July 94).....	137
E-15 Local Efficiencies over Filter Face (Diffuser, 204 m ³ /hr, 0.966 μm Particles, July 94).....	137
E-16 Axial Velocity Upstream (Diffuser, 255 m ³ /hr, 0.966 μm Particles, July 94).	137

Figure	Page
E-17 Number Density Upstream (Diffuser, 255 m ³ /hr, 0.966 μm Particles, July 94).....	138
E-18 Axial Velocity Downstream (Diffuser, 255 m ³ /hr, 0.966 μm Particles, July 94).....	138
E-19 Number Density Downstream (Diffuser, 255 m ³ /hr, 0.966 μm Particles, July 94).....	138
E-20 Local Efficiencies over Filter Face (Diffuser, 255 m ³ /hr, 0.966 μm Particles, July 94).....	138
E-21 Axial Velocity Upstream (Diffuser, 68 m ³ /hr, 5.3 μm Particles, July 94).....	139
E-22 Number Density Upstream (Diffuser, 68 m ³ /hr, 5.3 μm Particles, July 94)....	139
E-23 Axial Velocity Downstream (Diffuser, 68 m ³ /hr, 5.3 μm Particles, July 94)...	139
E-24 Number Density Downstream (Diffuser, 68 m ³ /hr, 5.3 μm Particles, July 94)	139
E-25 Local Efficiencies over Filter Face (Diffuser, 68 m ³ /hr, 5.3 μm Particles, July 94).....	140
E-26 Axial Velocity Upstream (Diffuser, 119 m ³ /hr, 5.3 μm Particles, July 94)....	140
E-27 Number Density Upstream (Diffuser, 119 m ³ /hr, 5.3 μm Particles, July 94)..	140
E-28 Axial Velocity Downstream (Diffuser, 119 m ³ /hr, 5.3 μm Particles, July 94).	140
E-29 Number Density Downstream (Diffuser, 119 m ³ /hr, 5.3 μm Particles, July 94).....	141
E-30 Local Efficiencies over Filter Face (Diffuser, 119 m ³ /hr, 5.3 μm Particles, July 94).....	141
E-31 Axial Velocity Upstream (Diffuser, 255 m ³ /hr, 5.3 μm Particles, July 94).....	141
E-32 Number Density Upstream (Diffuser, 255 m ³ /hr, 5.3 μm Particles, July 94).....	141
E-33 Axial Velocity Downstream (Diffuser, 255 m ³ /hr, 5.3 μm Particles, July 94).....	142

Figure	Page
E-34 Number Density Downstream (Diffuser, 255 m ³ /hr, 5.3 μm Particles, July 94).....	142
E-35 Local Efficiencies over Filter Face (Diffuser, 255 m ³ /hr, 5.3 μm Particles, July 94).....	142
E-36 Axial Velocity Upstream (Diffuser, 68 m ³ /hr, 0.966 μm Particles, Feb. 95)...	142
E-37 Number Density Upstream (Diffuser, 68 m ³ /hr, 0.966 μm Particles, Feb. 95)	143
E-38 Axial Velocity Downstream (Diffuser, 68 m ³ /hr, 0.966 μm Particles, Feb. 95).....	143
E-39 Number Density Downstream (Diffuser, 68 m ³ /hr, 0.966 μm Particles, Feb. 95).....	143
E-40 Local Efficiencies over Filter Face (Diffuser, 68 m ³ /hr, 0.966 μm Particles, Feb. 95).....	143
E-41 Axial Velocity Upstream (Diffuser, 136 m ³ /hr, 0.966 μm Particles, Feb. 95)	144
E-42 Number Density Upstream (Diffuser, 136 m ³ /hr, 0.966 μm Particles, Feb. 95).....	144
E-43 Axial Velocity Downstream (Diffuser, 136 m ³ /hr, 0.966 μm Particles, Feb. 95).....	144
E-44 Number Density Downstream (Diffuser, 136 m ³ /hr, 0.966 μm Particles, Feb. 95).....	144
E-45 Local Efficiencies over Filter Face (Diffuser, 136 m ³ /hr, 0.966 μm Particles, Feb. 95).....	145
E-46 Axial Velocity Upstream (Diffuser, 255 m ³ /hr, 0.966 μm Particles, Feb. 95).	145
E-47 Number Density Upstream (Diffuser, 255 m ³ /hr, 0.966 μm Particles, Feb. 95).....	145
E-48 Axial Velocity Downstream (Diffuser, 255 m ³ /hr, 0.966 μm Particles, Feb. 95).....	145
E-49 Number Density Downstream (Diffuser, 255 m ³ /hr, 0.966 μm Particles, Feb. 95).....	146

Figure	Page
E-50 Local Efficiencies over Filter Face (Diffuser, 255 m ³ /hr, 0.966 μm Particles, Feb. 95).....	146
E-51 Axial Velocity Upstream (Diffuser, 272 m ³ /hr, 0.966 μm Particles, Feb. 95).	146
E-52 Number Density Upstream (Diffuser, 272 m ³ /hr, 0.966 μm Particles, Feb. 95).....	146
E-53 Axial Velocity Downstream (Diffuser, 272 m ³ /hr, 0.966 μm Particles, Feb. 95).....	147
E-54 Number Density Downstream (Diffuser, 272 m ³ /hr, 0.966 μm Particles, Feb. 95).....	147
E-55 Local Efficiencies over Filter Face (Diffuser, 272 m ³ /hr, 0.966 μm Particles, Feb. 95).....	147

NOMENCLATURE

a	size parameter for light scattering
a_e	elemental surface area of filter media (m^2)
A_{pv}	cross-sectional area of the probe volume (m^2)
c	dimensionless packing density of filter
C	log normal distribution function
C_c	Cunningham slip correction factor
CMD	count median diameter of the droplets (m)
d	diameter of the droplets (m)
D	diameter of the monodisperse spheres (m)
D_f	diameter of fiber (m)
D_p	diameter of particle (m)
e	base of the natural logarithm
e_c	elementary unit of charge (1.6×10^{-19} coulomb)
f	frequency of droplet generator (Hz)
f_D	signal Doppler frequency (Hz)
F	fraction by volume of the particles in the original solution
h	filter depth (m)
I	measured current (amperes)

I_p	interception parameter
K_n	Knudsen number
K_u	Kuwabara hydrodynamic factor
L	length of all fibers in a unit volume of filter media (m)
m	average number of particles in a droplet
m_f	refractive index of surrounding fluid
n	number of elementary units of charge
n_i	total number of particles
N	concentration of small ions of either polarity (per ml)
N_i	particle number density (m^{-3})
$P(x)$	probability of x spheres in a droplet
r_p	particle radius (m)
R	singlet ratio
R_f	radius of fiber (m)
R_p	radius of particle (m)
s_f	fringe spacing (m)
St_c	Stokes number corrected for slip
t_i	run time (seconds)
u	measured upstream velocity (m/s)
u_o	velocity near filter pleats (m/s)
u_∞	velocity inside filter media (m/s)
U	average flow velocity (m/s)

v_i	average measured velocity (m/s)
VMD	volume median diameter (m)
x_e	width of an element of filter media (m)
X	axis along the center line of the transceiver
y	dilution ratio
y_e	length of an element of filter media (m)
Y	axis perpendicular to the center line of the transceiver
Z	vertical axis along the center line of the housing
Z	ion mobility ($\text{cm}^2/\text{statV}\cdot\text{sec}$)
α	beam crossing angle
η_1, η_2	independent collection efficiencies
η_{coll}	overall collision efficiency
η_e	elemental efficiency
η_I	local efficiency
η_{IR}	combined inertial interception efficiency
η_{overall}	overall efficiency averaged over all of the grid points
η_s	single fiber efficiency
λ	wavelength of light (m)
μ	dynamic viscosity of air (Pa s)
ρ_p	density of seeding particle (kg/m^3)
σ_g	geometric standard deviation of the droplets produced by the atomizer

CHAPTER I

INTRODUCTION

The performance of an engine greatly depends on the quality of air supplied to it. Better air filtration improves engine durability and performance by reducing engine wear. Engines equipped with properly designed filters last longer and are more fuel efficient. In addition, they will consume less oil, give more power and create less emissions. A properly designed engine filter not only reduces the dust concentration in the engine intake air to an acceptable level, but also has less restriction, attenuates engine noise, is not a source of flow noise and has high operational reliability (Jaroszczyk et al., 1993b).

Two types of filter are commonly used for intake air filtration in automotive engines, circular type and panel type. Engine air filters operate at variable flow rates and in unpredictable environmental conditions. These factors have a significant influence on filter behavior. Unfortunately many variables involved in the filtration process change randomly. The factors influencing the performance of air filters are varied. Dust concentrations, particle size distribution, flow distribution over the filter, and the location of the air intake are some of them. Although particle distribution is closely related to the

air flow distribution for an air filter, the presence of particles actually changes the flow pattern. Critical operating characteristics of filtration process include filtration efficiency, air flow resistance, and dust holding capacity (Davies, 1973). The filtration efficiency is the measure of the air cleaner's ability to remove particulate matter from an air stream. Smaller particles are typically the most difficult to filter, resulting in lower filtration efficiencies than larger particles. In general, the filtration efficiency of dry type filters and filters exposed to low dust concentrations increases with dust loading (Davies, 1973). The air flow resistance is the pressure loss across the filter, at a specified air flow rate which typically increases with the amount of dust loading. Dust holding capacity defines the amount of dust that the air cleaner can hold when it is operated at a specified air flow rate to some maximum resistance value. A properly designed filter must provide a very high dust removal efficiency and dust holding capacity with least possible flow restriction across the filter.

There have been numerous studies on mechanisms of air filtration and the flow velocity across the filter media. There are several theories predicting the flow field around fibers and single fiber efficiency due to interception, impaction, diffusion, reentrainment and gravity (Sabnis et al., 1994a). Several methods have been proposed to incorporate these theories into an overall description of filter efficiency which will apply to a wide range of parameters. Experimental work has followed to corroborate or to improve these theories. In addition experimentally measured parameters such as flow velocity profiles within a test housing have been used with these theoretical models to predict overall filtration performance (Sabnis et al. 1994b).

The efficiency of filtration and the pressure drop across the filter are both strong functions of the aerosol velocity through the filter media. The velocity distribution across the filter is determined by the configuration of the housing that holds the filter and the filter itself. To maintain uniformity of standards for testing the pressure drop, efficiency, and dust holding capacity characteristics of automotive air filters, the Society of Automotive Engineers has produced the "Air Cleaner Test Code," J726 (1987). This code governs the testing of both dry and oil bath type air filters. Flow visualization and velocity measurements performed with this housing show that the housing provides strongly recirculating separated flow at the walls leading to a very non-uniform flow that resembles that of an impinging jet (Newman, 1994). More details on the SAE housing are given in Chapter II.

Standard gravimetric test methods such as the SAE test evaluate a filter in terms of an "overall efficiency". The test simulates the entire life of a filter by passing an extremely large amount of dust through it, until a specified terminal pressure drop is reached. The weight gained by the filter during the test is the dust capacity of the filter. The ratio of the weight of the dust collected by the filter to the weight of the dust to which it was exposed, gives the overall efficiency of the filter. Gravimetric testing does not provide information concerning the dynamic changes in filter performance caused by deposited dust or any time and location dependent variation in the performance of the filter. Knowledge about these could change the overall approach to filtration system design and testing.

The present work employed Laser Doppler Velocimetry, a state-of-the-art technique to obtain knowledge of flow fields within the test housings of air filter tests.

Particle number densities were measured at various points in planes upstream and downstream of the filter. Particle concentrations at corresponding points of the grid upstream and downstream were used to obtain “local efficiencies”. The local efficiencies were averaged to get overall efficiency for a given flow rate and particle size. Only monodisperse polystyrene latex (PSL) particles were used in these experiments. Since aerosol velocity (flow rate) and size of the particles are two of the most important factors affecting the filtration efficiency, we felt that it was important to study the effects of different flow rates and particles sizes on filtration performance.

The experiments were performed on actual automotive panel air filters (Purolator A13192) in both the SAE J726 housing and a very small angle diffuser housing designed to yield more uniform flow field. The small angle diffuser housing was similar to that specified by the SAE J1669 (1993) for automotive cabin filter testing. The filter media was tested in an essentially clean condition giving initial efficiency of the filter. Variations in filter performance as regards to local efficiencies at different points on the filter face and when exposed to different particle sizes and different face velocities were studied. Pressure drop across the filter was also monitored during some of these experiments.

The measured efficiencies were compared with theoretical filtration models proposed by Sabnis (1993), and modified by Duran (1995), two of the previous researchers in this project. Both the theoretical and measured efficiencies were compared based on Stokes number.

CHAPTER II

LITERATURE REVIEW

2.1 Filter Testing Methods

2.1.1 SAE J726 Standard

The standards for testing performance of automotive engine air filters are laid down by the Society of Automotive Engineers (SAE) J726 Air Cleaner Test code (1987). Under this test code, the panel filter is mounted and tested in a standardized panel filter test housing. Typically, the test consists of injecting dust onto the filter until the pressure difference across the filter reaches a specified terminal restriction or pressure drop. An "absolute filter" is employed in-line to collect the dust particles passing through the test filter. The dust holding capacity and filtration efficiencies are arrived at by weighing the dust captured by the filter and that passing through into the absolute filter. Organizations that test filters have reported problems in terms of performance test result repeatability from test to test and from one test facility to another (Sabnis et al., 1994a). Difficulties also arise in comparing results between different sized filters. The test housing consists of a section which is similar to a wide angle diffuser diverging in two planes, with the diffuser exit blocked by a plate in which the panel air filter is mounted. This construction has been proved to be a cause for the flow being separated from the walls of the housing (Newman, 1994) and providing the filter under test with a non-uniform flow distribution. Figure 2.1 shows the sketch of the overall test apparatus of the SAE J726 standard.

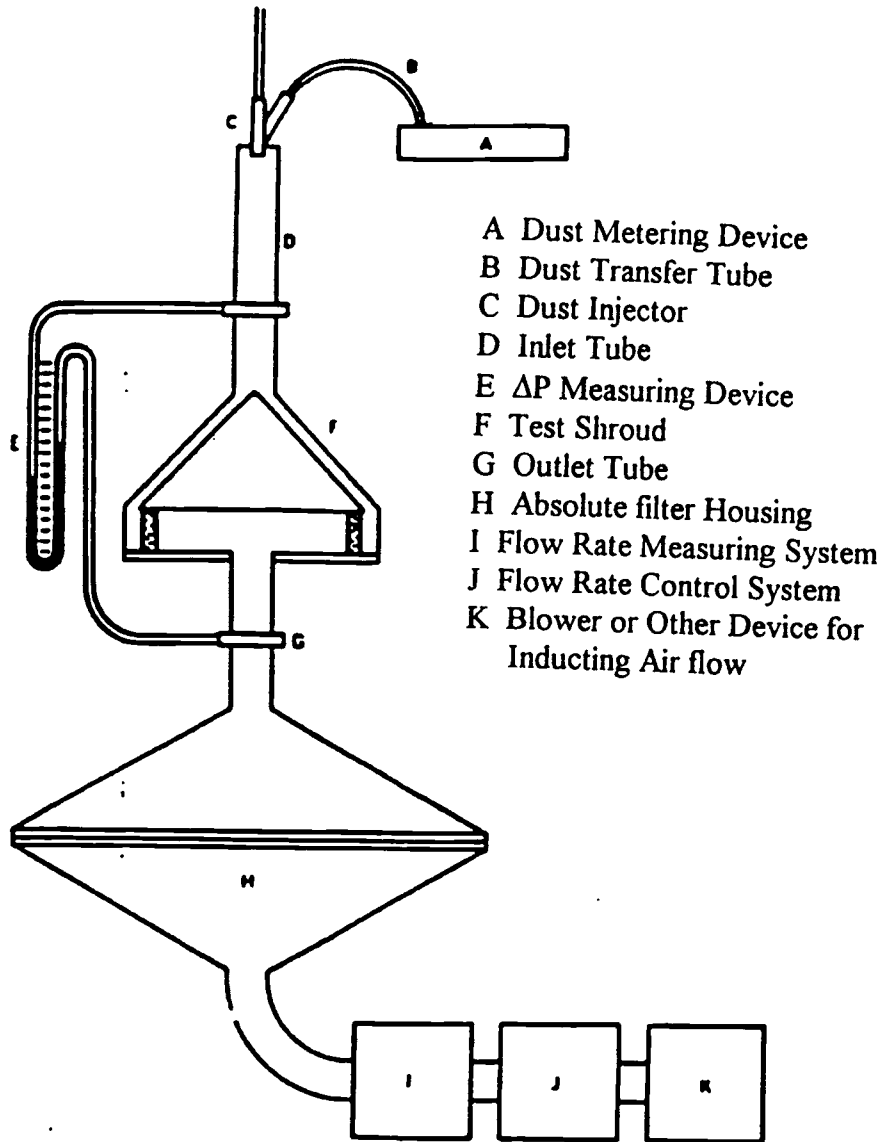


Fig. 2.1 Sketch of Test Housing and Overall Testing Apparatus as Per SAE J726 Standard (SAE, 1987)

In order to have a thorough understanding of the filtration process and the performance of a particular filter under actual operating conditions, information on

particle number and size distribution should be considered along with the average filter efficiency as determined by the aforementioned gravimetric method. This need has led several researchers to develop particle counting methods to test filters. These experimental procedures measure the average upstream and downstream particle concentrations using representative sampling procedures which disturb the flow fields within the test housing. Sampling typically occurs at one location upstream and downstream of the filter. The following is a review of some of these alternate procedures for arriving at filtration efficiencies by particle counting procedures.

2.1.2 Continuous Aerosol Monitoring System

A universal test stand for air filter media testing developed by Nelson Industries, Inc. employs the Continuous Aerosol Monitoring system (CAM) to determine overall and fractional efficiency of flat filter media (Jaroszczyk et al., 1987). Efficiencies, pressure drop, and dust holding capacity can all be obtained as a function of time, dust loading, dust particle size, or flow velocity. The schematic diagram of the stand is shown in Fig. 2.2. The on line CAM system simultaneously analyzes the upstream and downstream concentrations and size distributions using either AC fine dust or other test dusts. Two filter holders are available, one smaller 50 mm diameter and another 152 mm diameter. A laminar type flow meter provides accurate flow measurements in the range of 0 to 35 m³/hr (0 to 20.5 cfm) to give flow velocities in the range of 1 to 500 cm/s.

The CAM system uses near forward light scattering using an LED to determine particle concentration and size distribution of any aerosol that is moved through an optical sensor which is a small volume in the center of the aerosol volume. An isokinetic aerosol sampling technique is employed to supply aerosol to the sensors. In isokinetic sampling, the velocities in the aerosol tube of the filter holder and the sensor sampling probe are the same. The main advantage of this system is, due to the continuous monitoring of dust

concentrations, overall and fractional filter efficiencies can be obtained as a function of time every 5, 15, 30, or 60 minutes or as a function of dust loading.

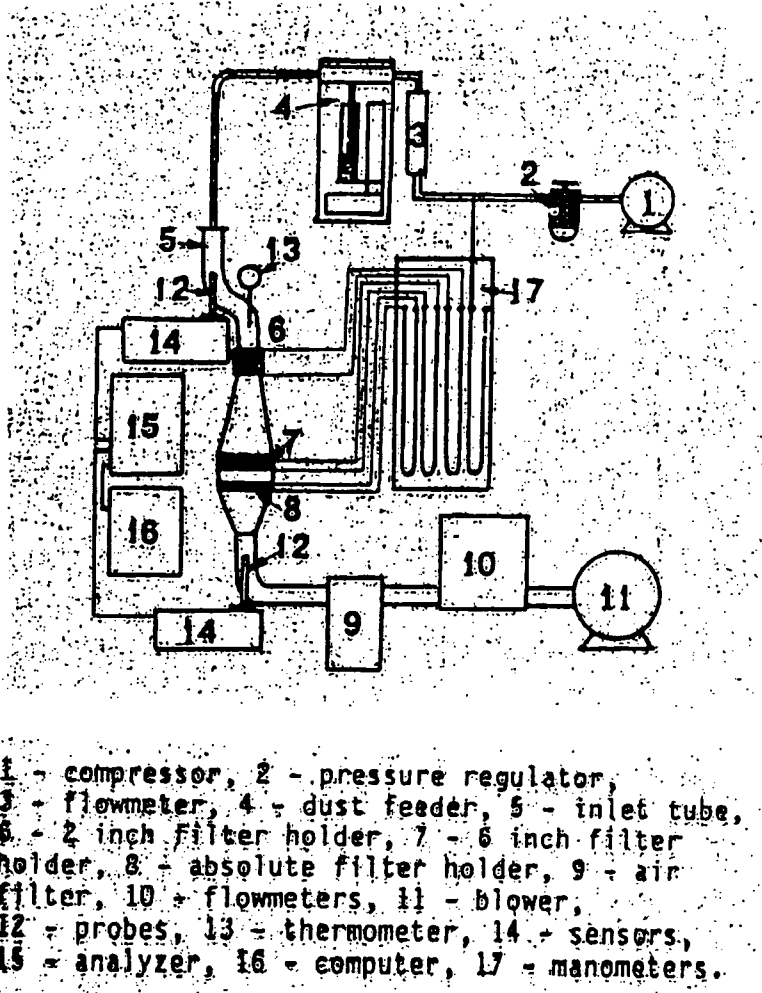


Fig. 2.2 Schematic Diagram of the Universal Test Stand for Air Filter Media Testing
 (Jaroszczyk et al., 1987)

Jaroszczyk et al. studied the changes in filtration efficiency and pressure drop as a function of dust loading. Their results clearly show the effects of re-entrainment after certain amount of dust loading. They used both AC coarse test dust and 0-10 μm test dust on nonwoven fabric and cellulose filter paper. In the case of AC coarse dust, the re-dispersion of dust particles begins at a lower flow restriction (40 mm of H_2O), as

compared to fine particles (100 mm of H₂O). The efficiency steadily increases with dust loading for both types of dust, until it reaches 99%. Then it drops below 99% at a restriction of 80 mm of H₂O for coarse dust, and is more than 99% throughout the course of fine dust filtration even at a restriction of over 280 mm of H₂O.

2.1.3 ASTM Standard for Testing Flat Media

The American Society for Testing and Materials Committee F21, developed ASTM F 1215-89, Standard Test Method for Determining the Initial Efficiency of a Flatsheet Filter Medium in an Airflow Using Latex Spheres (ASTM, 1989). As the name implies, the method covers techniques for measuring the initial particle size efficiency of flatsheet filter media using monodisperse polystyrene latex spheres in the range of 0.5 μm to 5.0 μm at airflow velocities of 1-25 cm/s. The method applies to efficiencies of less than 99.9% or penetrations of greater than 0.001 at 1 μm. Figure 2.3 shows a schematic of the test method. Some of the recommendations of this standard are briefly stated here.

Filtered and dried air must be used in the atomizer to produce an aerosol containing suspended latex particles. The aerosol must then be passed through a charge neutralizer. Typically, an ionizing flux of 10³ mCi/m³/s will provide the required aerosol neutralization. The aerosol is then mixed and diluted with additional preconditioned air to produce a stable, neutralized and dried aerosol of latex spheres to be used in the efficiency test. The aerosol mixing must be completed a minimum of 8 duct diameters before the inlet sampling probe and 10 duct diameters before the filter medium test sample. The filter medium testing is to be conducted in a relative humidity range of 30 to 50% and be held to no more than ±5% excursions during a given test. The aerosol generator must be capable of a latex sphere concentration output of 10⁷ to 10⁸ particles/m³. Static pressure taps should be flush with the duct walls at a distance of 1 duct diameter upstream and downstream of the filter medium faces. With no filter medium in the sample holder, there is to be no appreciable pressure drop between the inlet-side and outlet-side pressure taps.

The filter medium specimen will generally be of a form and flexibility so that it can be clamped or sealed in a specimen holder. It is also necessary that the sealing force not distort or influence the integrity or continuity of the filter medium matrix. Preconditioning is recommended for each filter medium sample at test duct conditions (30 to 50% \pm 5% relative humidity and 70 \pm 2°F temperature).

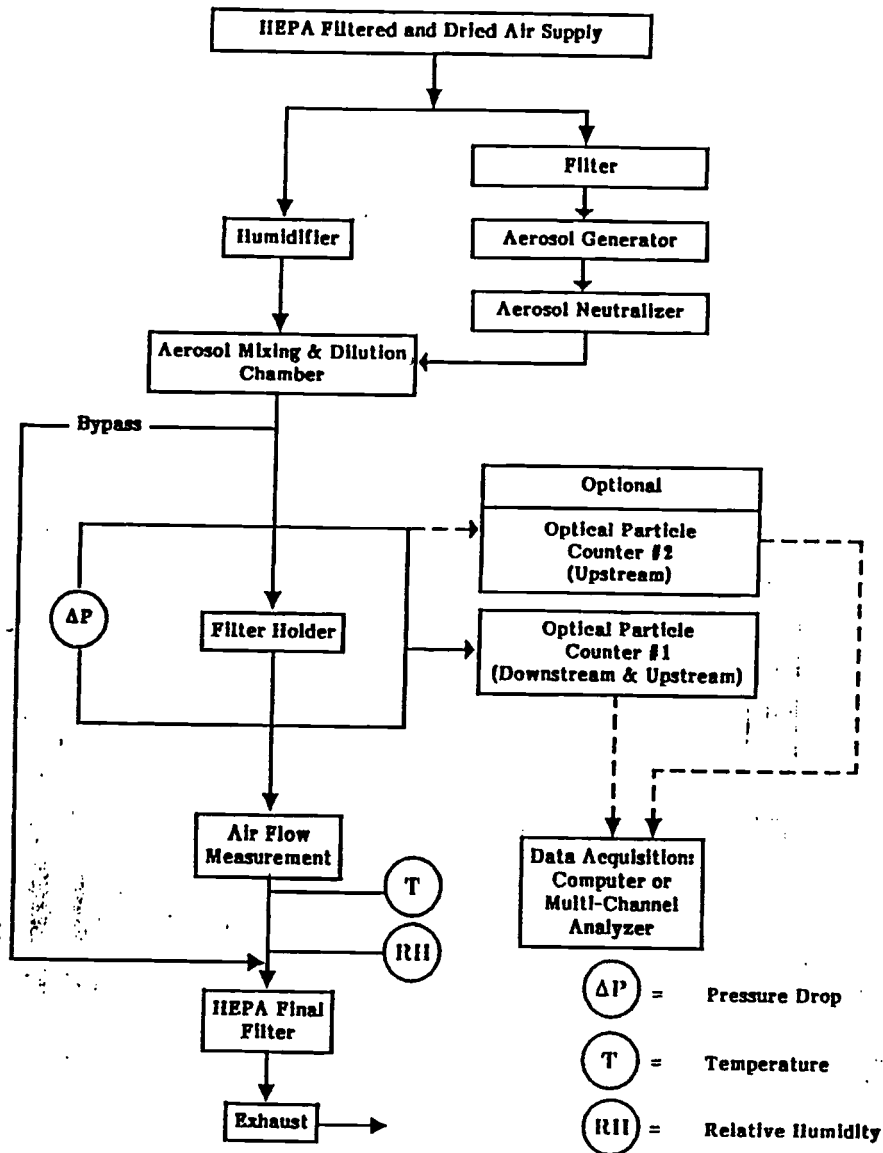


Fig. 2.3 Schematic Diagram of Air Filter Media Test Method (ASTM F 1215-1989)

A subsequent paper by Davis (1994) illustrates the utility of the above test standard for determining the efficiency of nonwoven materials (used as filtration media) as a function of particle size and velocity. Figure 2.4 provides a schematic of the experimental set up used for these tests. A commercial single particle light scattering counter (called the Optical Particle Counter) capable of measuring particle sizes of 0.5 to 10.0 μm was used to measure the particle concentrations upstream and downstream of the medium. While the counter used here met the ASTM requirements, a Multi-Channel Analyzer (MCA) card mounted in a standard personal computer was used to effectively convert the OPC into a high resolution counter. The software associated with MCAs allowed the user to specify the region of interest (ROI) for summation of the counts. In this case, ASTM specifies that the counts consist of all channels with $\geq 50\%$ of the peak. Figure 2.5 shows the results of a series of tests conducted at three different particle sizes for velocities ranging from 1.2 cm/s to 40 cm/s. As the velocity increased, the efficiencies for both electret and non-electret media increased. Davies points out that effect of electrostatic charge is significant only at low velocities.

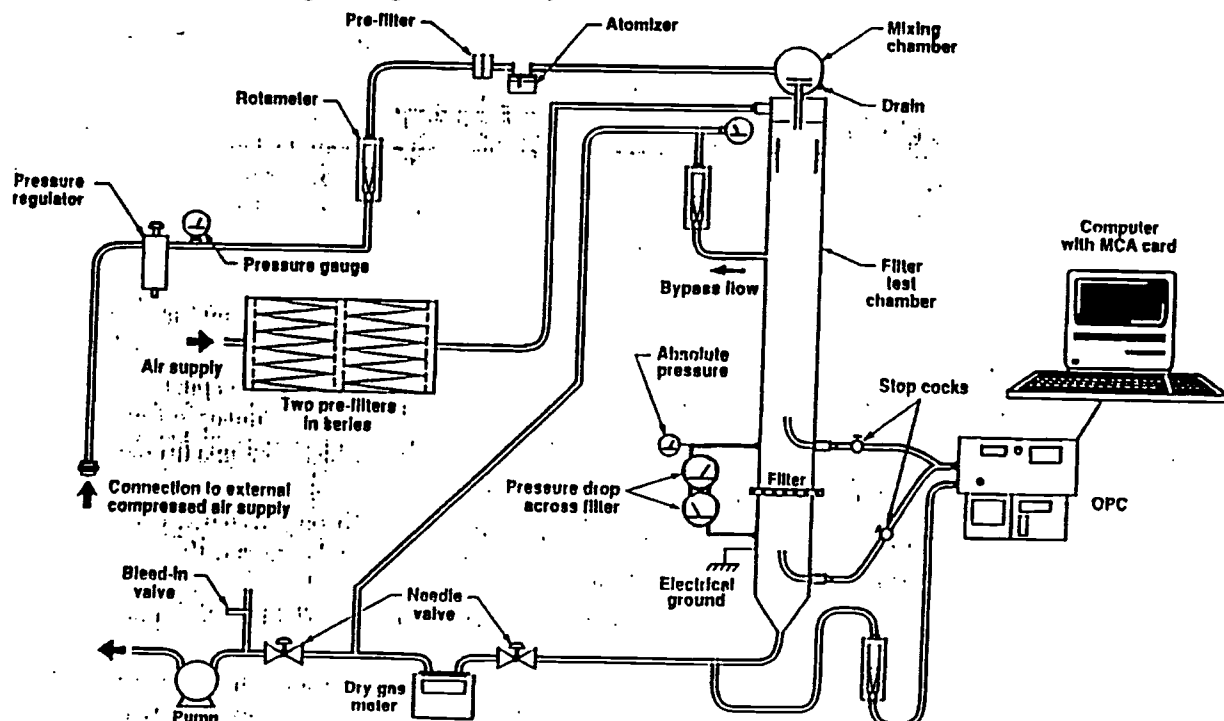


Fig. 2.4 Air Filtration Test Stand Used by Davis (1994)

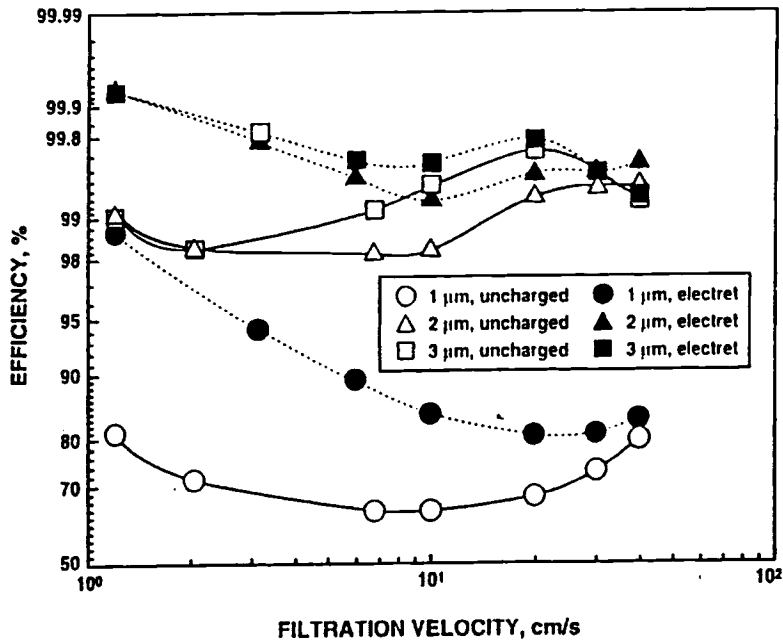


Fig. 2.5 Collection Efficiency for Three Particle Sizes (Davis, 1994)

2.1.4 Other Testing Methods

Although fibrous filtration is a transient process by nature, most of the research work carried out in this area is concerned primarily with the initial period of filtration during which the effect of deposited aerosol particles is negligible. The accumulation of particles at the surfaces of packing fibers results in an increase of the collection efficiency as well as pressure drop (Emi et al., 1982). In the study conducted by Emi et al., the results indicated that the collection efficiency increases monotonically with the increase in particle deposition at low flow velocities. At high flow velocity, the efficiency first increases, reaching a maximum, it either remains at this value or suffers a slight decrease with further increase in deposition, suggesting the effect of particle reentrainment and/or

particle bounce-off. On the other hand, the pressure drop was found to increase monotonically with the amount of particle deposition for all flow velocities.

This test used model filters composed of layers of wire screens of different dimensions. The experiments were conducted under conditions such that inertial impaction was the dominant mechanism. The test aerosol used in the above experiments was polydisperse droplets of a stearic acid-ethanol solution. The influent and effluent particle concentrations were based on Tyndallometer readings which provide a relative measurement of particle concentrations using sampling techniques. The aerosol particle size was determined by depositing the aerosol particles on a glass slide placed in an electrostatic sampler and examining them under a microscope.

A series of investigations were carried out by Baczewski and Jaroszczyk (1981) consisting of a selection of test dust from actual road samples, laboratory investigation of filtration materials and filters, and field investigation of filters. The concentration of dust in vehicle surroundings were determined at different points around the vehicles driving under various road conditions. The concentration of dust in air sucked into filters did not exceed 0.25 mg/m^3 for a vehicle driving on asphalt roads just after rain and approximately 0.8 mg/m^3 when the surrounding roads were dry. During tests in towns, dust collected in a filter contained 60 - 80% by weight of organic materials such as carbon black. They comment that, it is impossible to describe the process of filtration of actual, polydisperse aerosol in actual fibrous filters with dynamical laws that would cover the complete range of filtration kinetics, i.e. the range in which structure of a filter is conditioned by the dust accumulating on the filter. It is easier to obtain simplified and generalized conclusions

during the initial period of filtration, when the filter structure has not been changed by the accumulated dust.

The laboratory investigations were carried out with filtration paper 20/66 manufactured by Bosso Company (paper thickness 0.60 - 0.68 mm, basis weight 107 - 110 g/m^2). Figure 2.6 shows that the efficiency of paper filters increases for particle sizes of $1 \mu\text{m}$ and larger with an increase of aerosol flow velocity. Figure 2.7 shows the filtration efficiency as a function of dust loading. For lower velocities up to 0.2 m/s, the efficiency of filtration increases for dust load growth up to 50 g/m^2 , due to the fact that the accumulating dust results in an increase of filter packing density. If an excessive increase of the packing density increases the velocity of aerosol flow in spaces around the fibers in

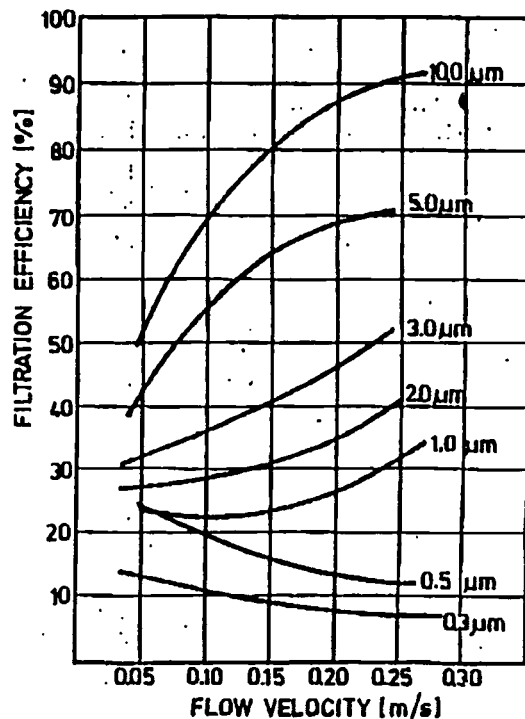


Fig. 2.6 Filtration Efficiency of 20/66 Paper Versus Flow Velocity of Aerosol for Different Sizes of Particles (Baczewski and Jaroszczyk 1981).

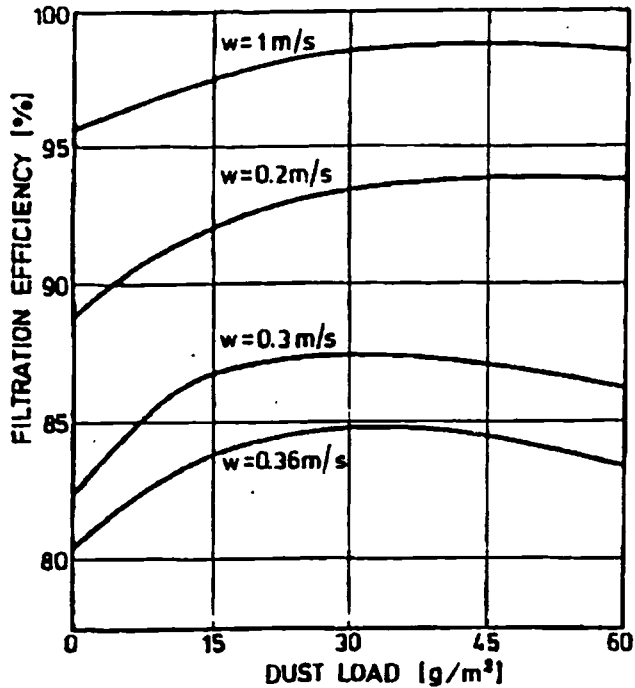


Fig. 2.7 Filtration Efficiency of 20/66 Paper Versus Accumulated Dust Load. (w =average flow velocity) (Baczewski and Jaroszczyk 1981).

the filter, then forces of aerodynamic separation of the dust particles exceed the forces of adherence, and the filtration efficiency diminishes. For higher velocities, this phenomenon begins earlier. At very high velocities, the majority of the particles could be deflected from the fibers and would not be deposited in the filter. They conclude that, as a result of limited forces of adherence of the dust particles to fibers in the range of filtration kinetics, the dust reentrainment occurs, caused by a lack of equilibrium between the forces of aerodynamic separation of the dust particles and their adherence to the fibers. Larger particles are easily blown off from the fibers. For each polydisperse dust and type of filter material, there is an optimum flow velocity that should be the basis for selection of a suitable filter area for a specific engine. In actual filters, this principle is frequently not observed and filter areas are often too small.

2.1.5 Aerosolization

A successful filter test can be defined as one that provides an accurate measurement under meaningful test conditions. The two most important factors for the success of a filter test are the accuracy of the aerosol generator and the aerosol particle counter. The aerosol may be monodisperse or polydisperse depending on the objective of the test. Monodisperse aerosols are produced by atomizing liquid suspensions of relatively uniform spheres. Commonly used monodisperse suspensions are those of polystyrene latex spheres in water. These are available as 10% solids by weight in deionized water with trace amounts of surfactants. Their sizes are determined by the manufacturer either by electron microscopes or, for particles above 0.5 microns, by optical microscopes and/or electrical resistance type particle size analyzers.

When producing an aerosol by atomizing liquid suspensions, it is desirable to produce droplets with only one sphere in them. Many droplets will contain no spheres, and many droplets will contain more than one sphere. When the liquid of the droplet evaporates, a droplet with no spheres dries to a relatively tiny particle of residue of impurities in the liquid. When a droplet with a single sphere evaporates, the resulting aerosol particle is that individual sphere. If more than one sphere is contained in a droplet, the resulting particle is an undesirable aggregate. It is therefore desirable to calculate the dilution required in a given application to provide a satisfactory fraction of single spheres. It is also useful to calculate the corresponding fraction of droplets that will have no spheres in estimating the resulting aerosol concentration.

A formula was developed by Raabe (1968) for estimating the dilution required to produce a satisfactory ratio assuming that the atomizer produces a droplet distribution which is log normal. To make these calculations, the droplet distribution of the generator used to atomize the suspension must be known. The droplet distributions are usually described as log-normal distributions.

$$C(\ln d) = \frac{1}{\ln \sigma_g \sqrt{2\pi}} e^{-\frac{(\ln \text{CMD} - \ln d)^2}{2 \ln^2 \sigma_g}} \quad (2.1)$$

where C is the log normal distribution function, CMD is the count median diameter of the droplet (median of the droplet sizes), σ_g is the geometric standard deviation of droplets produced by the atomizer, and d is the diameter of the droplets. When a droplet is produced, the probability of a sphere being in the droplet is given by the Poisson probability distribution. Thus the probability of x spheres being found in a drop of size d is

$$P(x) = \frac{m^x e^{-m}}{x!} \quad (2.2)$$

where 'm' is the average number of spheres in the droplet and is given by

$$m = Fd^3 / yD^3 = nd^3 \quad (2.3)$$

with 'F' being the fraction by volume of the particles in the original stock suspension, 'y' the dilution ratio, 'D' the diameter of the monodisperse spheres, and 'n' is a parameter defined for simplicity. The dilution ratio 'y' is defined as the ratio of the new volume to the old volume after the original suspension is diluted with pure liquid. The ratio of the probability of finding one sphere among the droplets to the probability of finding droplets with one or more spheres is taken as the singlet ratio, R:

$$R = \frac{P(1)}{1 - P(0)} \quad (2.4)$$

$$R = \frac{n(\text{CMD})^3 e^{[4.5 \ln^2 \sigma_g]} - n^2(\text{CMD})^6 e^{[18 \ln^2 \sigma_g]} + \frac{n^3}{2} (\text{CMD})^9 e^{[40.5 \ln^2 \sigma_g]} \dots}{n(\text{CMD})^3 e^{[4.5 \ln^2 \sigma_g]} - \frac{n^2}{2} (\text{CMD})^6 e^{[18 \ln^2 \sigma_g]} + \dots} \quad (2.5)$$

Since the process of obtaining a solution from the above equation would be cumbersome, the following form of empirical equation has been developed:

$$R = 1 - [n(\text{CMD})^3 e^{13.5 \ln^2 \sigma_g}] [f(n, \text{CMD}, \sigma_g)] \quad (2.6)$$

where $f(n, \text{CMD}, \sigma_g) \cong 1 - (e^{\ln^2 \sigma_g}) / 2$ (2.7)

The authors then go through some manipulations to arrive at the dilution ratio 'y' as,

$$y \cong \frac{F(\text{CMD})^3 e^{13.5 \ln^2 \sigma_g}}{(1 - R)D^3} [1 - (e^{\ln^2 \sigma_g}) / 2] \quad (2.8)$$

Droplet distributions are sometimes described in terms of the volume median diameter, VMD. Employing the identity (Raabe, 1968),

$$\text{VMD} = \text{CMD} e^{3 \ln^2 \sigma_g} \quad (2.9)$$

the dilution y, required to yield a singlet ratio, R, is given by

$$y \cong \frac{F(\text{VMD})^3 e^{4.5 \ln^2 \sigma_g}}{(1 - R)D^3} [1 - (e^{\ln^2 \sigma_g}) / 2] \quad (2.10)$$

for $R > 0.90$ and $\sigma_g < 2.1$.

The fraction of droplets with no spheres is approximately given by

$$P(0) \cong 1 - \frac{(1 - R)}{e^{9 \ln^2 \sigma_g} (1 - 0.5 e^{\ln^2 \sigma_g})} \quad (2.11)$$

Figure 2.8 shows a portion of the results of computations performed by Raabe (1968) for a singlet ratio of 0.95 as points plotted with full logarithmic coordinates in conjunction with the theoretical lines. Probabilities of various numbers of spheres in drops

for a variety of monodisperse sphere sizes from 0.088 μm to 1.305 μm and for various droplet distributions with VMD from 0.5 μm to 20.0 μm and with σ_g from 1.2 to 3.0 were used in the computations. The fraction by volume (F) of spheres in the stock suspensions was assumed to be 0.1 in all cases.

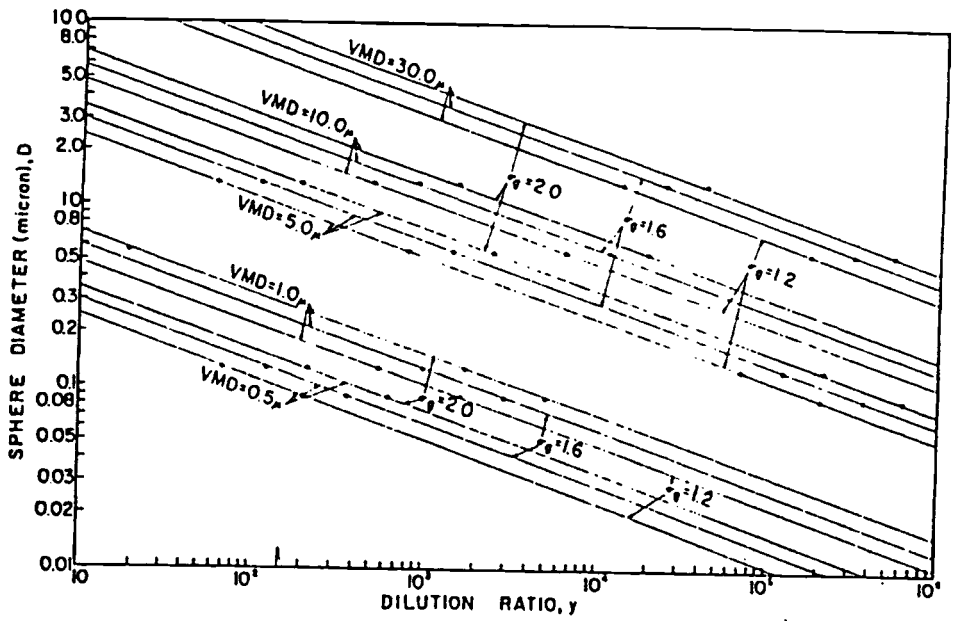


Fig. 2.8 The Dilution Ratio, y , for a Singlet Ratio, $R=0.95$, Versus the Sphere Diameter for Various Values of Volume Median Diameter (Raabe, 1968)

Coagulation of particles in an aerosol is an important phenomenon which reduces the number concentration, alters the size distribution, and changes the shape of solid particles (Melling and Whitelaw, 1975). Coagulation depends strongly on the size of the particles rather than on the particle material. Between equally sized particles, coagulation occurs more rapidly when they are small, and coagulation between unequal particles is increasingly probable as the difference between their diameters increases. Similarly, if a monodisperse aerosol is generated at high concentration, it will tend to become polydisperse by coagulation. When measurements are made in confined flows, particles

depositing on test section windows will cause deterioration of the Doppler signals. But they add that, when using dual beam scatter fringe systems, problems of particle coagulation will be encountered, if at all, only in the equipment used to generate the seeding particles rather than in the flow where laser anemometer measurements are required.

2.1.6 Electrostatic Effects

Gillespie (1955) lists two possible ways in which the electric charges may affect the filtration process: (1) particles or drops may be pulled to the fibers from a distance; and (2) the presence of electric charges may help to ensure that particles or drops which have come in contact with the fibers are retained. A series of measurements were performed by Gillespie to quantitatively measure the electric charge distributions of typical aerosols and the net electric charge per unit length on the fibers of various filters. Two types of aerosol were used; first, a homogeneous stearic acid aerosol from a La Mer-Sinclair generator, and second, spherical polystyrene particles. With the types of instruments used to determine the electric charge, it was possible to determine the electric charge, only for particles above the limit of visibility of the optical microscope ($> 0.2 \mu\text{m}$). When the aerosol generator was generating a homogeneous aerosol, less than 5% of the particles had an electric charge. It is interesting to note that when the generator was yielding a heterogeneous aerosol, as many as 70% of the particles were charged. These electric charge data collected were then applied along with a simple theory of filtration which included electric and mechanical effects to get appropriate filtration results.

Liu and Pui (1974) describe methods of neutralizing the aerosols to avoid unwanted electrostatic effects in laboratory tests. The level of charge on an aerosol can be reduced by means of small bipolar ions. By exposing an aerosol to a source of ionizing radiation, small bipolar ions can be created and the gaseous medium around the particles can be made electrically conductive. The particles can then discharge themselves by

capturing ions of the opposite polarity. Alternatively, small bipolar ions can be produced in an a.c. corona discharge and then can be mixed with the aerosol to be neutralized.

In the design or application of aerosol charge neutralizers, it is necessary to know the time, t , required for an aerosol to be neutralized. This time is estimated from the following equation (Whitby et al., 1965),

$$t = 1/[4\pi Ne_c Z] \quad (2.12)$$

where N (ions/ml) is the concentration of small ions of either polarity and Z ($\text{cm}^2/\text{statV}\cdot\text{sec}$) is the ion mobility. However Liu and Pui (1974) opine that Gunn's equation provides only a rough estimate of the actual neutralization time required, since the actual neutralization time depends both on the initial particle charge and the kinetics of the charge neutralization process. They go on to describe several radioactive aerosol charge neutralizers including a Kr^{85} radioactive charge neutralizer. It consists of a radioactive source placed along the center of a cylindrical metal container. The β -radiation produced by the radioactive Kr^{85} gas is capable of penetrating through the thin wall stainless steel tube to ionize the gas molecules inside. The outer metal cylinder serves to confine the β -radiation from the source and to provide the necessary neutralization volume for the aerosol. The aerosol used was generated from a solution of DOP (di-octyl phthalate) in isopropyl alcohol using a vibrating orifice droplet generator. The aerosol charge was measured by spraying the solution droplets directly into a Faraday cup and measuring the current with an electrometer. The droplet charge, n , was calculated from the equation

$$n = I/f e_c \quad (2.13)$$

where f is the operating frequency of the droplet generator, I is the measured current and $e_c = 1.60 \times 10^{-19}$ coulomb is the elementary unit of charge. The solution droplets were allowed to evaporate and the DOP aerosol (2.53 μm dia.) obtained was passed through the 2mCiKr^{85} charge neutralizer at flow rates ranging from 23.6 to 94.4 liters/min. The corresponding residence time of the aerosol was between 3.83 and 0.95 sec.

2.2 Laser Doppler Velocimetry

2.2.1 Basic Principles

Pre-laser flow measurements were nearly exclusively carried out by means of mechanical probes (pitot tube, hot-wire, or hot-film probes) supported at the point of measurement by mechanical means. Such methods obviously exert uncontrollable influence on the flow phenomenon under study. In cases where the flow region is accessible by light beams, either through windows or through transparent sections, optical methods have the great advantage of introducing negligible distortions into most flow fields. The laser Doppler method, which is based on the detection of the Doppler shift of laser light scattered from small particles moving with the medium, has the potential of complete linearity between transducer response (Doppler frequency shift) and velocity. In contrast, other commonly used transducers such as the pitot tube or hot wire are only approximately linear within limited ranges. The laser is a source of coherent highly collimated light. In the following paragraphs, some of the basics of Laser Doppler Velocimetry (LDV) will be outlined. Further details can be obtained from many references such as Liang (1994).

The main ingredients of an LDV arrangement are the laser source, the optical transmitter/receiver, and the electronic signal processor. The function of LDV optics is partly to transmit and direct the laser light into a small well-defined volume at the desired point of measurement, and partly to receive the scattered light and direct it to the photodetector. There are different modes by which the laser Doppler systems may work: (1) the reference beam mode, in which one beam, the reference beam, is derived directly from scattered light from the measuring volume; (2) the dual beam mode, known as the differential fringe system mode, in which the two recombined beams are composed of scattered light from the same measuring volume, but scattered from two different incident beams intersecting in the measuring volume; and (3) the dual scattered beam mode in

which, by means of a beam splitter and mirrors, two beams of light scattered in two different directions from one incident beam are recombined on the surface of the detector (Buchhave et al., 1975). The detector can be arranged to collect either the forward scattered or the backscattered light with a combined transmitter/receiver, called a 'transceiver', which is most favored in applications where space and optical access are limited. Systems employing backscattered light do not differ from forward scattering systems in principle, but the low intensity of backscattered light from small particles necessitates special care in the design of backscattering systems.

One of the first signal processors used in LDV work was the conventional spectrum analyzer (Buchhave et al., 1975). The measured probability density distribution of frequency allows the mean velocity and correlations of the fluctuating velocity to be determined. Another averaging system is the photon correlator which directly constructs the time averaged autocorrelation function of the detector signal. All time averaging systems are unable to provide information relating to the short time history of the flow fluctuations, thus preventing the formation of turbulence spectra and related information. The third system, known as the burst counter, is again basically a timing device which measures the time for a certain number of zero crossings of the high pass filtered Doppler signal. The measured time is the time of flight of a particle through a corresponding number of interference fringe planes in a fringe mode LDV. Fast digital electronics calculate the velocity by inversion and multiplication by the appropriate scale factor and present a digital output immediately following each measurement.

The fringe-mode dual-beam LDV is the most commonly used system now. A typical fringe mode dual-beam laser system is shown in Fig. 2.9. The laser beam is split into two beams and then focused on a point where flow measurements have to be taken. The two intersecting beams create an interference fringe pattern. The light is scattered by the seeding particles passing through the fringes, and the scattered light is collected by the receiver and then sent to photomultiplier tubes (PMT). The PMTs convert the optical

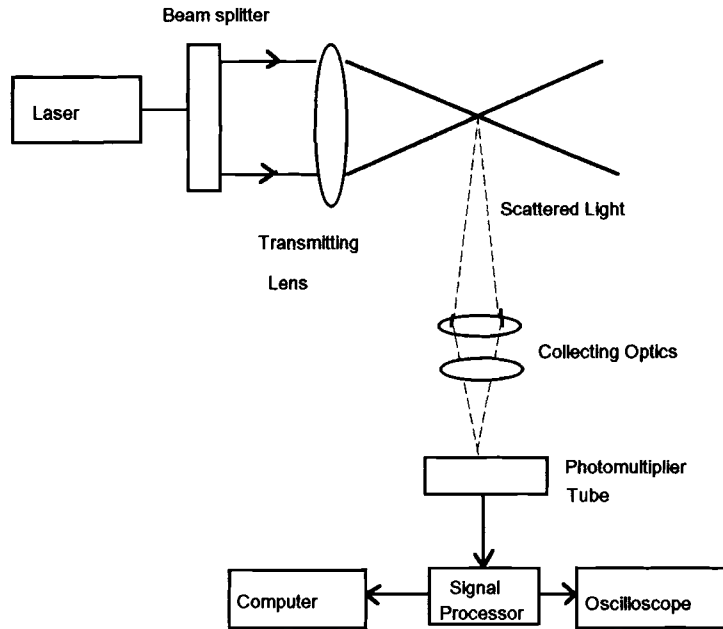


Fig. 2.9 Schematic Sketch of a Typical Dual-Beam LDV System

signals into electronic signals which are processed by appropriate signal processors. A microcomputer controls the whole process of data collection and analysis and also stores the data. The ensemble-averaged flow velocity is obtained at the end of the signal processing and is related to the Doppler frequency of the signal by

$$U = f_D s_f \quad (2.14)$$

where 'U' is the flow velocity in the direction perpendicular to the optical axis of the crossing beams, f_D is the Doppler signal frequency, and 's_f' is the fringe spacing given by

$$s_f = \frac{\lambda}{2\sin(\alpha / 2)} \quad (2.15)$$

where 'λ' is the light wavelength and 'α' is the beam crossing angle (Aerometrics, 1992).

An important concept in the LDV measurements is that of optical frequency shift between the two beams. It allows the direction of flow velocity to be determined. The point of intersection of the two beams is called the 'probe volume', and it is typically described as an ellipsoid. It contains an alternate dark and light interference pattern called the 'fringe pattern'. When a seeding particle in the test flow passes through the probe volume, the light will be scattered by this particle and the detected signal will match the incident dark-light pattern as shown in the Fig. 2.10. The amplitude variation reflects the original Gaussian intensity distribution across the laser beam as shown in Fig. 2.11.

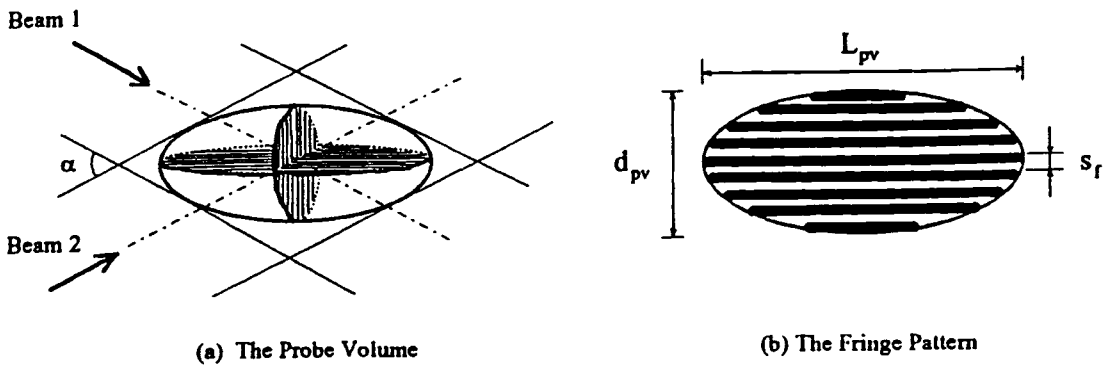


Fig 2.10 The Probe Volume and the Fringe Pattern (Liang, 1994)

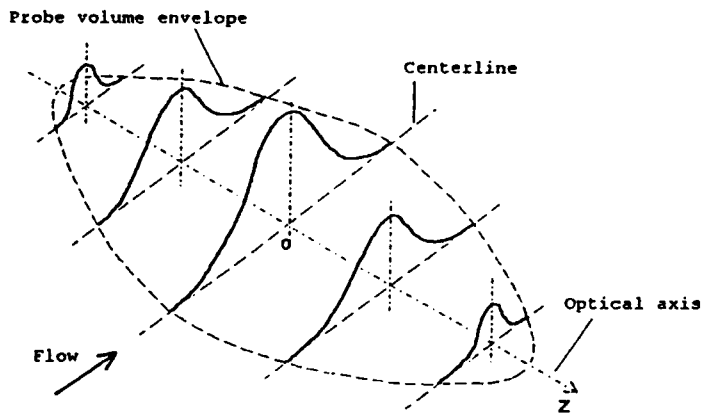


Fig. 2.11 Gaussian Intensity Distribution in the Probe Volume (Liang, 1994)

2.2.2 Laser Doppler Signals and Particles

One of the main disadvantages of the LDV system is that the seeding particles have to be present in the flow field in order to measure the flow velocity. The LDV typically measures the velocity of the seeding particle rather than that of the fluid itself. This requires that the seeding particles are sufficiently small to follow the flow and at the same time must be sufficiently large to produce good signals. It is also necessary that the particle be uniformly distributed in the flow so that measurement errors can be eliminated or reduced. The properties of the scattered light waves detected by the receiver of an LDV depend largely on the size and the optical properties of the particle. To obtain low noise signals with high measuring accuracy, the size of the particles has to be matched to the optical system. When considering the theory of light scattering by particles, the following size parameter is very important.

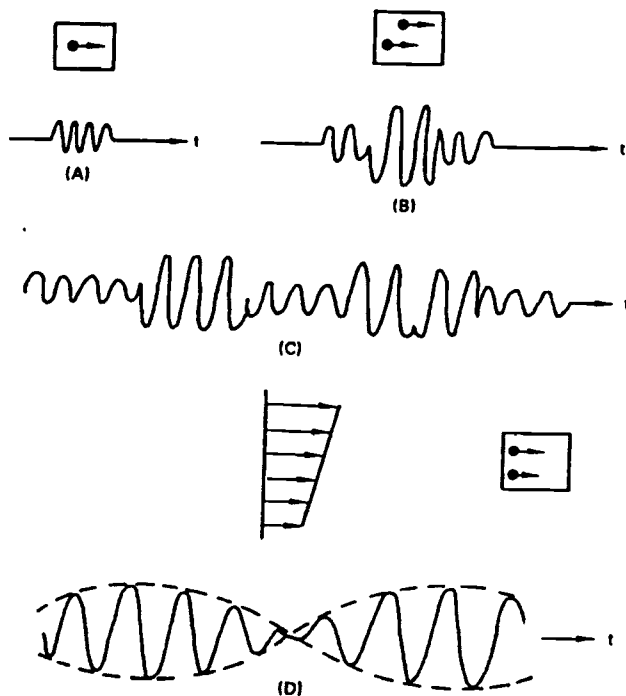
$$a = \frac{2\pi r_p m_f}{\lambda} \quad (2.16)$$

where ' r_p ' is the particle radius, ' m_f ' is the refractive index of the surrounding fluid, and ' λ ' is the wavelength of the light wave. Depending on the size parameter's range, light scattering is characterized as follows:

Rayleigh Scattering	$a \leq 1$
Mie Scattering	$1 \leq a \leq 500$
Geometrical Optics	$a \geq 500$

In most situations in which the fluid velocity has to be measured, particle sizes corresponding to $a \geq 500$ are prohibited due to requirements imposed on the dynamic behavior (Durst and Eliasson, 1975). Particles in the size range $a \leq 1$ don't normally provide scattered waves with adequate signal-to-noise ratios to permit laser Doppler signals to be recorded with sufficient accuracy. This leaves the particle size range $1 \leq a \leq 500$ as the most important one for an LDV.

In a paper presented in an LDA symposium in Copenhagen, George, Jr. (1975) discusses the various limitations on the accuracy of measurements inherent in laser Doppler signals. Among other things, his paper gives an idea of the resulting signal when more than one particle is present in the control volume. Figure 2.12 illustrates the effect of particles entering and leaving the control volume for four different cases. If there is only one scattering particle in a steady uniform flow, the signal is shown in Fig. 2.12a. In Fig. 2.12b, there are two particles present in the control volume. A typical signal for particles entering and leaving is shown in Fig. 2.12c, in which not only the Doppler current changes, but also the amplitude and the phase change abruptly. A frequency determining device cannot distinguish these anomalous crossing from velocity fluctuations. In Fig. 2.12d is depicted a situation where two particles enter at the same time.



- a) Signal generated by passage of single particle in steady, uniform flow.
- b) Signal generated by two particles which entered the flow at different times.
- c) Typical signal that would be obtained from many particles.
- d) Signal generated by two particles having different velocities.

Fig. 2.12 Doppler Signals Generated for Four Different Situations in a Steady, Uniform Flow (George, 1975).

Experiments have been conducted to thoroughly understand the signal properties of individual particles. By using a “Biomation Transient Recorder”, Durst and Eliasson (1975) photographically recorded the individual Doppler bursts. Figure 2.13 shows the LDA signals recorded for particles passing through center and off-center of the control volume. They point out that, in the presence of two or more particles as well as two or more incident coherent light waves, light scattering becomes more complex. Due to the coherent illumination of all particles, all of the scattered light waves will interfere. The complex amplitudes, and not the intensities in the field, are added prior to measurement. Therefore a photodetector will always record the resultant field intensity which is given by the square of the magnitude of the resultant field vector.

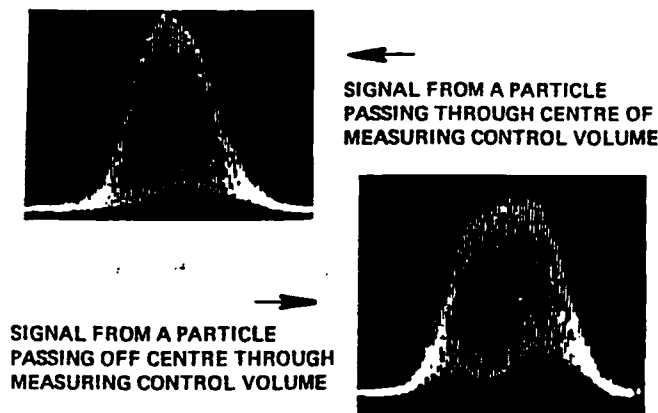


Fig. 2.13 LDA Signals Recorded with the Biomation Transient Recorder (Durst and Eliasson, 1975).

According to the theory, a band pass filtered LDV signal must not show significant variations in period length. However, Ruck and Pavlovski (1993) demonstrated that, in a systematic gas flow investigation, the period variations occur irrespective of the choice of flow regime, laminar or turbulent flow conditions, optical set up, data processing

electronics, and seed particle concentration. The differences in period lengths are caused due to multiple scattering, noise effects, and imaging and biasing errors (Ruck and Pavlovski, 1993). Subsequent experiments confirmed that the period variations were caused by particles located inside and outside of the actual control volume. The outside particles in the light beam path of the laser just outside the control volume scatter light, generating diffraction lobes in the forward direction, as shown in Fig. 2.14. The scattered light of the particles intersects with parts of the undisturbed light and causes distortions of the fringe pattern within the control volume. This results in a scatter of the measured velocity data for those particles passing through the center of the measuring volume at the same time. Depending on the intensity of the phase noise, and on the number of cycles evaluated, the error in fluctuation velocity measurements was found to be up to 4%. The scatter in individual FFT frequency determination can be reduced by increasing the validated cycles within a burst.

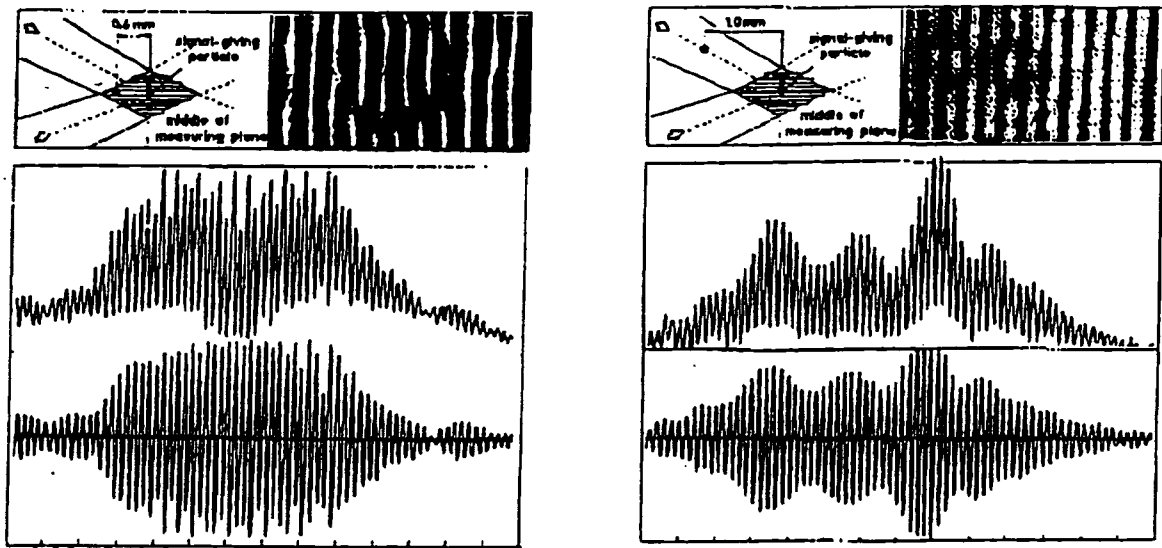


Fig. 2.14 Burst Analysis of a Doppler Signal in the Presence of Another Disturbing Particle Away from the Middle of the Measuring Volume (Ruck and Pavlovski, 1993).

2.3 Filtration Models

Paper or cellulose, which is a nonwoven filtering media, consists of fibers of various diameters. If the media has a certain thickness, it is assumed to be made up of a number of layers of randomly oriented fibers. This randomness in the construction of filter media makes it difficult to mathematically model a filter. Models have been proposed with varying degrees of complexity and none of them are generic models (Sabnis, 1993). Detailed literature review of various filtration theories and models have been done by previous researchers (Sabnis, 1993, Newman, 1994, Duran, 1995) in this project. One model based on the fundamentals of fluid flow around a single fiber was proposed by Davies (1973). The overall particle collection efficiency, η_{coll} , for a fiber cylinder is commonly obtained by considering the various mechanisms of particle capture by the fiber and then combining the individual efficiencies (Duran, 1995). The probability that a particle will be captured by any two mechanisms 1 and 2 is given by

$$\eta_{\text{coll}} = 1 - (1 - \eta_1)(1 - \eta_2) \quad (2.17)$$

By combining the Lee and Liu (1982) interception model, and the Landahl and Hermann (1949) inertial impaction model into Eq. (2.17) (refer to Duran's thesis for further discussion of these models), one can obtain the following expression for the combined effects of interception and inertial impaction (Duran, 1995):

$$\eta_{\text{IR}} = 1 - \left(1 - \frac{1 - c}{\text{Ku}} \frac{I_p^2}{1 + I_p} \right) \left(1 - \frac{\text{St}_c^3}{\text{St}_c^3 + 0.77\text{St}_c^2 + 0.22} \right) \quad (2.18)$$

where I_p is the interception parameter defined as the diameter ratio of particle to fiber, Ku is the Kuwabara hydrodynamic factor given as:

$$\text{Ku} = c - \frac{3}{4} - \frac{c^2}{4} - \frac{1}{2} \ln c \quad (2.19)$$

'c' is a dimensionless packing density or packing fraction, defined as the volume fraction of the fibers, and is given by:

$$c = \pi R_f^2 L \quad (2.20)$$

St_c is the dimensionless Stokes number corrected for slip using Cunningham correction factor approximated as:

$$C_c = 1 + 1.257Kn \quad (2.21)$$

where Kn is the Knudsen number, the ratio of the mean free path of the air to particle radius. Then the Stokes number corrected for slip, St_c, is defined as:

$$St_c = \frac{C_c R_p^2 \rho_p u_\infty}{9\mu R_f} \quad (2.22)$$

'R_f' is the radius of uniform fibers in the media, 'L' is the length of all fibers in a unit volume of the media, 'ρ_p' is density of seed particles, 'μ' is the dynamic viscosity of air.

The uncorrected Stokes number as defined by Davies (1973) is

$$St = \frac{R_p^2 \rho_p u_\infty}{9\mu R_f} \quad (2.23)$$

The trajectory of a particle can be mathematically tracked by inserting the Kuwabara flow field velocities into the equation of motion of a particle (Duran, 1995). Flagan and Seinfeld (1988) presented both an approximate solution, using average velocities, and an exact solution, using Kuwabara velocities, to obtain the isolated collision efficiency due to interception and inertial impaction. Sabnis (1993) used the model as given by Eq. 2.18 to compare with the exact and approximated solutions obtained by Flagan and Seinfeld (1988).

All of the filtration theories and models have been based on a flat filter media. However the same models could be used for pleated air filters using the velocity within the filter media, 'u_∞', and the packing density factor 'c'. If the axial velocity upstream of the filter is 'u₀', then the velocity near the filter pleats, 'u' is obtained by,

$$\mathbf{u} = \mathbf{u}_0 \frac{x_e y_e}{a_e} \quad (2.24)$$

where 'a_e' is the elemental surface area of an element of width 'x_e', and length 'y_e'. The air velocity inside the filter media is greater than the velocity near the filter pleats, u_∞ > u, and the measured axial velocity upstream of the filter is greater than the air velocity near the filter pleats, u₀ > u (Duran, 1995). The velocity within the filter media is given by

$$\mathbf{u}_\infty = \frac{\mathbf{u}}{1 - c} \quad (2.25)$$

If one assumes that the filter has uniform packing density c and fiber radius R_f, and that the filter efficiency is also uniform through a filter media of height 'h', then the elemental efficiency through the filter bed, is given by

$$\eta_e = 1 - \exp\left(\frac{2c\eta_s h}{\pi(1 - c)R_f}\right) \quad (2.26)$$

The elemental fiber efficiency represents an overall efficiency of a small element of a filter having thickness 'h' (Duran, 1995). Depending on how the single fiber efficiency 'η_s' is defined, the elemental fiber efficiency may or may not include the various mechanisms of particle collection. Duran (1995) developed a FORTRAN program EFFMODEL.FOR to incorporate various filtration models including the above described elemental efficiency model and using Eq. (2.18) for single fiber efficiency 'η_s'. For Purolator A13192 filter, he used a packing density of 0.345 and an effective fiber diameter of 51.78 μm.

2.4 Automotive Filter Media

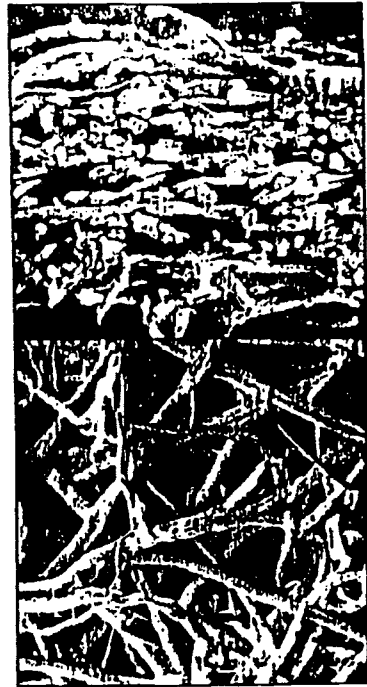
Nonwoven fibrous materials have been commonly used as filtration media for automotive air filters. They are manufactured as a sheet of paper consisting of a blend of coarse, fine, and curled cellulose fibers derived from various wood pulps (Rodman and Lessman, 1988). In some cases, it contains a small amount of synthetic fibers. The media

is then pleated to increase the effective surface area of filtration. It has a resin binder that supports the medium in its pleated filter state. There are two popular pleated filter configurations: one is the panel filter and the other is the circular filter. The work presented here was carried out for rectangular panel filters manufactured by Purolator Products, Inc. Rodman and Lessman (1988) took scanning electron microscope (SEM) pictures of the top surface and cross section of two wet laid nonwoven papers commonly used in pleated air filters. Figure 2.15a shows a picture of a wet-laid non-woven filter media commonly used in pleated air filters. In Fig. 2.15b is a high performance, water-laid non-woven filter media which has the same coarse fiber interlacing and pore structure as in Fig. 2.15a, but the large pores are crisscrossed with much finer micro-fibers.

Using an ordinary microscope, we took some photographs of the filter media and the filter used in this work. Figure 2.16 shows a top layer view of the flat filter media used in making A13192 filters. Figures 2.17 and 2.18 show two views of the surface of a filter sheet carefully cut out of a pleated filter loaded with SAE dust. The terminal pressure drop of this loaded filter was 254 mm of water over and above the initial pressure drop across the clean filter. All of the photographs were taken at a magnification of approximately 440. In Fig. 2.17 the void space between the fibers is large enough that the space is not filled with the dust. One can clearly see the dust particles clinging to the fibers. Whereas in Fig. 2.18 the fibers are so intermingled that the space between them is filled with the dust particles. The Polaroid camera used for these photographs automatically adjusted the exposure time depending on the light falling on the object. It also had a manual setting for the exposure time ratio to control the contrast of the photos. Figure 2.16 was taken at an exposure setting of 0.63 (equivalent to 1 to 3 sec), whereas Figs. 2.17 and 2.18 were taken at an exposure setting of 1.26 (equivalent to 16 to 25 sec). Figure 2.19 shows a scale engraving (comes with the microscope) used for obtaining the exact scale ratio used in the photos. With the help of the scale, a measurement of fiber diameter in the clean filter media gives a maximum value of approximately 40 μm .



(a) Wet-laid Automotive Filter Paper



(b) With Microscopic Fibers

Fig. 2.15 SEM Pictures of the Top Surface and Cross-section of Wet-laid Automotive Filter Papers (Rodman and Lessman, 1988)



Fig. 2.16 Top Surface Photograph of Purolator A13192 Clean Flat Filter Media (440 x)



Fig. 2.17 Top Surface Photograph of Purolator A13192 Pleated Filter Media Loaded with Dust to 254 mm of H₂O Pressure Drop (440 x)

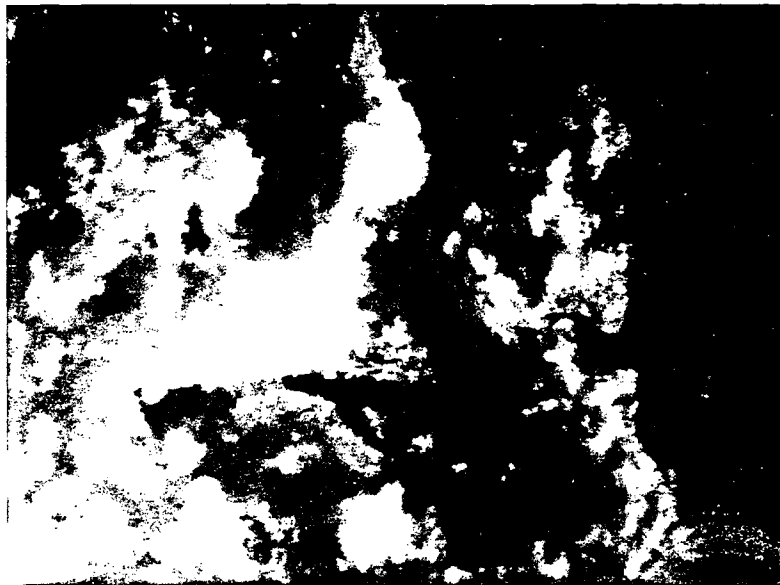


Fig. 2.18 Top Surface Photograph of Purolator A13192 Pleated Filter Media Loaded with Dust to 254 mm of H₂O Pressure Drop (440 x)

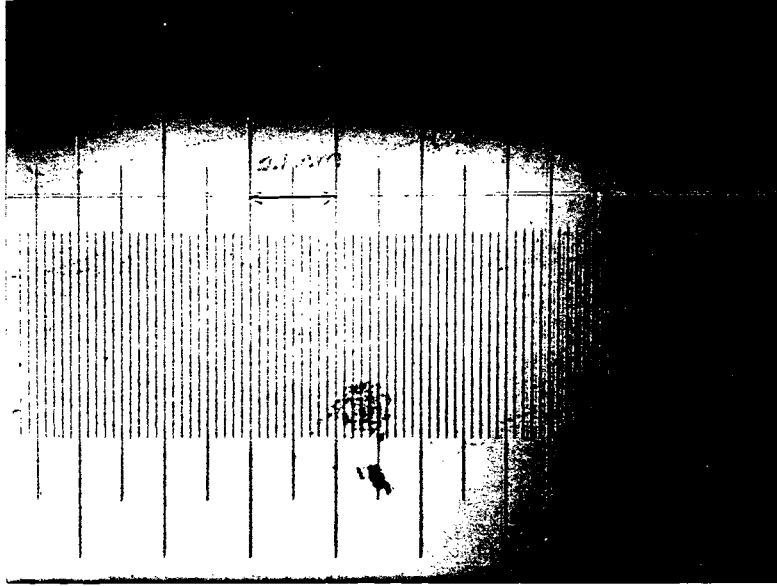


Fig. 2.19 Photograph Showing the Scale Engraving Used for Comparison (Smallest Division = 10 μm)

2.5 Present Work

In this present work, particle number density measurements were made using dual beam Laser Doppler Velocimeter in conjunction with a particle counting technique called the “swept volume” technique. The particle number density was computed using velocity information and the number of particles passing the probe volume in a given run time, all of which were obtained from DSA software, used for LDV signal processing. This is discussed in detail in Chapter III. This method differed from the various particle counters found in literature, used for filter testing, in that, it did not use any sampling techniques which disturb the flow. Further, the LDV probe volume could be positioned anywhere within the flow duct, making it possible to obtain the so-called local efficiencies, at various locations for a given filter. In-situ measurements were made at 35 locations upstream and downstream of the filter, to compute the local and overall efficiencies.

Both the SAE J726 prototype housing and the small angle diffuser housing were used as test housings. A six jet atomizer (TSI, model no. 9306) was used to atomize the PSL solution mixed with distilled water. Compressed air supply from a central reservoir was used to atomize the solution. No special effort was made to filter the compressed air. Small electric heaters were used to dry the air to vaporize the water droplets. No aerosol electrostatic charge neutralization procedure was employed during these experiments. Some of the recommendations given in the ASTM standard (1989) were followed. Though the standard was meant for flat filter media, it applies for panel filter testing also. A mixing chamber was used to mix the aerosol and dry air thoroughly. This mixing was done at approximately 9.8 equivalent duct diameters before the filter. The pressure taps were made flush with the housing walls, at four places connected together circumferentially. Initial efficiencies were measured using clean filters, and hence no effects of dust loading on filter performance were studied. A complete description of the experimental setup is given in Chapter III.

With the measured upstream axial velocity values, filtration efficiencies were calculated using the program EFFMODEL.FOR (Duran, 1995). Once the individual elemental efficiencies were known, an overall filter efficiency, η_f , was calculated as a weighted average of the elemental efficiencies. A comparison was made between the measured and calculated overall efficiencies for a particle diameter of 0.966 μm . Only the velocity values obtained from the new diffuser housing were used for the calculations.

CHAPTER III

EXPERIMENTAL PROCEDURE

3.1 Experimental Setup

The Laser Doppler Velocimeter used in these experiments was a 4 beam, 2 component laser system supplied by Aerometrics, Inc. The laser used was a 4 watt Argon-ion laser provided by Coherent (Innova 70-A). The system operates in the dual-beam fringe-mode with two colors, blue and green. A Doppler Signal Analyzer (DSA) processes Doppler bursts in the frequency domain using Fast Fourier Transform (FFT) techniques. The instrument is hosted by a 486 DX2-66 MHz personal computer. Figure 3.1 shows a line sketch of the system.

The multi-line laser beam coming out from the laser box (1) is directed by the two reflecting mirrors into the fiber drive (3), where the laser beam is split into four beams of two colors each. The fiber drive incorporates a Bragg cell (4) which splits the beam into two beams of equal intensity. One beam is the zeroth order beam and the other one is first order beam which is shifted by 40 MHz. Two dispersion prisms are used to separate the beams into two colors, blue and green, with wavelengths of 488 nm and 514.5 nm,

respectively. Thus four beams are obtained, one shifted in frequency and another unshifted, for each color. The beams then are transmitted to the transceiver (9) through fiber optic cables. The fiber optic coupler (3) which aligns the four beams with the fiber optic cables is a very important part of the whole system. The alignment has to be done carefully using five alignment screws one each on the X, Y, and Z axes, and two for angular fine adjustment.

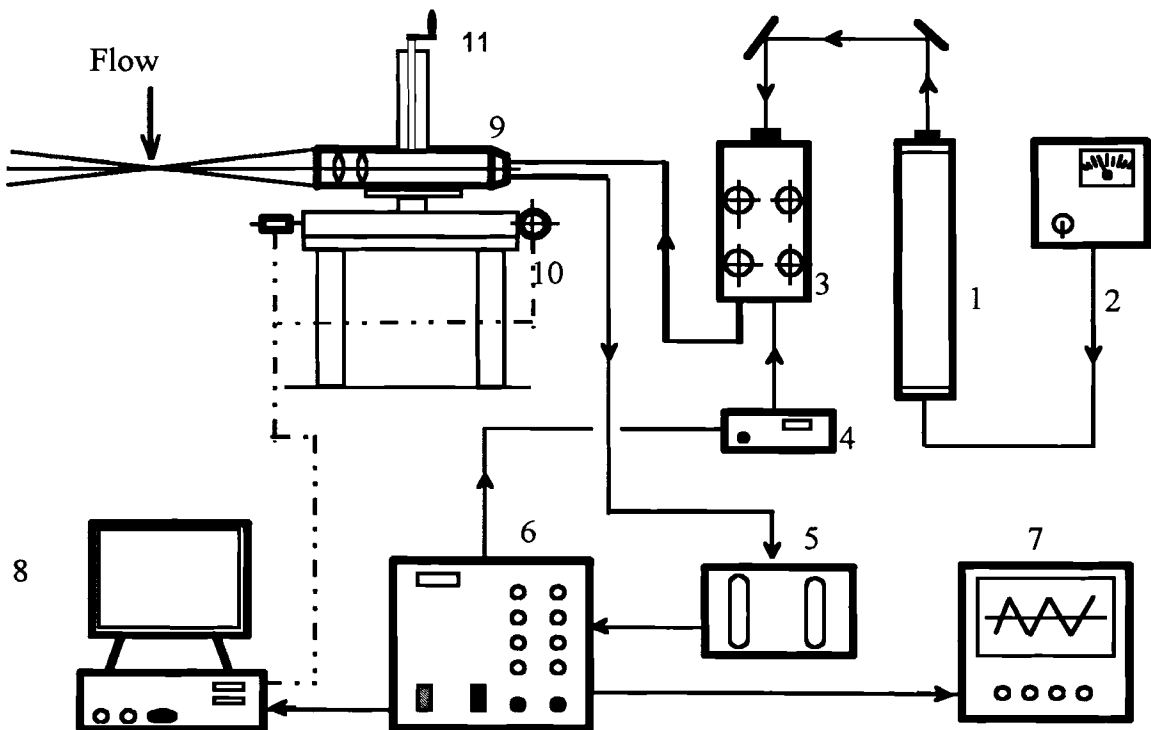


Fig. 3.1 Schematic of LDV System (Modified from Liang, 1994)

The transceiver is a combination of transmitting and receiving optics built into one unit, assembled and aligned by the manufacturer. The beams are focused in the test region

to generate the probe volume. This volume is located at the locus of the four beams which is 50 cm from the transceiver lens. The transceiver receives back scattered laser light from the particle passing through the probe volume, and transmits through the fiber optic cable, back to the two Photo Multiplier Tubes (PMT) (5), one for each color. The back scattered optical signal received by the PMT is converted into an electronic signal identified as a raw Doppler signal. This signal is taken to the Doppler Signal Analyzer (DSA) (6) which does all the further signal processing. A digital oscilloscope (7) is used to display the raw and other processed signals which helps in the DSA parameter setup. The DSA operates through software installed in the personal computer (8), which controls the whole process of collecting, processing, and storing data.

The transceiver is supported on a completely automated, three-dimensional, computer controlled traverse table (10). The vertical travel in the third axis was manually controlled previously (11), to position the transceiver in the two measuring planes upstream and downstream of the filter. Then it also was automated by this author (Appendix D). Details about the signal processing and DSA software can be obtained from the User's Manual for DSA (Aerometrics, 1992). The highlights of the principles of signal processing are fully explained elsewhere (Liang, 1994, Haldhani, 1993). After data processing, the results are given in two formats, namely, the averaged properties and the raw data listing. The first one provides the mean velocities, the flow angles, the number of total samples, the number of samples validated, the sampling time (called run time), number of rejected samples in different categories (such as velocities over or under range or low signal-to-noise ratio [SNR] and above all, the velocity histogram, which is a

distribution of sample counts in different velocity bins. Figure 3.2 shows a sample velocity histogram from DSA software.

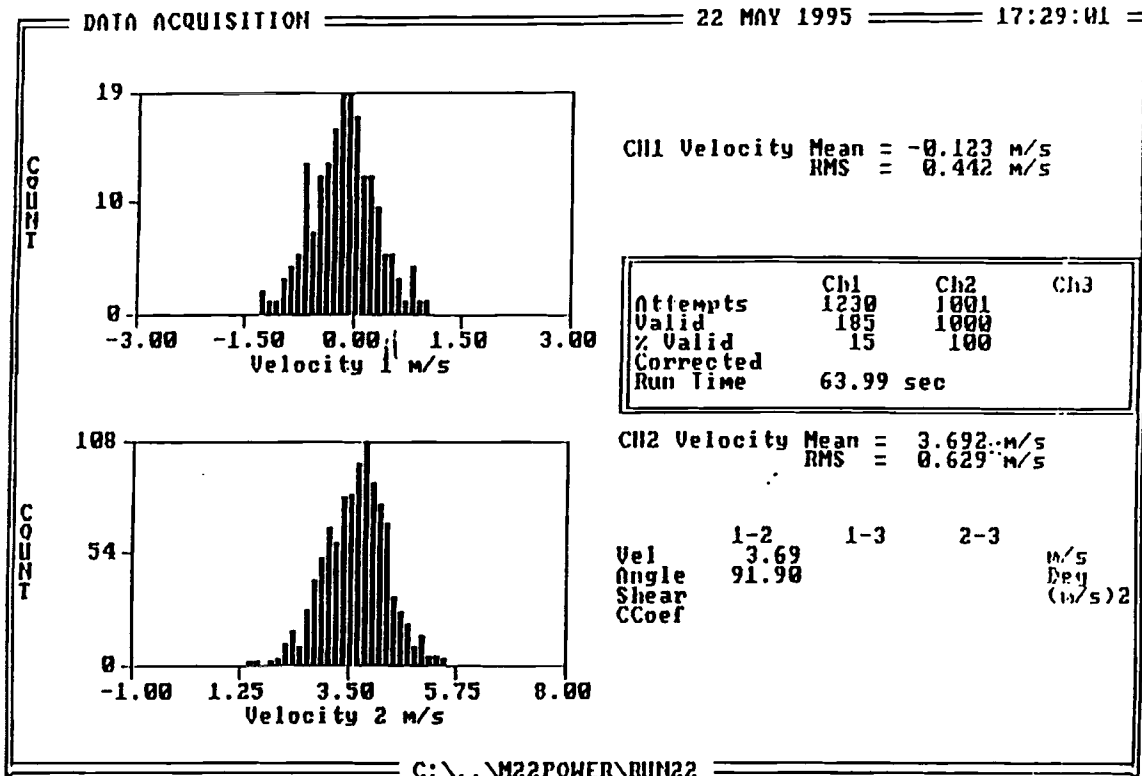


Fig. 3.2 Sample Velocity Histogram

The DSA raw data gives the sampling time, instantaneous velocities and scattered intensities for every sample validated, or, if not validated, the reason for rejection. This list is useful when individual signals are of interest. The transceiver focuses the 4 beams at an angle of 5.16° to the transceiver axis. The probe volume which is located at the focal point of the beams, is an ellipsoid with a major axis of about 734 microns and two minor axes of about 66 microns each (Fig. 3.3). The cross-sectional area along either of the minor axes is then approximately $3.357 \times 10^{-8} \text{ m}^2$. The two components of velocity

measured were along these two minor axes, and velocity was not measured along the major axis. As mentioned before, the computer controlled traverse system allowed the probe volume to be positioned at various locations within a given plane parallel to the filter face.

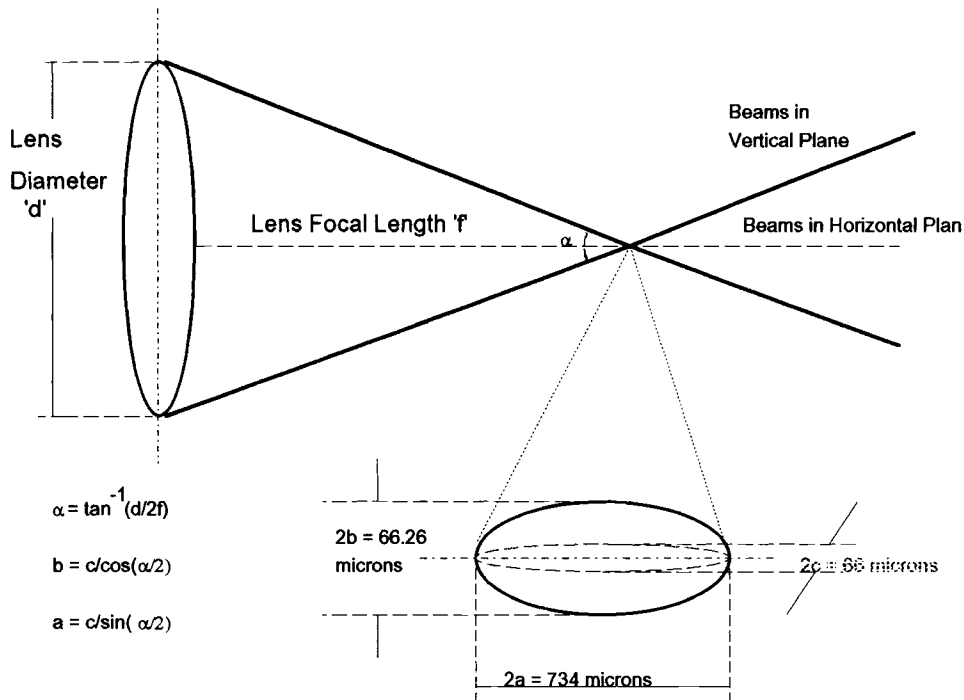


Fig. 3.3 Probe Volume Location and Geometry

Several particle counting techniques were reviewed by Haldhani (1993) and Liang (1994), and they found none of them suitable for the present system. Therefore a method called the “Swept Volume “ technique was developed and presented as the earlier work of this project (Liang, 1994, Haldhani, 1993). The idea of this technique is to use the sample counts, mean velocity and the sampling time or run time, which are all available from the DSA, along with the information about the probe volume dimensions, to calculate the particle number density. The swept volume technique is based on the volume effectively

swept by the particles with certain velocities passing through the cross-sectional area of the probe volume per unit time. The particles in the probe volume are assumed to move at a constant velocity which is the average velocity of all of the samples. Then the swept volume is a volume with the probe volume cross-sectional area and the mean velocity times the run time as its length. It is true that the particles move through the probe volume with different velocities, in different directions, and through different sections of the probe volume. But this procedure assumed that all of the particles (n_i), contained in an imaginary volume of elliptical cross-section (A) and length $v_i t_i$ passed through the center of the probe volume with the mean velocity v_i (and in the direction of v_i) during the recorded measurement time (t_i). The number of particles counted in each sample (number of signals) is used along with the mean velocity and probe volume cross-section to compute the average particle concentration as follows:

$$N_i = \frac{n_i}{v_i \cdot A_{pv} \cdot t_i} \quad (3.1)$$

where N_i is the particle number density (m^{-3}) at the 'i'th location in either the upstream or the downstream plane, n_i is the total number of particles counted (samples), v_i is the average measured velocity (m/sec), A_{pv} is the cross-sectional area of the probe volume (m^2), and t_i is the time required to sweep this volume, which is the run time (sec). Swept volume can be visualized as an elliptically shaped cylinder as shown in Fig. 3.4.

As mentioned earlier, the probe volume can be moved to various grid locations along the X and Y axes, within a measurement plane using the table traverse. Also the

probe volume can be moved between upstream and downstream planes by using the vertical traverse. Initially, after taking measurements in all of the 35 grid locations in one

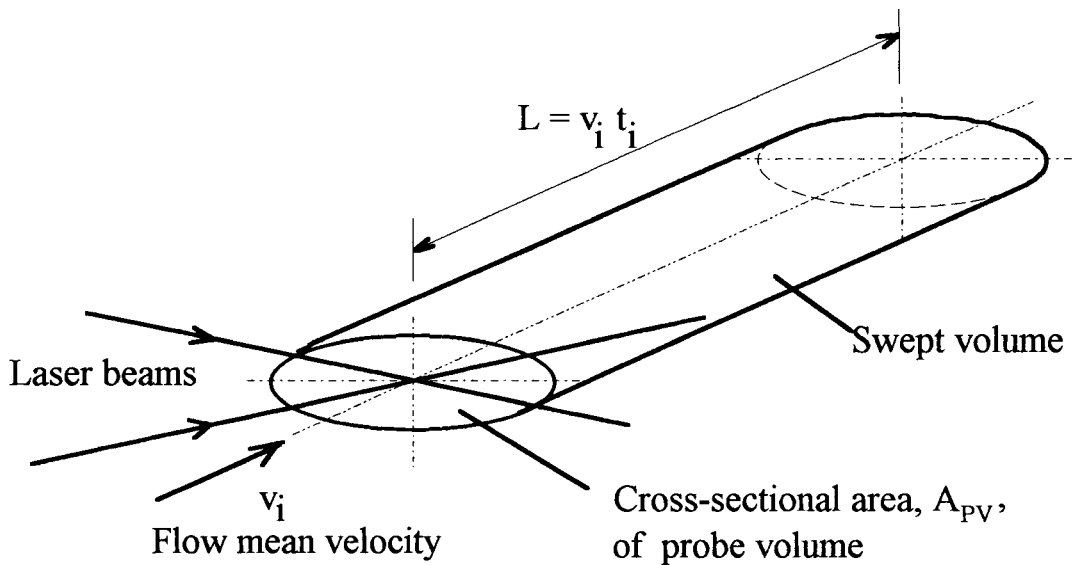


Fig. 3.4 Swept Volume Technique for Particle Counting

plane, the transceiver was moved manually to the other plane to measure particle concentrations. But subsequently the vertical traverse was automated using computer control and stepper motors. The software controlling the stepper motors was written by my colleague (Tian, 1995). Thus particle concentration measurements were made at a downstream point immediately after measuring at an upstream point, and the local efficiencies were calculated for each location. The local efficiency was computed as

$$\eta_i = 1 - \frac{N_{i(\text{downstream})}}{N_{i(\text{upstream})}} \quad (3.2)$$

and the overall efficiency was computed as

$$\eta_{\text{overall}} = 1 - \frac{\Sigma(N_i(\text{downstream}))}{\Sigma(N_i(\text{upstream}))} \quad (3.3)$$

The overall efficiency could be obtained by taking a weighted average of the local efficiencies at various grid locations by considering the corresponding areas of the filter covered by the grid location. But in our case, Eq. 3.3 was used and the difference between the values of overall efficiency arrived at with the two methods was very small since most of the elemental areas were equal.

The swept volume technique takes the total sample counts, both validated and rejected, as the number of particles (n_i). This is true only when one independent signal is obtained for each particle passing through the probe volume (refer to section 2.1.5). Suppose the flow is heavily seeded so that there is more than one particle simultaneously present in the probe volume. Since these particles are illuminated simultaneously, the detecting optics will receive the scattered light from all of these particles at the same time. Though the individual signals may be of different intensities, the receiver will receive only one signal which is a combination of scattering information from all these particles. This means that when a particle enters the probe volume, the previous particle must have already left the probe volume. Thus the LDV cannot easily differentiate between two simultaneously present particles in the probe volume. Therefore care must be taken to make sure to a reasonable extent, that no more than one particle is present in the probe volume at a time. One practical way to do this is to limit the particle concentration to the lower limit of instrument accuracy.

Validation rate is a percentage of the validated signals to the total attempts. Most of the rejected signals are rejected due to a poor signal-to-noise-ratio. If the validation rate is low, a large number of the total attempts, which could have been rejected for low SNR, would be counted as particles. At the same time, it is not advisable to push it to 100% validation rate, because, that may ignore some perfectly good signals. Therefore, it is suggested that the validation rate be maintained between 80 and 95%. This is to make sure that the total number of counts being used as the number of particles is an accurate reflection of the actual particles going through the control volume.

3.2 Test Housing and Flow Setup

Both the small angle diffuser housing and the SAE J726 housing were used in the present study. As mentioned earlier in Chapter II, the SAE J726 universal test housing (Fig. 3.5) provided a non-uniform flow to the filter (Sabnis, 1993). In order to present a relatively uniform flow to the filter, the small angle diffuser housing (Fig. 3.6) was developed and preliminary particle number density measurements upstream of the filter were made by Haldhani (1993). Flow field measurements done by Newman (1994) in the new diffuser housing showed a relatively uniform flow field above the filter. A dimensioned figure of the new diffuser housing is shown in Fig. 3.6. For comparison, a dimensioned sketch of the SAE J726 housing is given in Fig. 3.5. As can be seen from the figures, the SAE test housing consists of a section which is similar to a wide angled diffuser in two planes. The exit of the diffuser is partially blocked by a pair of mounting

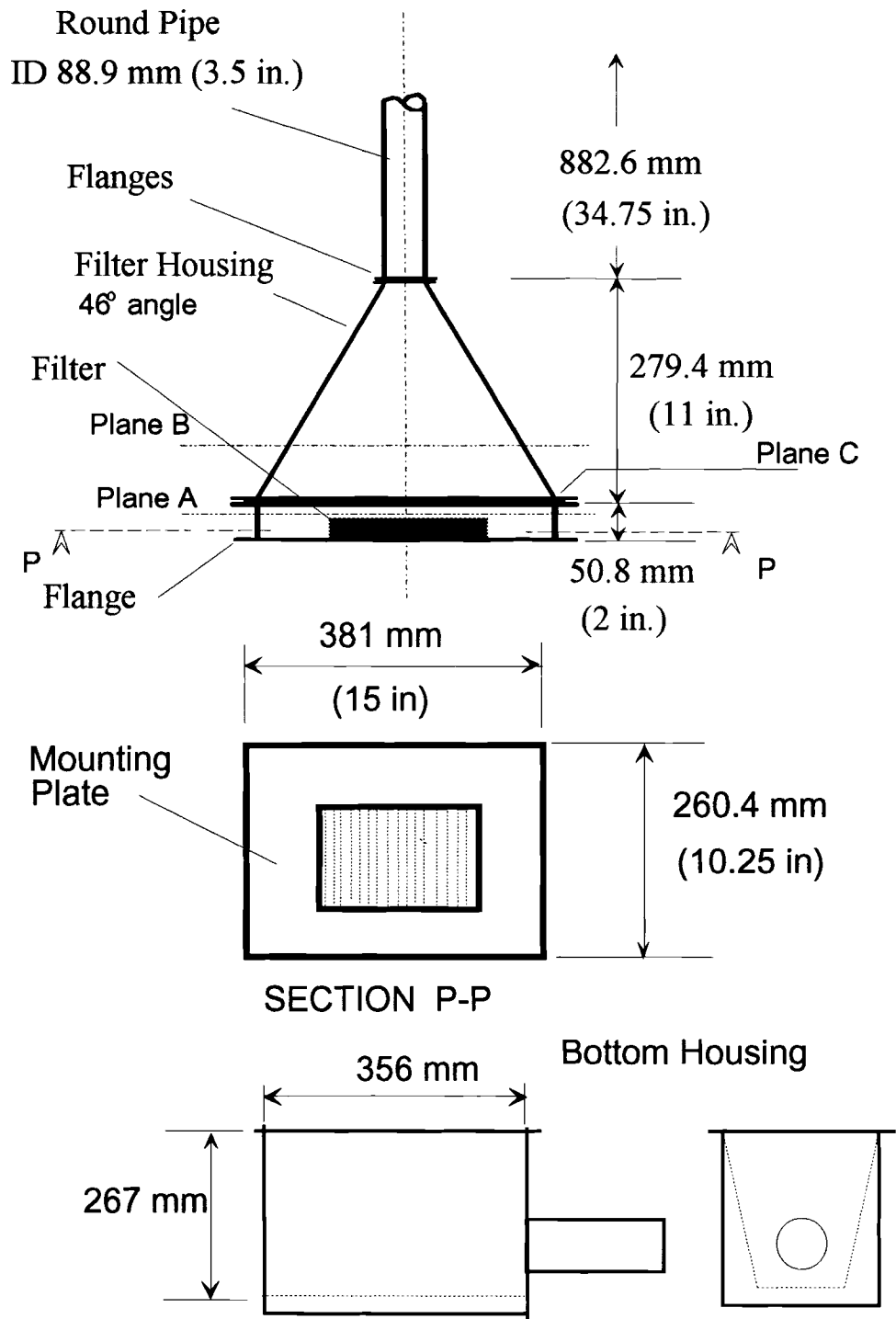


Fig. 3.5 Sketch of the SAE J726 Housing

plates, with which the panel air filter is secured in position. The flow takes place only through the filter area. This partial blocking of the exit leads to recirculating non-uniform flow.

The small angle diffuser housing's shallow angle walls (Fig. 3.6) tend to reduce the potential for separation and recirculating flows upstream of the filter. Though not built specifically to satisfy the cabin air filter test code, SAE J1669 (1993), the housing fits some of the geometric requirements of that code by having its largest cross-sectional area be less than 13.5% (less than 10% is required by SAE J1669) larger than the area of the filter being tested. The diverging wall angles are 2° and 6.34° for each pair of diverging walls (less than 7° is required by SAE J1669).

The first task of this author was to build a manual positioning table (#11 of Fig. 3.1) to position the transceiver between the two planes upstream and downstream of the filter. Details of this table and a dimensioned sketch are given in Appendix D. This table, working like a screw jack, can be moved by rotating the handle at the top. Figure 3.7 shows the setup for the new housing. The test filter was mounted in the test housing which was made of plexiglass, to facilitate taking readings with the LDV. The housing was supported on a stand which could be adjusted manually to alter its vertical position with respect to the transceiver. This was needed mainly due to the difference in overall heights between the SAE housing and diffuser housing. The top and bottom housings were clamped together with eight adjustable clamps. A mixing chamber was mounted on top of the housing, whose primary purpose was to mix the flow thoroughly. This was one of the important factors in providing a uniform flow field to the filter. Previous

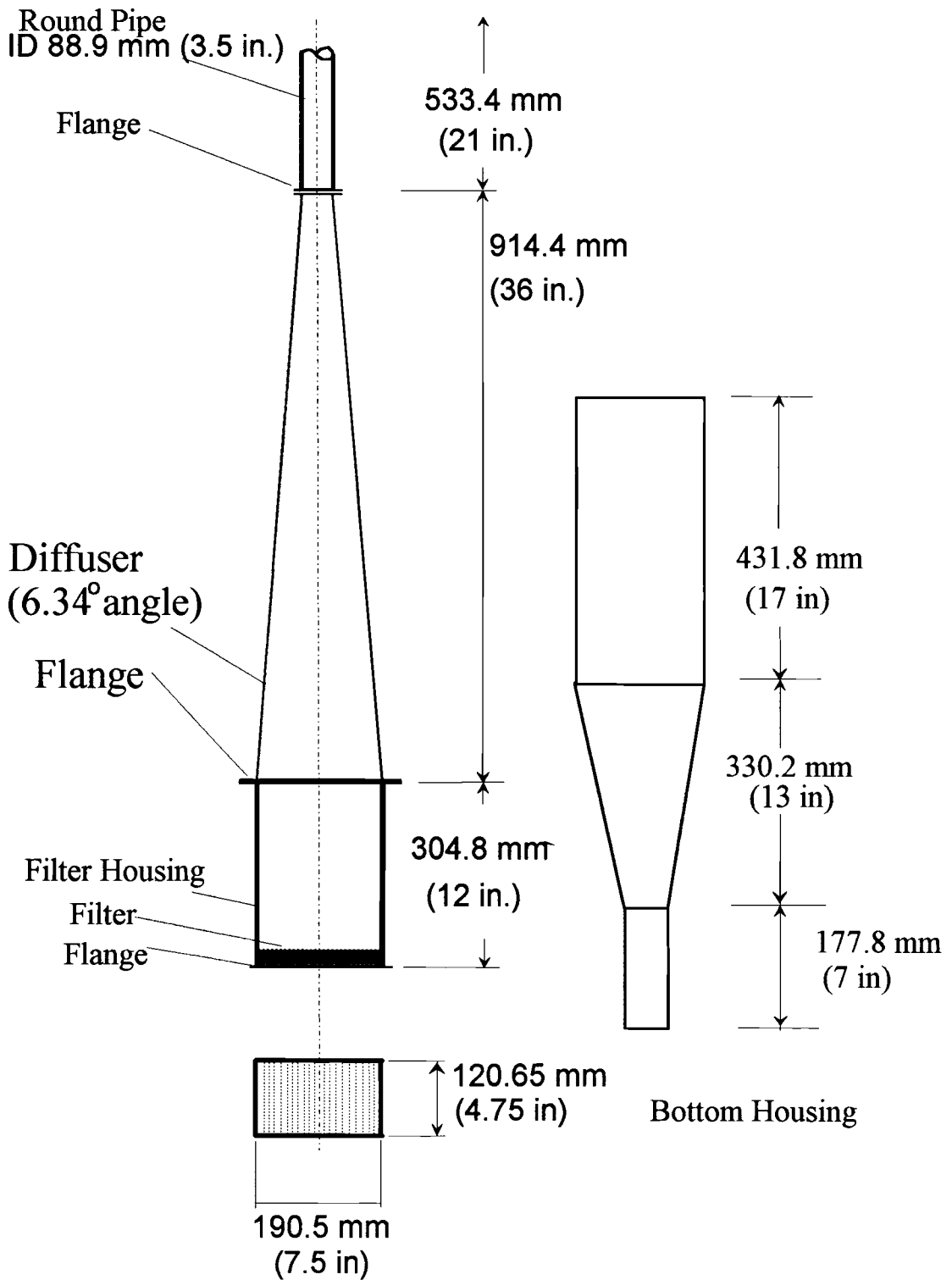


Fig. 3.6 Sketch of the New Diffuser Housing

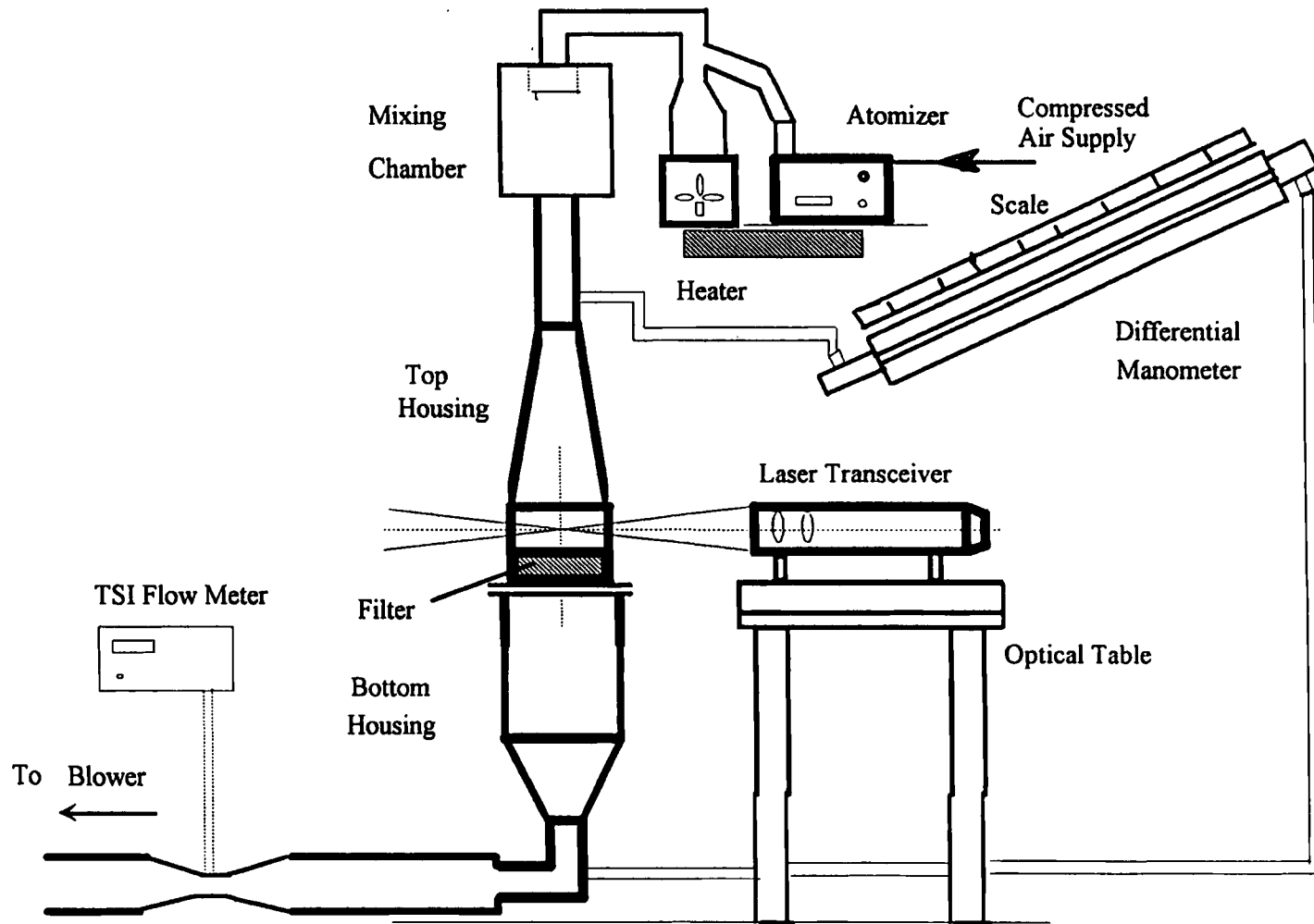


Fig. 3.7 Experimental Setup for the New Housing

experiments with a small mixing chamber with an inlet from one side provided a skewed velocity profile. Hence the present mixing chamber was built by my colleague, Charles Tebbutt, on the advice of Dr. Chambers with an inlet at the top and a deflector plate to uniformly distribute the flow.

Exact alignment of the four laser beams was accomplished by carefully focusing the beams on the center of the housing. When the probe volume is located at the center of the housing, the distance between the blue beams (and the green beams) on the front wall must be equal to that on the rear wall of the housing. The transceiver travel along the Y direction had to be parallel to the face of the housing. This was checked by focusing the probe volume outside the housing and measuring the distances between the beam crossing and the face of the housing at both ends of the housing along the Y axis. If these distances were equal, then it was assumed that the travel would be parallel in the X direction also. The flatness of mounting the housing on the mounting table was checked with a level.

The bottom housing was connected to the blower through a flexible hose connection. Initially a 15 hp blower was used along with a TSI model 2012 mass flow sensor to produce and monitor the necessary flow through the filter. Pressure taps were placed in the housing upstream and downstream of the filter by my colleague Charles Tebbutt. Four taps were made circumferentially around the duct and connected to a common tube which was attached to either end of an inclined manometer to read the pressure drop across the filter. The seeding particles for these experiments were produced by atomizing the polystyrene latex (PSL) solution mixed in distilled water in proper ratios. The ratio of dilution initially used was 10 cc of 10% PSL solution to 1000 ml of distilled

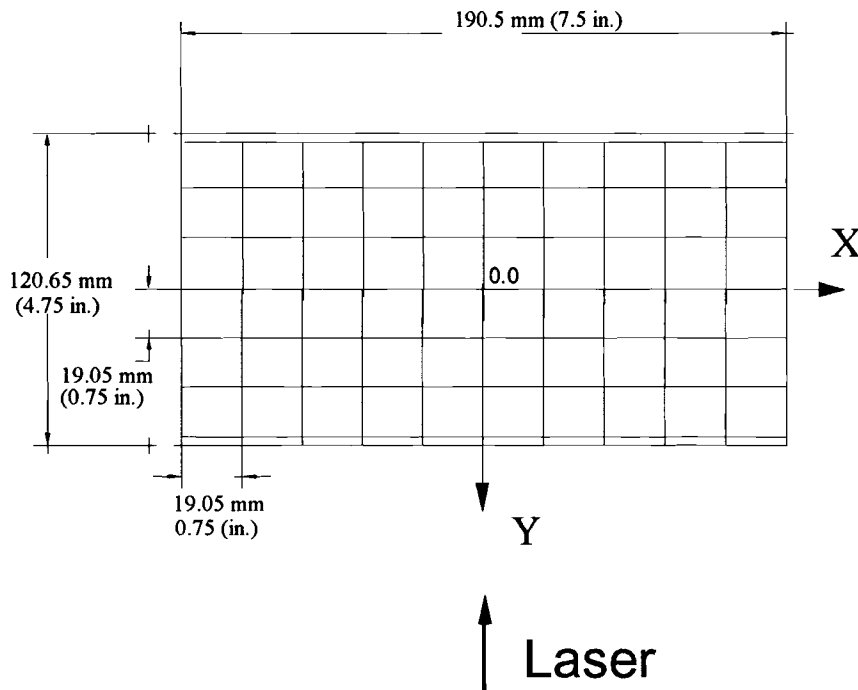


Fig. 3.8 Measurement Grid in Two Dimensions

water. But subsequent experiments done with a ratio of 5 cc of solution to 1000 cc of distilled water giving a concentration of 500 ppm were successful, in the sense that enough signals were detected by the LDV. This was same as the dilution ratio given in Fig. 2.8 for 1 μm particles with a VMD of 5.0 and standard deviation of 1.2 (Raabe, 1968). The PSL solution was poured into a 6 jet atomizer (TSI model 9306), and compressed air was supplied to it to atomize the particles. The atomizer has six jets, and can be operated with between 0 and 6 jets. The atomizer also has a built-in valve by which the pressure of compressed air supplied to the jets can be controlled. Also the air dilution rate can be controlled. All these experiments were performed with all the six jets operating, at a pressure setting of 55 psi and air dilution ratio between 40 and 60 lpm.

The stream of PSL particles and water droplets coming out of the atomizer was heated by a small room heater to vaporize the water, so that only dry PSL particles entered the test housing. In tests done to check this assumption, the LDV did not detect any particles when pure water was used with the atomizer and heater for approximately thirty minutes.

Particle concentration measurements were made at 35 locations upstream and downstream of the filter. The two measuring planes were located at 15.875 mm (0.625 in.) above the filter and 38.1 mm (1.5 in.) below the filter. These distances were the closest the probe volume could be positioned to the filter without the beams interfering with the housing walls. Initially, when the vertical movement was done manually, the transceiver would be moved to the bottom plane only after making all the 35 measurements in the top plane. This led to some concern about the time lag between measurements at the same X-Y location in the two planes. Hence the vertical traverse was also automated by this author with stepper motors and computer control. This facilitated fast movement of the traverse between upstream and downstream planes. Thus measurements could be taken at a downstream point immediately after measuring at an upstream point. Measurements could be continued with the next downstream point and on to the corresponding upstream point.

Great care must be taken to align the top and bottom housings and to properly seal the filter joints. Any misalignment or improper sealing could cause air leakage through the joint, leading to incorrect flow rate measurement. Leakage could also create recirculation zones, leading to incorrect particle concentration measurements. All of the housing edges were tested for leaks with a soap solution by slightly pressurizing the housing by

connecting the housing to a small blower that blew air through the housing. A small opening was left at the top of the housing so that approximately 1 to 2 inches of water pressure was maintained inside the housing. Then a soap solution was applied over all of the joints, such that any leakage could be detected by the formation of air bubbles. This was done before using a newly fabricated or rebuilt housing.

Note that the present LDV could make velocity measurements only in two components. The third component of velocity was not measured, the effect of which was unknown for these experiments. The dimension of the diffuser housing along the small side of the filter (direction of the third component) is smaller than the corresponding dimension of the SAE housing. Hence, I believe that the effect of the third component would be minimal for the diffuser housing compared to the SAE housing.

Flow visualization is an effective technique to get an overall perspective of the flow field. Water and intermittent smoke flow visualizations have been used in the past to get a qualitative insight of the flow field within the SAE test housing (Sabnis, 1993). Intermittent smoke and water mist flow visualizations using laser sheet lighting were conducted for the small angle diffuser housing and are presented in the results section. The smoke generator is described in Appendix E. These flow visualization tests were also used to check for any leakage through the housing flange joint or anywhere else in the setup. Refer to Section 4.9 on flow visualization for further discussion.

CHAPTER IV

RESULTS AND DISCUSSION

4.1 Flow Directions

The Laser Doppler Velocimeter used for these experiments was controlled by the Doppler Signal Analyzer (DSA). The DSA was responsible for collecting, processing, and storing the data, and was controlled by software through a 486 personal computer. There were several parameters and variables in the software which had to be initialized and adjusted from time to time, by the user, depending on the purpose for which it was used. Some of the parameters were set by Aerometrics, Inc., depending upon the light characteristics of the laser beams and the nature of the optics used in this LDV system. Those parameters which needed adjustments by the user had a range of values for each of them, within which the adjustments could be made. These parameter settings needed a thorough understanding of the manner in which DSA worked for this particular application. A detailed discussion of these parameters and the values used for the experiments are given in Appendix B.

The data collection by the DSA could be terminated either after reaching a user specified number of samples, or after a user specified elapsed time. The number of samples mode was selected for our purpose. The user had to enter a number for this mode, which was 500 samples for these experiments. Previous experiments by Newman (1994) showed that 500 was the smallest number of samples which could give reasonable accuracy and repeatability. The LDV measured velocities in two components, axial and transverse. The DSA had two channels to measure these velocities, channel 1 with green beams for transverse velocity and channel 2 with blue beams for axial velocity.

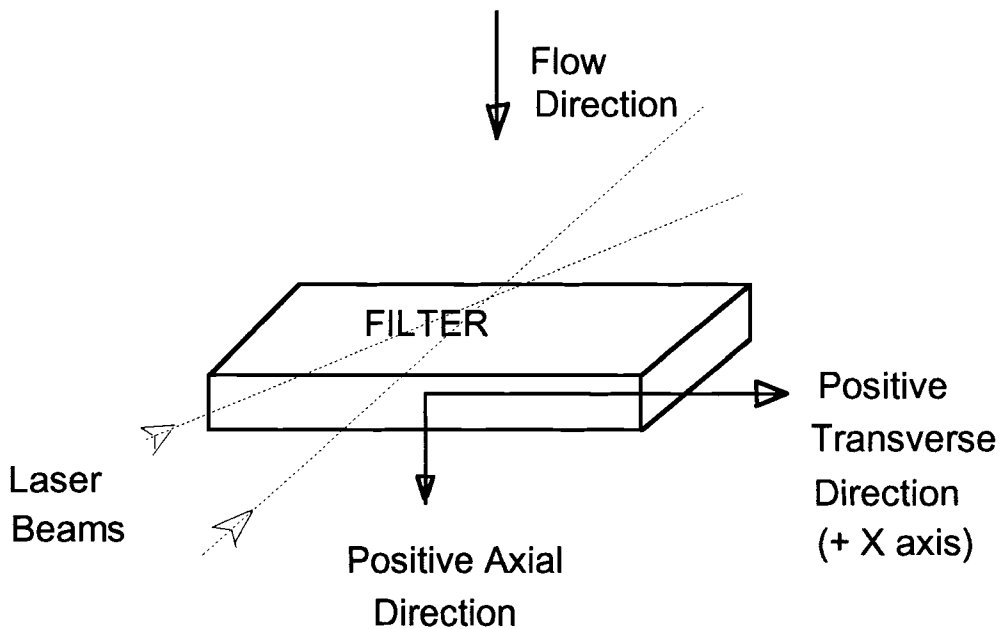


Fig. 4.1 The Two Components of Velocity Measurements

The directions of positive and negative axial and transverse velocities are illustrated in Fig. 4.1. Since the axial velocity component was predominant in our flow setup, channel 2 was the dominant channel.

4.2 SAE J726 Housing Results

The local efficiency measurements were conducted using the SAE J726 housing and an A13192 panel air filter, using $0.966\ \mu\text{m}$ PSL particles, atomized by the 6 jet atomizer. As was mentioned in Chapter III, the mixing chamber for these experiments with the SAE J726 housing was relatively of a smaller size with an inlet from the sides. Comparison between the old mixing chamber and the new one is shown in Fig. 4.2. Results with the new mixing chamber are given later in the chapter.

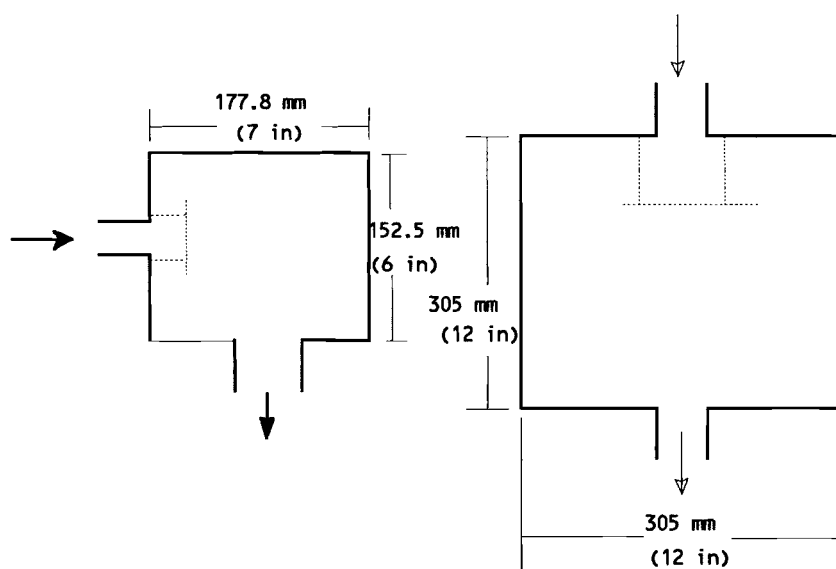


Fig. 4.2 Old and New Mixing Chambers

There were some scratches on the vertical wall below the slanted wall on the front side of the top housing. Due to these scratches, the LDV could not detect signals in the measurement plane close to the filter face (plane A in Fig. 3.5). Therefore the upstream measurement plane (plane B) was at a height of 3" above the plane C, where the straight

wall of the SAE housing meets the slanted wall of the housing. The downstream plane was located at 2" below the flange of the bottom housing (refer to Fig. 3.5). This was the reason that we could take 35 measurements covering the whole area of the filter in each plane. Otherwise only one-half of the filter face towards the front could be covered. This also might be a reason that the velocity profile was not as expected. Figure 4.3 shows the axial velocity profile upstream of the filter for a flow rate of 120 cfm (204 m³/hr). As was reported by Newman (1994), the velocity profile is non-uniform, with the precise form of non-uniformity dependent on the manner in which the air enters the inlet pipe of the housing. Figure 4.4 shows the corresponding particle number density profile upstream of the filter. One can observe that the particle concentration profile has a peak at some of the locations of minimum axial velocities.

Due to our measurements having been made only over the filter face, the strong recirculation zones beyond the edges of the filter are not visible in the above figures. However, beyond the filter's dimensions, flow visualization results from Sabnis (1993) showed the existence of such zones. These zones cause significant mixing of the flow, and thus the measurements presented may not give an accurate representation of the microscopic filtration process. Figure 4.5 depicts the axial velocity profile downstream of the filter. Again, this is similar to the upstream velocity profile with very high velocities on one side of the filter. It should be noted that the downstream particle concentration profile on Fig. 4.6 is relatively flat, except for a spike at one point which is possibly due to the side exit from the bottom housing (refer to Fig. 3.5). The spike is probably due to the

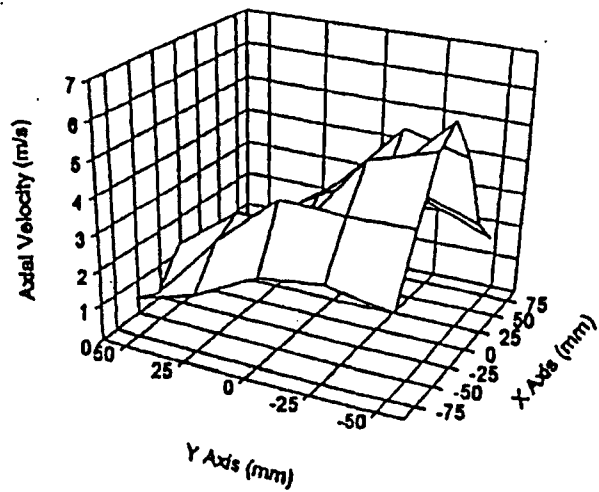


Fig. 4.3 Axial Velocity Upstream (SAE, 204 m³/hr, 0.966 μm Particles)

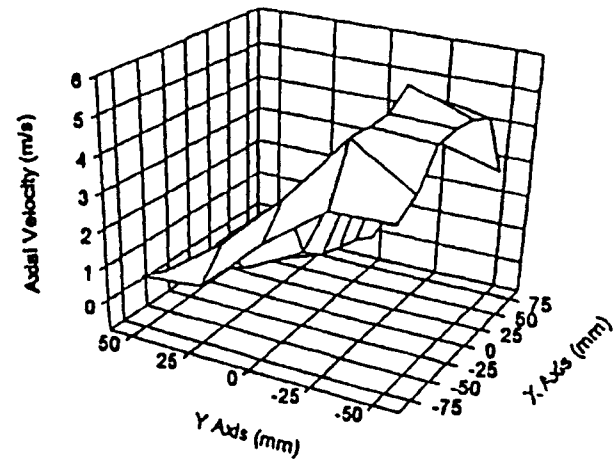


Fig. 4.5 Axial Velocity Downstream (SAE, 204 m³/hr, 0.966 μm Particles)

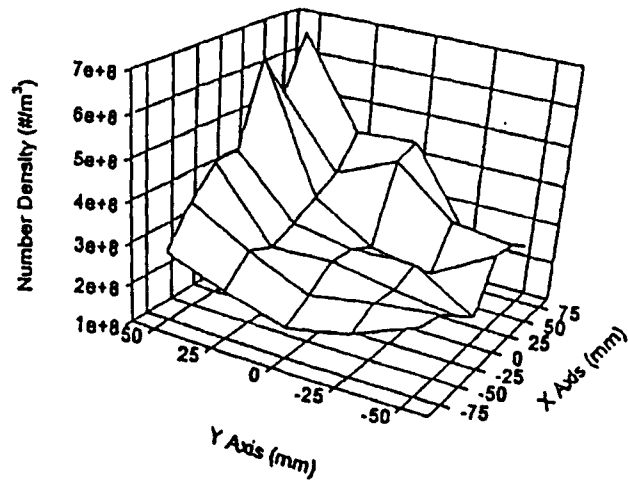


Fig. 4.4 Number Density Upstream (SAE, 204 m³/hr, 0.966 μm Particles)

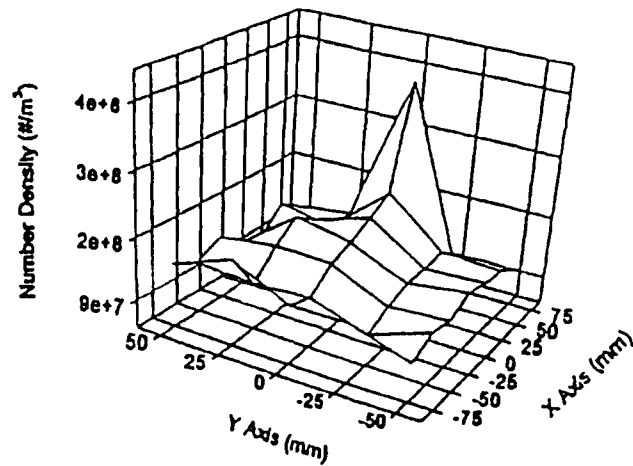


Fig. 4.6 Number Density Downstream (SAE, 204 m³/hr, 0.966 μm Particles)

recirculating flow in that portion of the bottom housing, due to which the LDV detects more particles. There is reason to believe that, apart from counting the particles exiting the filter at the point of measurement, the LDV counts some of the particles exiting the adjacent portions of the filter due to the recirculating flow. The upstream transverse velocity profile in Fig. 4.7 shows that the transverse velocities are higher wherever the axial velocities are lower. Figure 4.8 shows the corresponding downstream transverse velocity profile, which has large variations, again due to the significant recirculation in the bottom housing. Figure 4.9 presents the local efficiencies computed from the upstream and downstream particle concentrations at each location. As can be seen, the local efficiencies vary considerably over the filter face, the lower efficiencies being at the central portion of the filter. This might be due to the higher velocities at the center of the filter, which could cause re-entrainment of the particles. The axial velocity profile might have changed after the present plane of measurement, into a jet like flow at the center, as it reached the filter, as had been shown by previous researchers (Newman, 1994).

The inaccuracies in the present study with the SAE J726 housing can be summarized as: 1) the measurement planes were not close enough to the filter face to capture a clear picture of what was going on, and 2) the entry and exit points from the sides had an undesirable effect on the flow profiles, which adversely affected the accuracy of these particle concentration measurements. Figure 4.7 shows the overall efficiency's dependence on flow rate, from a very low flow rate of 40 cfm ($68 \text{ m}^3/\text{hr}$) to the maximum

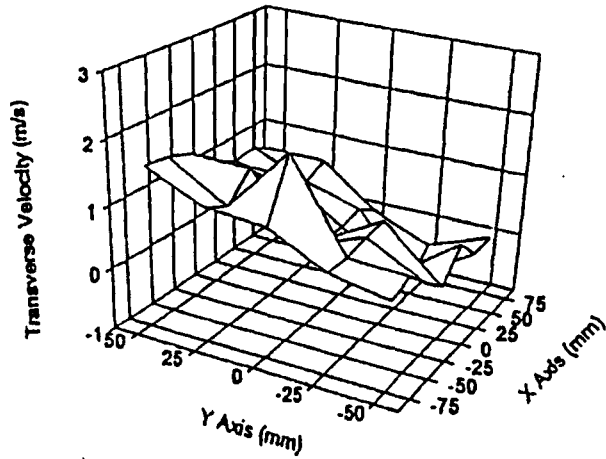


Fig. 4.7 Transverse Velocity Upstream (SAE, 204 m³/hr, 0.966 μm Particles)

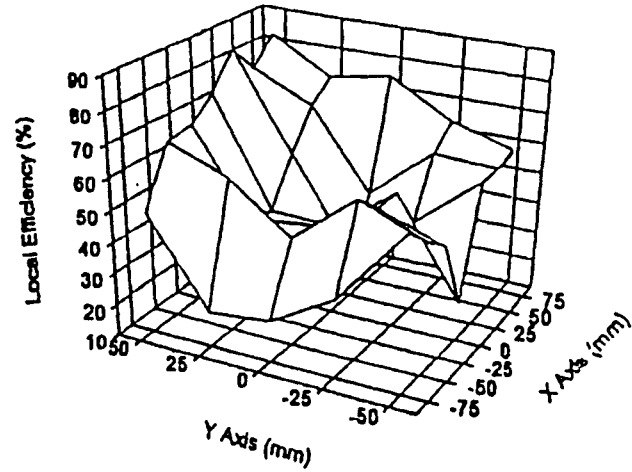


Fig. 4.9 Local Efficiencies over Filter Face (SAE, 204 m³/hr, 0.966 μm Particles)

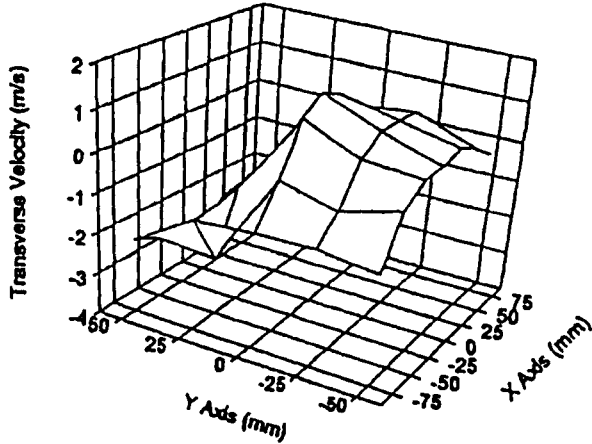


Fig. 4.8 Transverse Velocity Downstream (SAE, 204 m³/hr, 0.966 μm Particles)

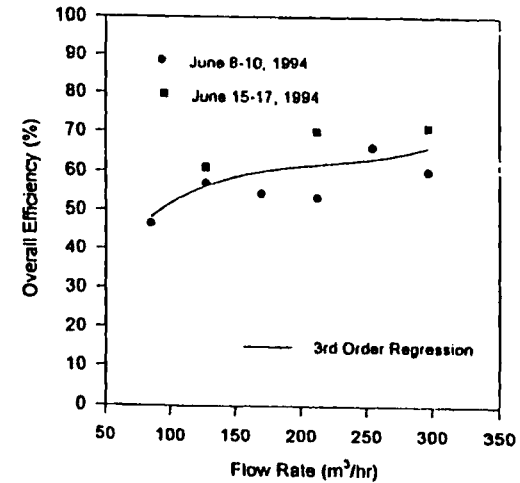


Fig. 4.10 Overall Efficiency vs. Flow Rate (SAE, 0.966 μm Particles)

of 225 cfm (382.28 m³/hr). One might deduce from this data that the filter's efficiency is relatively insensitive to the air flow rate. This fits with the simple predictive theory for impaction and interception which indicates that, for low Stokes number (less than 0.01 for a variety of particle sizes to fiber diameter ratios), the filter media has a constant single fiber and overall efficiency (refer to Fig. 4.43). It should be noted that, for all of the data presented herein, the filter was not changed. This might raise a question as to validity of the statement about these being "clean" filter tests. However, using the information given in Chapter III, with an overall filter efficiency for all tests of say 65%, there would be approximately 0.325 gm of dust deposited on the filter after all tests, which should cause only small changes in a typical cellulose filter's performance from its original condition.

4.3 Results of the Small Angle Diffuser Housing

4.3.1 One Micron Particles

The bottom housing for this small angle diffuser housing was different from the one for the SAE J726 housing as shown in Figs. 3.5 and 3.6. The upstream and downstream measurement planes were located at about 12.7 mm above and 50.8 mm below the filter. These planes were as reasonably close to the filter as the beams could clear the flange and other mounting arrangements and could be focused through the housing side walls. Figures 4.11 and 4.12 show the axial velocity and the corresponding particle concentration profiles upstream of the filter. The velocity profiles are more nearly uniform over the filter area as compared to the SAE housing.

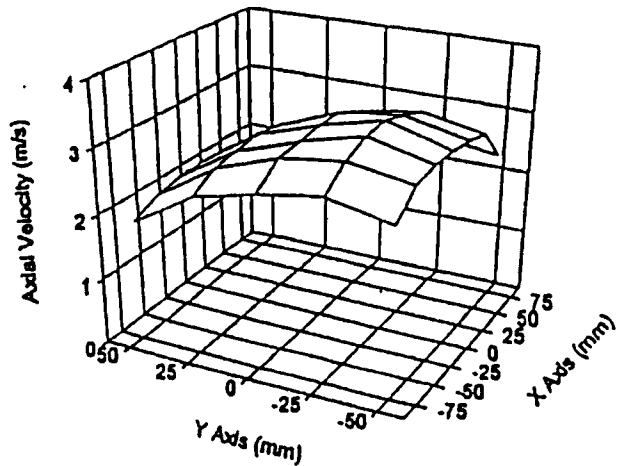


Fig. 4.11 Axial Velocity Upstream (Diffuser, 204 m³/hr, 0.966 μm Particles)

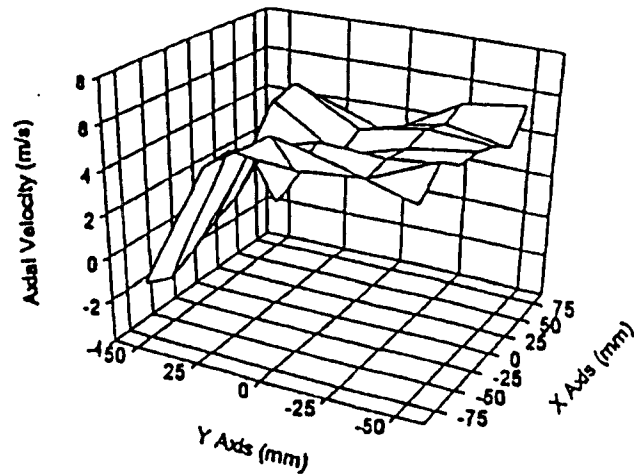


Fig. 4.13 Axial Velocity Downstream (Diffuser, 204 m³/hr, 0.966 μm Particles)

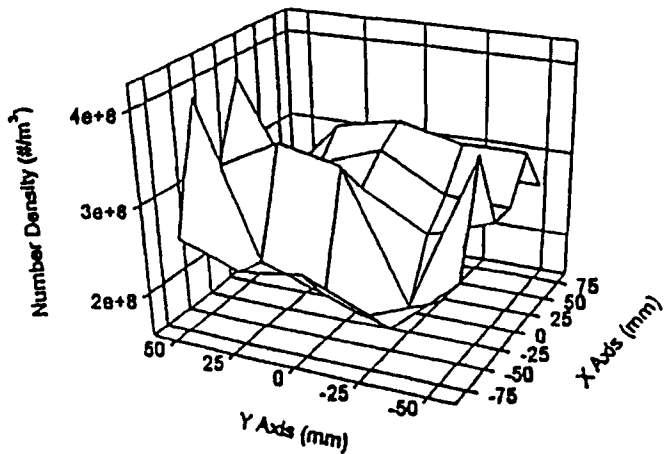


Fig. 4.12 Number Density Upstream (Diffuser, 204 m³/hr, 0.966 μm Particles)

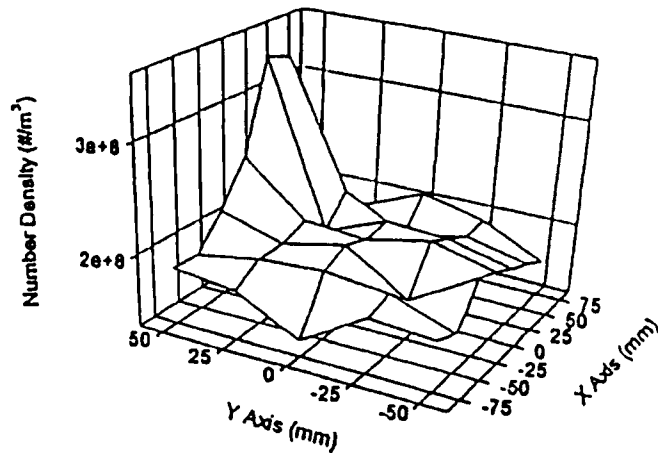


Fig. 4.14 Number Density Downstream (Diffuser, 204 m³/hr, 0.966 μm Particles)

This, one might expect would result in a more efficient use of all of the filter than would be the case for the SAE housing. The number density profile does not appear to follow the velocity profile upstream of the filter, as compared to the axial velocity and particle concentration profiles downstream of the filter given in Figs. 4.13 and 4.14. The downstream axial velocity and number density profiles are almost uniform over the filter area except at some corners where some recirculation zones are believed to have existed. One must note here that the cross-sectional area of the housing below the filter was the same as that above. Some recirculation in the flow might have happened near the filter's long side edges. This was due to the rubber sealing on the bottom of the filter along the long side edges, reducing the flow area from that of the top of the filter, by as much as 33% for some filters. Thus, though the mixing and the adverse effects of recirculation exhibited by the SAE housing were not seen upstream of the filter, they could not be totally eliminated downstream of the filter. One possible solution for this is to ensure a leak proof joint between the flanges of the top and bottom housings and locate the measurement points away from the filter's edges where negative axial velocities are not observed. This could be done by observing the velocity histograms to avoid negative velocity bins at measurement points near the edges of the filter.

The upstream and downstream transverse velocity profiles are shown in Figs. 4.15 and 4.16. Both of the profiles are almost flat with much smaller variations than the profiles with the SAE housing, the variations being in both positive and negative directions. Local efficiencies are shown in Fig. 4.17, providing a more uniform efficiency profile than that for the SAE housing, though the efficiency levels are lower.

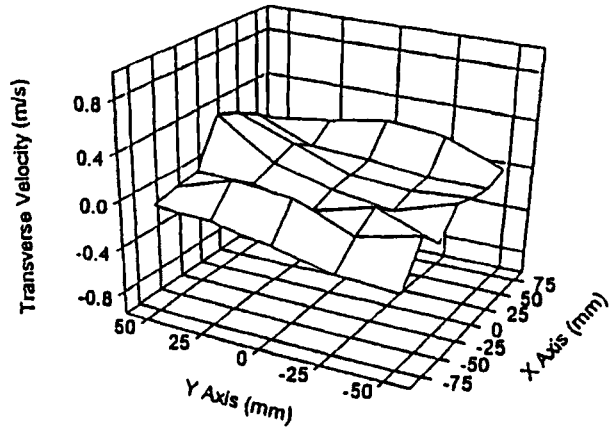


Fig. 4.15 Transverse Velocity Upstream (Diffuser, 204 m³/hr, 0.966 μm Particles)

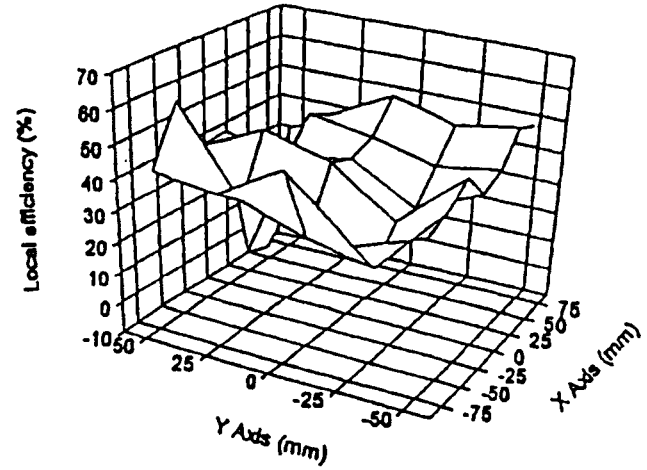


Fig. 4.17 Local Efficiencies over Filter Face (Diffuser, 204 m³/hr, 0.966 μm Particles)

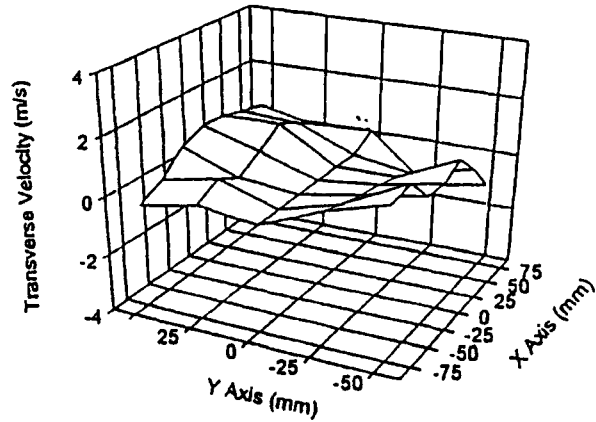


Fig. 4.16 Transverse Velocity Downstream (Diffuser, 204 m³/hr, 0.966 μm Particles)

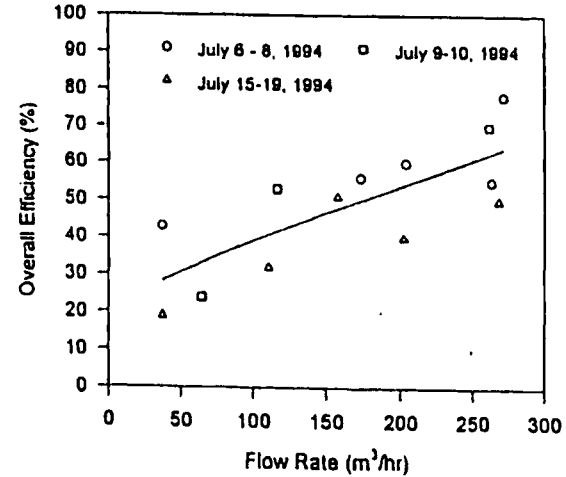


Fig. 4.18 Overall Efficiency vs. Flow Rate (Diffuser, 0.966 μm Particles)

In most of the locations, the efficiencies are in the range of 30 to 50%, with two negative local efficiencies. I believe this was the reason that the overall efficiency for this particular flow rate was lower than would be expected. The reason for this might have been either the recirculating flow, or some leakage through the filter joint at those points.

Figure 4.18 gives the dependence of overall efficiency on flow rate. Three sets of runs were conducted with the same 0.966 μm PSL particles. All of the other flow conditions also were the same for these sets of runs. There is a definite increasing trend with increasing flow rate, but not as predicted by the theory. One important observation was made at the end of all these runs, that the flow meter was not connected properly, resulting in an inaccurate flow measurement. This was due to a huge leakage at the blower motor, with the flow meter connected after the blower in the setup. Therefore, the actual flow rate through the filter would have been lower than was indicated by the TSI flow meter. The filter area was divided into 35 small areas. With these areas and the axial velocities at those 35 locations, an approximate estimate of the flow rate through the filter was calculated. They were lower than the TSI flow rates. Figure 4.18 was plotted with these estimated flow rates.

As compared to these results from the diffuser housing, the efficiencies from the SAE housing were higher. The local efficiencies for the SAE housing range from 21.48% to 84.49% whereas they range from -6.24% to 58.22% for the diffuser housing. Most of the axial velocities for the SAE housing are lower than those for the diffuser housing. These higher local efficiencies for lower axial velocities for a given flow rate could be attributed to the method of computing the number density values with the present LDV by

dividing the number of particles detected in each location by the axial velocity and the runtime (Eq. 3.1). The number of particles (number of signals) being the same for all of the locations, the number density is inversely proportional to the axial velocity and the run time. The effect of run time on the number density was not as pronounced as the effect of the axial velocity, resulting in higher local efficiencies for lower axial velocities.

4.3.2 Five Micron Particles

Figure 4.19 gives the axial velocity profile, upstream of the filter operating at 204 m³/hr flow rate using 5.3 μm seeding particles. The dilution used for 5.3 μm seeding particles was 50 ml of 10% solution to 1000 ml of distilled water giving a concentration of 5000 ppm. The axial velocity profile is still relatively uniform as compared to SAE housing, and the profile appear to match with that of 0.966 μm particles. This is an indication of even the 5.3 μm particles following the flow nearly as well as the 0.966 μm particles. The upstream particle concentration profile is shown in Fig. 4.20. In this, we could see the effect of side entry of seeding particles. Figures 4.21 and 4.22 show the corresponding two-dimensional slices along the filter's long axis, so that numerical comparisons could be made. One can see that the number density lines lie within a small band, except at one edge where the concentrations are higher. Figures 4.23 and 4.24 give the axial velocity and particle concentration profiles downstream of the filter. It was not known why the axial velocity values at both edges along the long side of the filter were negative. This could be due to recirculation zones all along those edges, either due to some leakage, or due to an unusually thick rubber sealing underneath that particular filter.

Figure 4.25 shows the local efficiencies for 5.3 μm particles. Comparing to Fig. 4.17 for 0.966 μm particles, these local efficiencies are much higher, in the range of 50 to

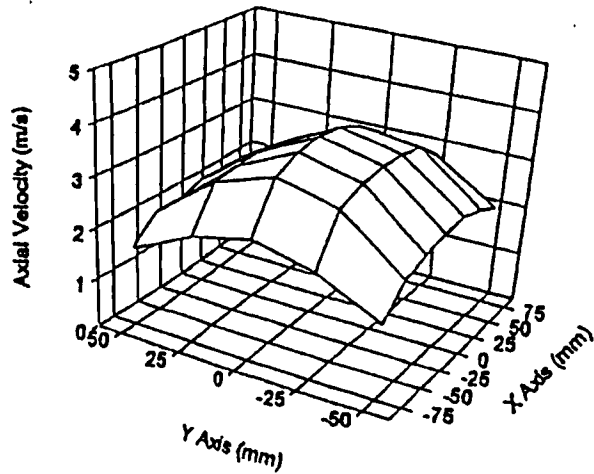


Fig. 4.19 Axial Velocity Upstream (Diffuser, 204 m³/hr, 5.3 μm Particles)

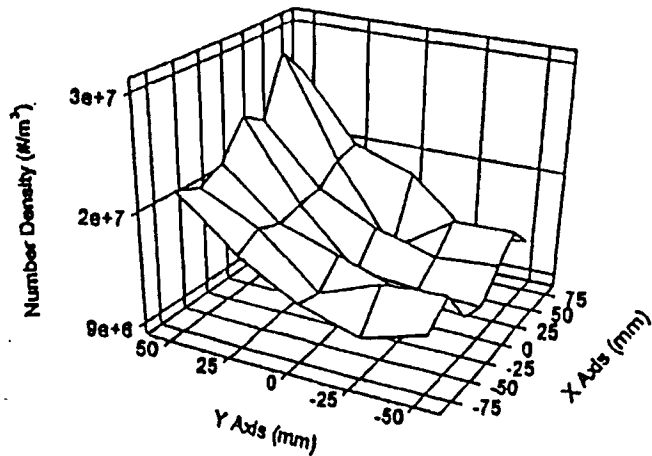


Fig. 4.20 Number Density Upstream (Diffuser, 204 m³/hr, 5.3 μm Particles)

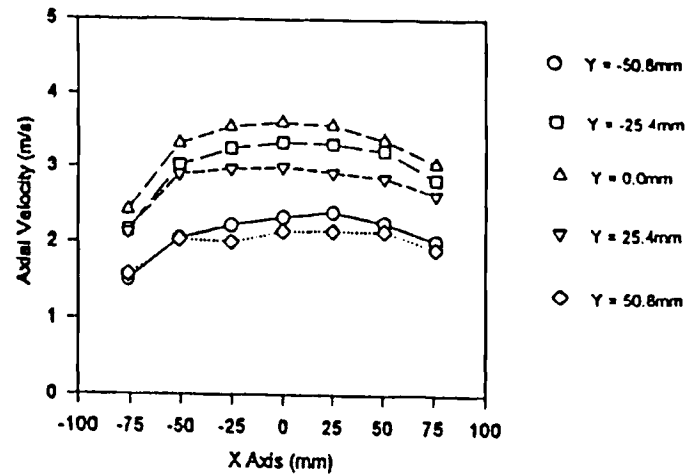


Fig. 4.21 2D Axial Velocity Upstream (Diffuser, 204 m³/hr, 5.3 μm Particles)

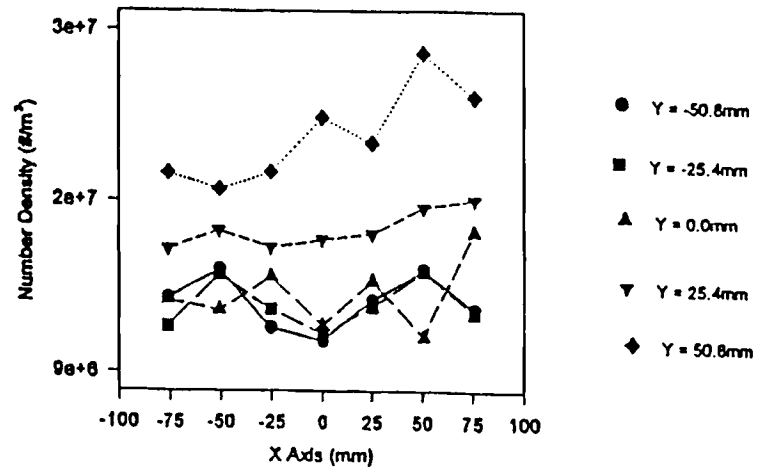


Fig. 4.22 2D Number Density Upstream (Diffuser, 204 m³/hr, 5.3 μm Particles)

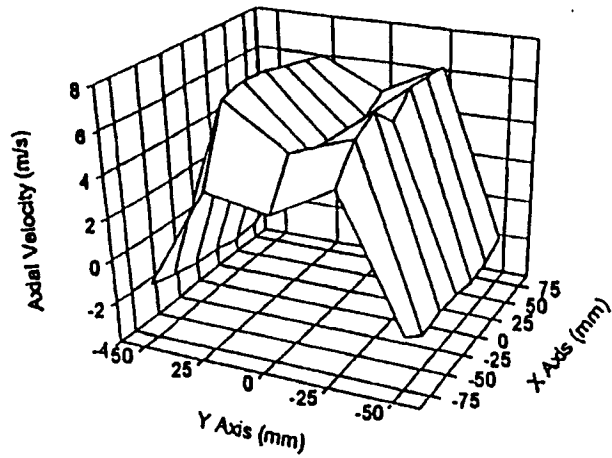


Fig. 4.23 Axial Velocity Downstream (Diffuser, 204 m³/hr, 5.3 μm Particles)

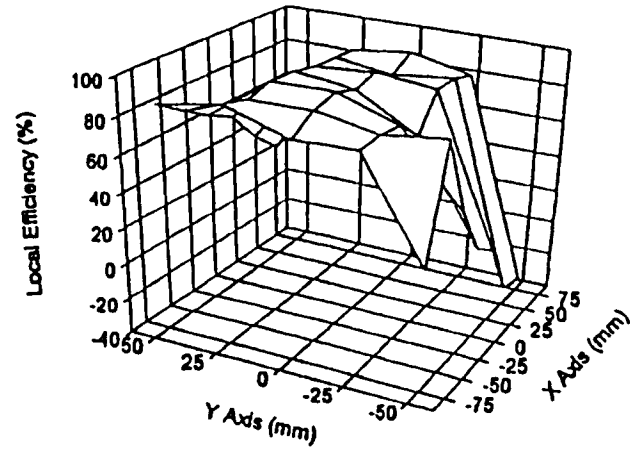


Fig. 4.25 Local Efficiencies over Filter Face (Diffuser, 204 m³/hr, 5.3 μm Particles)

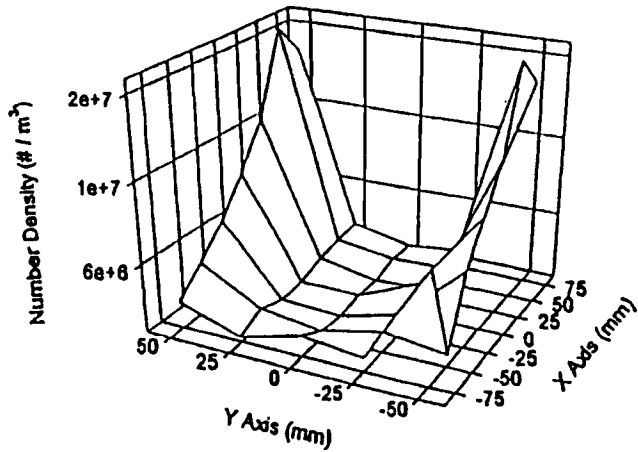


Fig. 4.24 Number Density Downstream (Diffuser, 204 m³/hr, 5.3 μm Particles)

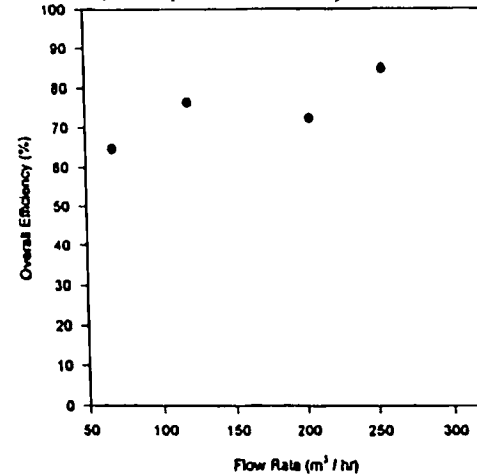


Fig. 4.26 Overall Efficiency vs. Flow Rate (Diffuser, 5.3 μm Particles)

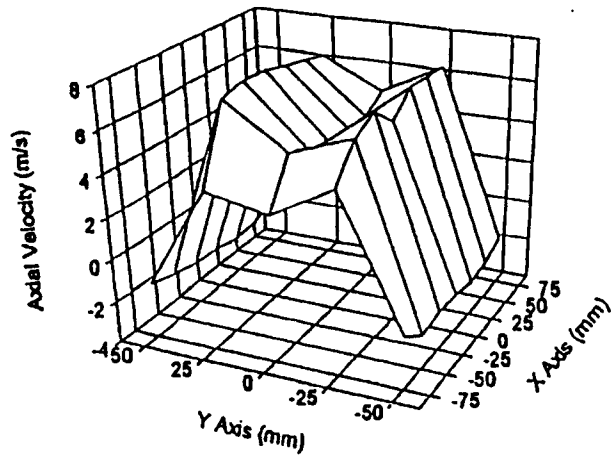


Fig. 4.23 Axial Velocity Downstream (Diffuser, 204 m³/hr, 5.3 μm Particles)

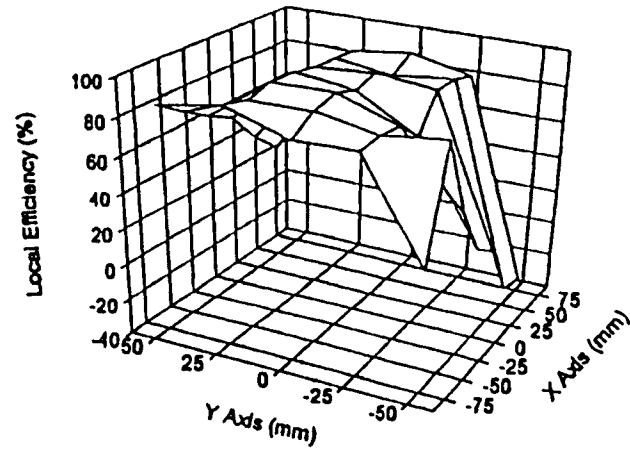


Fig. 4.25 Local Efficiencies over Filter Face (Diffuser, 204 m³/hr, 5.3 μm Particles)

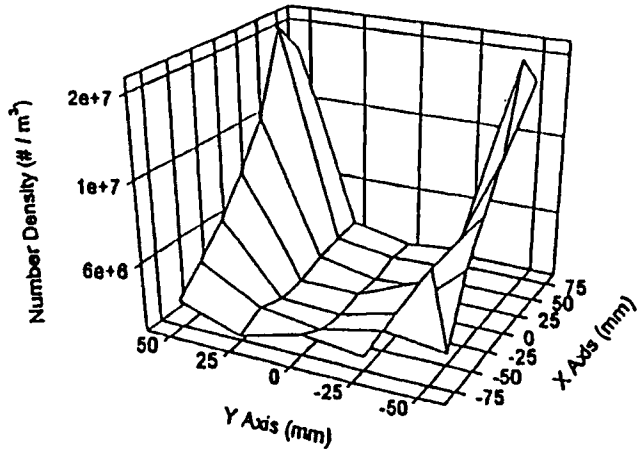


Fig. 4.24 Number Density Downstream (Diffuser, 204 m³/hr, 5.3 μm Particles)

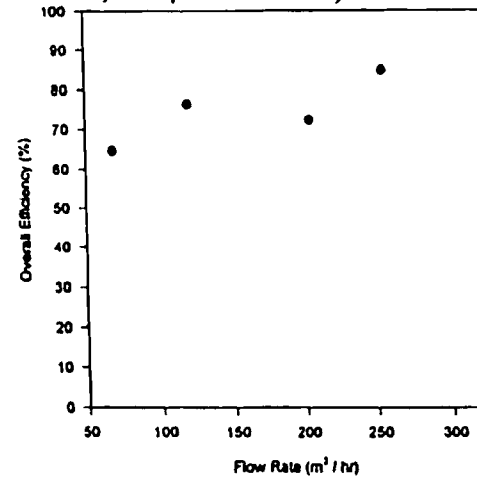


Fig. 4.26 Overall Efficiency vs. Flow Rate (Diffuser, 5.3 μm Particles)

75% at most of the locations, except a few much lower or negative efficiencies. Figure 4.26 depicts the effect of flow rate on overall efficiency for 5.3 μm particle filtration. Note that the 5.3 μm particle filtration was less sensitive to flow rate as compared to 0.966 μm filtration. It is interesting to note that the filter was new for the 68 m^3/hr (40 cfm) flow rate test, followed by the 119 m^3/hr (70 cfm) flow rate test. When the third test at 204 m^3/hr was started with the same filter, the data rate was noticeably lower downstream of the filter. Assuming 5 grams of seeding particles were input for each test run, for a maximum efficiency of 80%, approximately 4 grams of seeding particles would be deposited on the filter for each run. After two test runs, the filter was almost clogged with just 8 grams of particles so that the LDV could not detect enough particles downstream of the filter. Therefore the filter was changed for the third and fourth test runs. So, in order to measure a true initial filtration efficiency, the filter has to be changed for each run, especially for larger particles such as 5.3 μm particles.

4.4 Reliability of the Test Results

The results discussed in the previous sections were believed to be unrealistic and unreliable. There were several shortfalls in the manner in which the above tests were conducted. Some of them are discussed in this section and the measures taken to offset some of those shortfalls are detailed.

1. The mixing chamber was very small with an inlet from the sides and exit from the bottom. This caused insufficient mixing and actually introduced some preferential

entry to a portion of the flow into the main housing. This was the reason for the skewed velocity profile and a non-uniform distribution of particles (concentration) upstream of the filter.

2. Since these experiments were supposedly for measuring initial efficiency of the filter, a clean, new filter should have been used for each run. This was not followed strictly for all of the runs. All of the test runs with the SAE housing were done with the same filter. Using the dilution information for a particular particle size, it is possible to determine the approximate mass of particles deposited on the filter at the conclusion of all SAE tests. For those 0.966 μm particle tests, 5 ml of 10% solution were diluted with 1000 ml of distilled water, and the 1000 ml solution was sufficient to run the tests at all of the flow rates. Therefore 0.5 ml of particles at a specific gravity of about 1.0 were passed through the same filter. With an average overall efficiency for all tests of say 65%, there would be approximately 0.325 gm of seeding particles deposited on the filter.

In a typical SAE test with SAE fine dust, the gain in weight of the filter element at the end of a 10" of water pressure drop, ranges from 50 to 55 gm. The SAE standard mentions the initial efficiency as being taken after the addition of 20 gm of contaminant. 0.325 gm of dust deposition is well within that limit. Therefore this should cause only small changes in a typical cellulose filter's performance from its clean condition. On the other hand, for the 5.3 micron particles, particle deposition up to 8 gm caused a huge difference in the filter performance, as mentioned earlier. Hence, it would be better to use a new clean

filter for each run.

3. Though precautions were taken to avoid leakage through the system, this author believes that there was some leakage through the filter across the housing flange joints for all the above described test runs. This was one of the reasons for the re-circulation zones downstream of the filter. Another reason might have been due to the geometry of the bottom housing, which had a straight portion abruptly reducing in size to that of the outlet pipe. Therefore, the bottom housing was modified to incorporate a gradually decreasing diffuser shape towards the exit of the housing. These aforementioned test runs were conducted with only 4 clamps all around the flange joint. It was decided to secure with 4 more clamps so as to even out the clamping pressure and ensure leak proof clamping.
4. As mentioned in section 4.3.1, the flow meter was connected in the circuit assuming no leakage in the blower, leading to inaccurate flow measurement. This was overcome in the subsequent runs by using the Purolator test stand which has a built-in flow meter, and could account for temperature and barometric pressure variations.
5. For all of the above runs, the pressure drop across the filter was not monitored, resulting in an inability to correlate the behavior of the filter with the pressure drop.
6. Some of the local efficiencies were negative, which could not be true. As mentioned earlier, the rubber sealing underneath the filter also caused some re-circulation of the flow. Hence, the measurement grid was reduced from 1" by 1"

to 0.75” by 0.75” in the subsequent runs, whose results will be discussed in the following section.

Several modifications and improvements were made in the experimental setup to improve the reliability of the test results. Some of the changes made are tabulated in Table 4.1

Table 4.1 Modifications to the Experimental Setup

SL. No.	Cause for the modification	Modification made
1.	Mixing chamber not large enough.	A bigger mixing chamber was used with inlet at the top.
2.	Same filter must not be used for multiple test runs.	Separate filter was used for each flow rate.
3.	Leakage around the filter mounting plates and the flange joints.	Leakage was arrested by providing extra clamps.
4.	Flow measurement was inaccurate.	With Purolator test stand, flow rate measurement was believed to be accurate.
5.	Pressure drop was not measured.	Pressure drop was monitored for all the runs.
6.	Negative efficiencies.	Measurement grid was reduced to avoid negative efficiencies.

4.5 Results of New Diffuser Housing with Modified Setup

The upstream and downstream measurement planes were located at 12.7 mm above and 50.8 mm below the filter similar to the previous tests. As mentioned before, these runs were conducted using the Purolator test stand which incorporated an absolute filter, laminar flow element for flow rate measurement, and a temperature and barometric

pressure compensated flow meter. After the blower was started and the required flow rate was adjusted, it was allowed to run with the heater 'on' for about 20 to 30 minutes. This was to stabilize the temperature and the flow rate. The temperature of air passing through the laminar flow element was between 80° and 90° F for all of these runs.

Figure 4.27 shows the axial velocity profile, upstream of the filter for 0.966 μm particles at a flow rate of 204 m^3/hr (120 cfm). The profile is more uniform over the entire area of the filter even compared to the previous profile with the diffuser housing in Fig. 4.11. The particle concentration profile in Fig. 4.28 is also relatively uniform. The maximum to minimum number density ratio in this case is only around 1.6, whereas it was 2 in the previous case (Fig. 4.12). Two-dimensional slices of the axial velocity and number density profiles upstream, along the long axes of the filter are shown in Figs. 4.29 and 4.30 so that numerical comparisons could be made. It seems that the particle concentration varies a lot along the small axis $X = 0.0$.

The downstream axial velocity and the corresponding number density are shown in Figs. 4.31 and 4.32. The downstream axial velocity profile is also fairly uniform except at two corners of the housing. The downstream axial velocity and the number density profiles show a clear relationship between the two. Wherever the downstream axial velocity is lower, the number density seems to be higher, especially in the central portion of the filter. The upstream and downstream transverse velocity profiles are shown in Figs. 4.33 and 4.34. Both appear to be uniform over the filter area. Though there are a couple of points where the downstream axial velocity values are lower, they do not appear in the

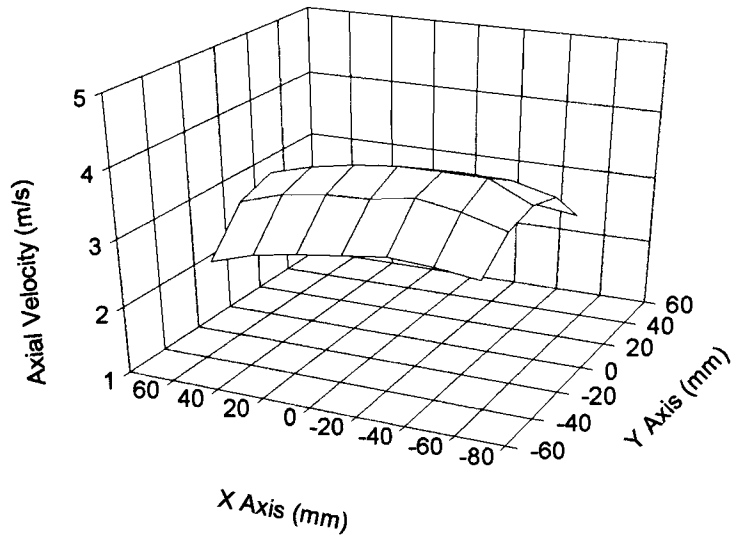


Fig. 4.27 Axial Velocity Upstream (Diffuser, 204 m³/hr, 0.966 μm Particles, Feb. 95)

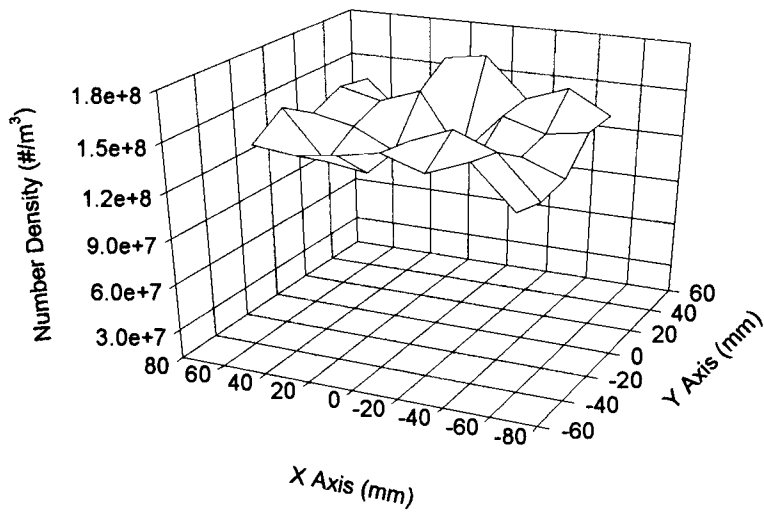


Fig. 4.28 Number Density Upstream (Diffuser, 204 m³/hr, 0.966 μm Particles, Feb. 95)

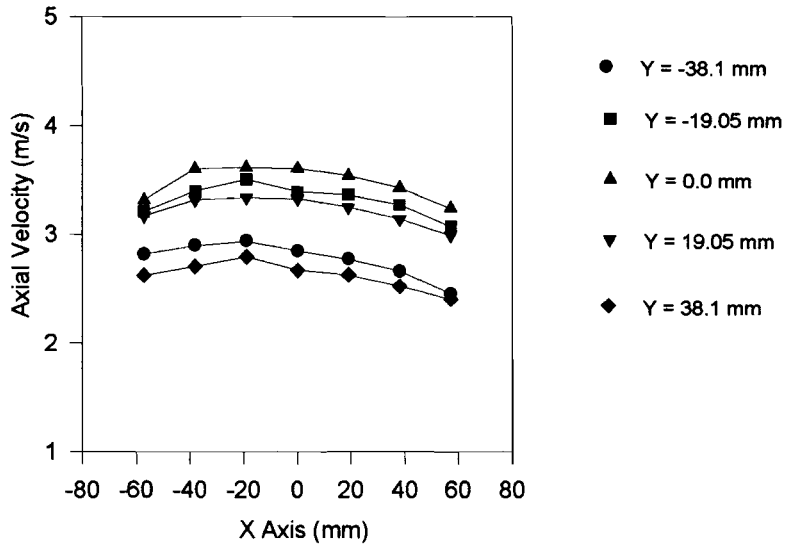


Fig. 4.29 2D Axial Velocity Upstream (Diffuser, 204 m³/hr, 0.966 μm Particles, Feb. 95)

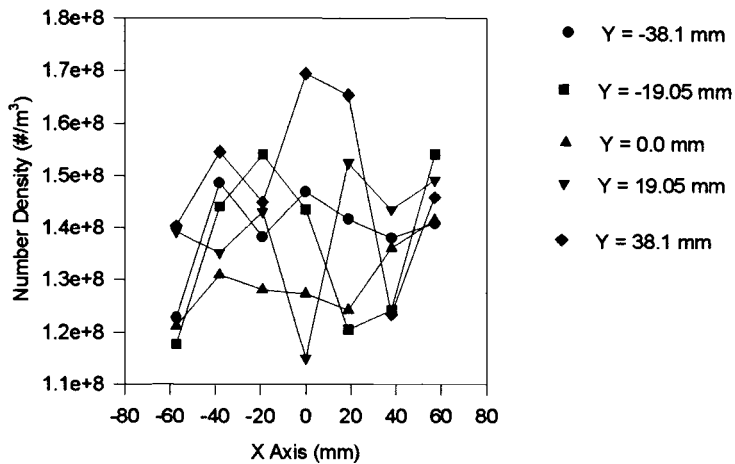


Fig. 4.30 2D Number Density Upstream (Diffuser, 204 m³/hr, 0.966 μm Particles, Feb.

95)

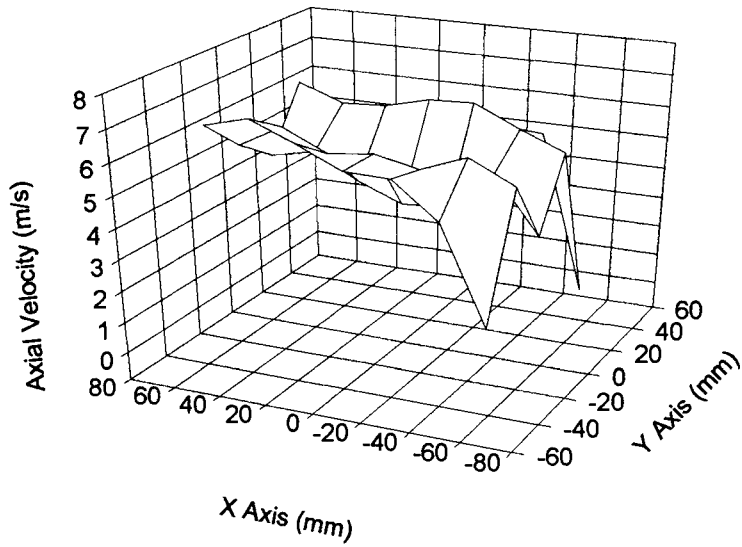


Fig. 4.31 Axial Velocity Downstream (Diffuser, 204 m³/hr, 0.966 μm Particles, Feb. 95)

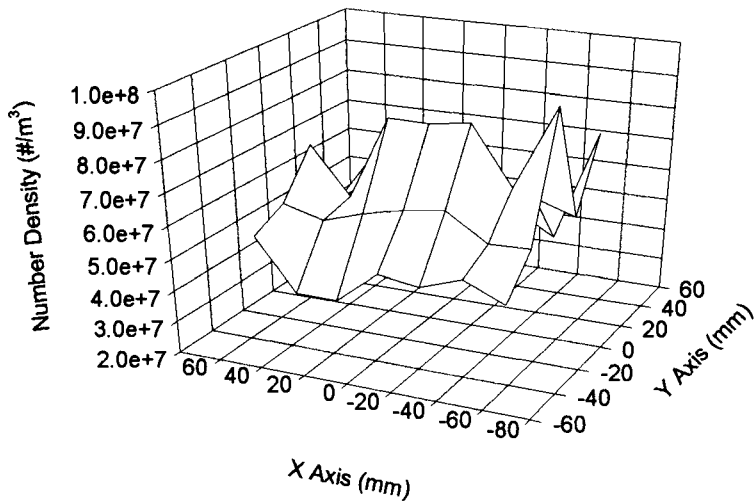


Fig. 4.32 Number Density Downstream (Diffuser, 204 m³/hr, 0.966 μm Particles, Feb.

95)

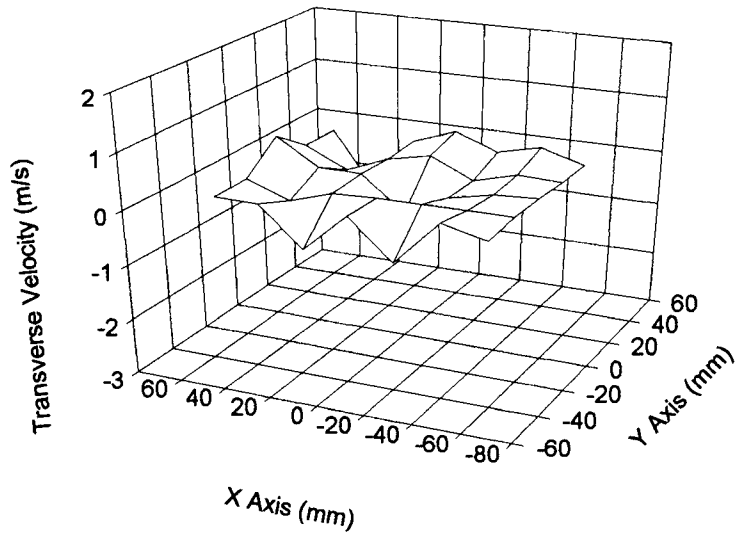


Fig. 4.33 Transverse Velocity Upstream (Diffuser, $204 \text{ m}^3/\text{hr}$, $0.966 \text{ }\mu\text{m}$ Particles, Feb.

95)

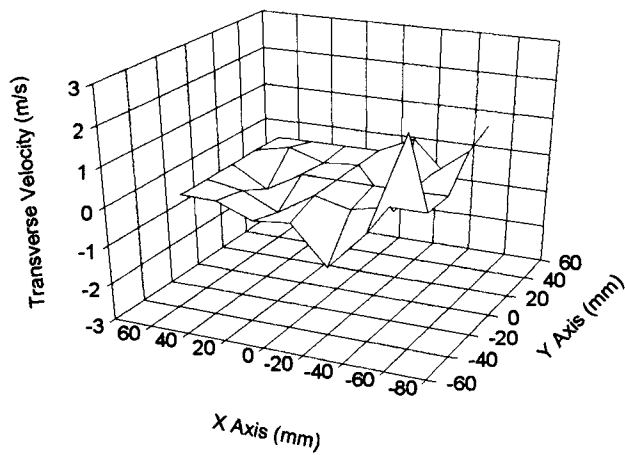


Fig. 4.34 Transverse Velocity Downstream (Diffuser, $204 \text{ m}^3/\text{hr}$, $0.966 \text{ }\mu\text{m}$ Particles, Feb.

95)

local efficiency profile shown in Fig. 4.35. Looking at the numerical values shown in the two-dimensional figure in Fig. 4.36, the local efficiencies lie in a small band, except at the center of the filter along the long axis ($Y = 0.0$) of the filter. One interesting point to be noted is that the lowest local efficiencies occur along this central axis. Comparing with the upstream axial velocity values along this axis in Fig. 4.29, it would appear that at some points, the higher the upstream axial velocity, the lower the local efficiency. This was true for many but not all of the other results with the diffuser housing at various flow rates. It should be noted that there are no negative efficiencies as compared to Fig. 4.17 for the previous run. For most of the locations, the local efficiency values are in the range of 40% to 70%, with the lowest value being 20%. Comparing these values with the ones for the SAE housing (Fig. 4.9), one could say that both are in the same range, even though there

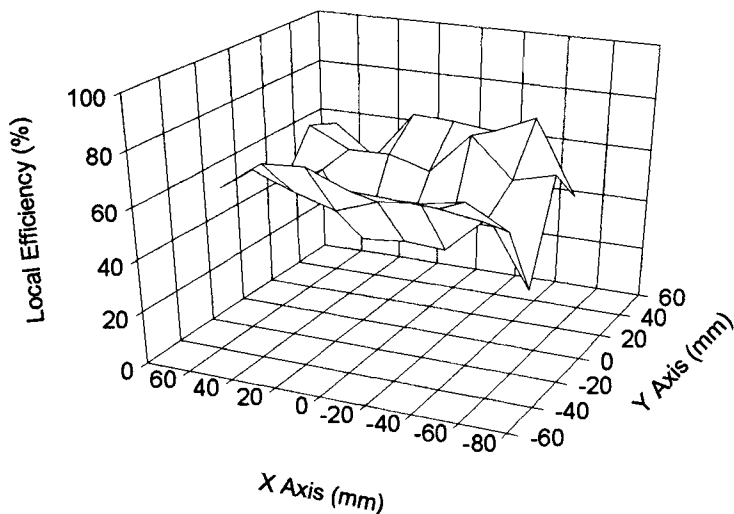


Fig. 4.35 Local Efficiencies over the Filter (Diffuser, $204 \text{ m}^3/\text{hr}$, $0.966 \mu\text{m}$ Particles, Feb.

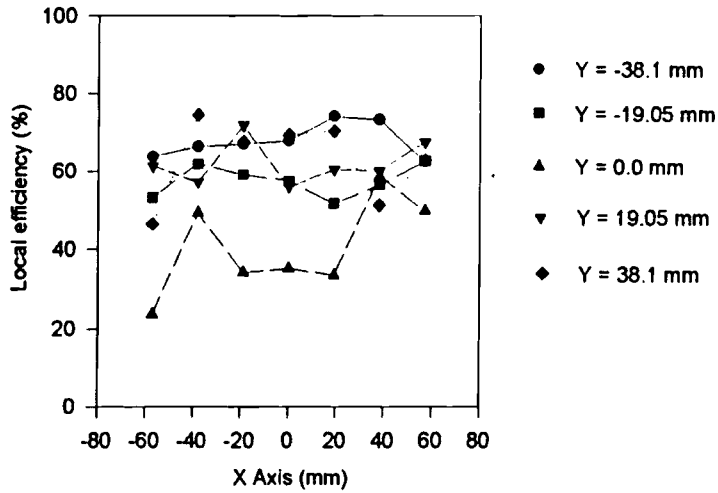


Fig. 4.36 2D Local Efficiencies over the Filter (Diffuser, 204 m³/hr, 0.966 μm Particles, Feb. 95)

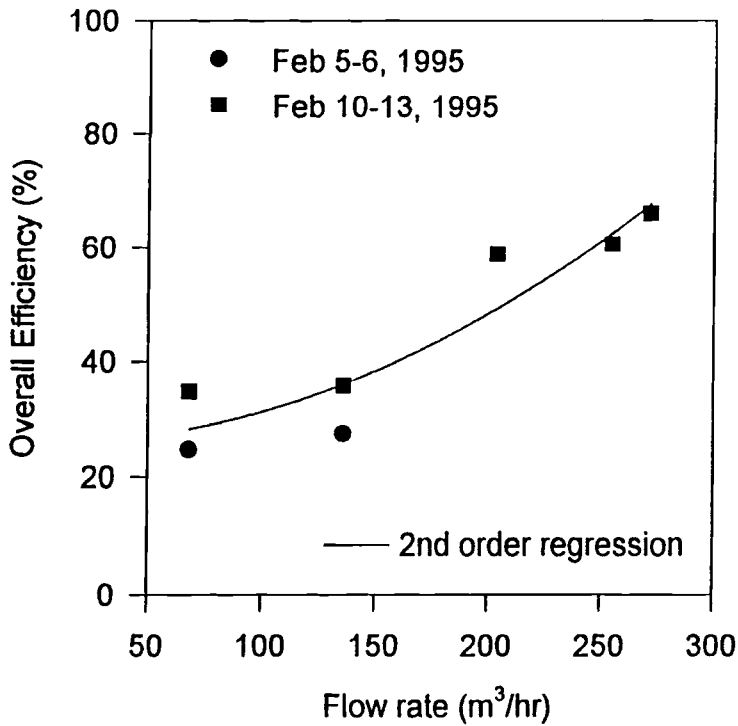


Fig. 4.37 Overall Efficiency vs. Flow Rate (Diffuser, 0.966 μm Particles, Feb. 95)

is a large variation of local efficiency values over the filter area for the SAE housing.

Tests were conducted with the same setup as above, at 68 m³/hr (40 cfm), 136 m³/hr (80 cfm), 255 m³/hr (150 cfm), and 272 m³/hr (160 cfm) flow rates. For each different flow rate, a new filter was used. The velocity, number density, and local efficiency profiles for each of the different flow rates above are given in Appendix C. The dependence of overall efficiency on the flow rate is shown in Fig. 4.37. Two tests conducted at 68 m³/hr and 136 m³/hr earlier on February 5 are shown in the figure by circles. For the later tests for the 68 and 136 m³/hr flow rates, the same old filter of that particular flow rate was used. This might be the reason for the slight increase in overall filter efficiencies for the above two flow rates. There was no appreciable increase in pressure drop during these tests for any flow rate. The pressure drop values are tabulated in Table 4.2.

A similar test was conducted using 0.5 μm PSL particles at a flow rate of 204 m³/hr. The 10% PSL solution was mixed with distilled water in the proportion of 2.5 ml of solution to 1000 ml of distilled water. One might raise a question that the dilution ratio for these 0.5 μm particles was higher compared to the dilution ratio used for 0.966 μm particles. Since the diameter of the particles is approximately one-half that of the 0.966 μm particles, the volume occupied by them would be one eighth of that of the 0.966 μm particles. Hence for achieving the same concentration of the particles in the final solution to be atomized, the dilution ratio for the 0.5 μm particles has to be one eighth of that used for the 0.966 μm particles, which was 5 ml of PSL solution to 1000 ml of distilled water.

Table 4.2 Pressure Drop Measurements

Date of Test	Flow Rate m ³ /hr	Initial Reading mm of H ₂ O	Final Reading mm of H ₂ O	Pressure Drop mm of H ₂ O
02-05-95	68	5.588	5.588	0.0
02-05-95	136	14.478	14.605	0.127
02-10-95	136	14.605	14.732	0.127
02-10-95	272	50.8	50.8	0.0
02-13-95	68	5.588	5.588	0.0
02-13-95	204	29.972	30.099	0.127
02-13-95	255	44.958	45.085	0.127

But the dilution ratio used was low enough that the upstream particle number density was actually lower than that obtained for the 0.966 μm particles. The upstream axial velocity profile in Fig. 4.38 and the upstream number density profile in Fig. 4.39 are more uniformly distributed over the area of the filter. The upstream number density values for the 0.5 μm particles were in the range of 2×10^7 to 7×10^7 as shown in Fig. 4.39. Comparing this with the values for 0.966 μm particles (in Fig. 4.30) which were in the range of 1.2×10^8 to 1.7×10^8 , it is obvious that the dilution ratio used was not too high.

The downstream axial velocity profile and the corresponding number density profiles are shown in Figs. 4.40 and 4.41. It appears that the downstream axial velocity values do not vary as much along the Y axis as they do along the X axis. The downstream

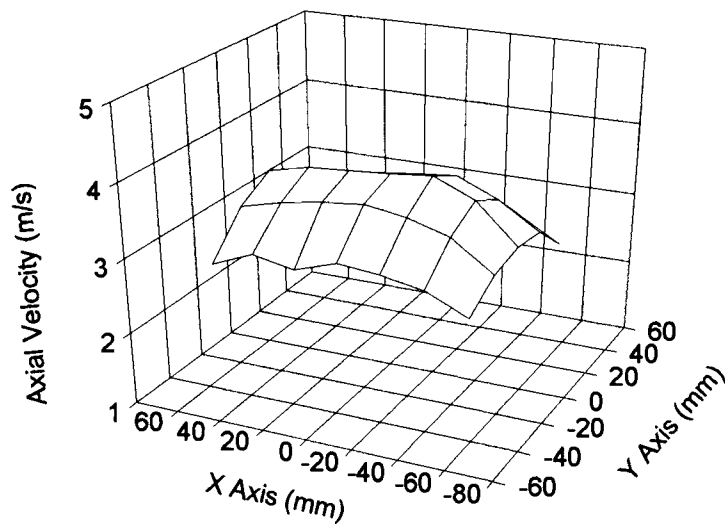


Fig. 4.38 Axial Velocity Upstream ($0.5 \mu\text{m}$ Particles, $204 \text{ m}^3/\text{hr}$, Feb. 95)

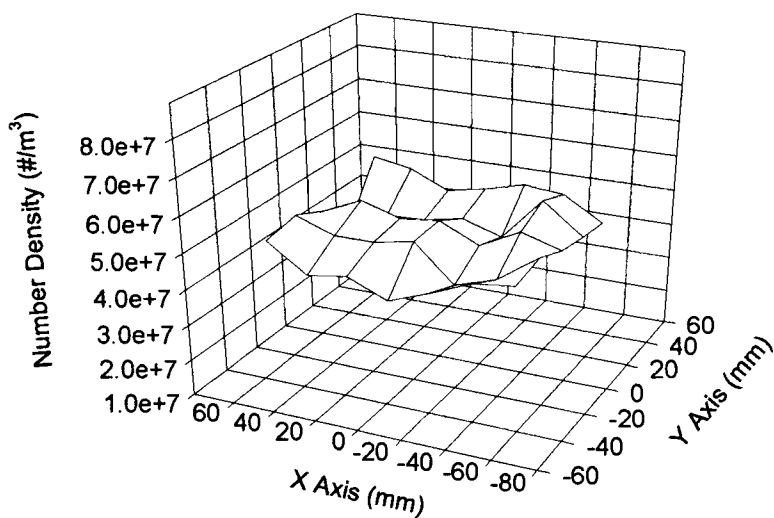


Fig. 4.39 Number Density Upstream ($0.5 \mu\text{m}$ Particles, $204 \text{ m}^3/\text{hr}$, Feb. 95)

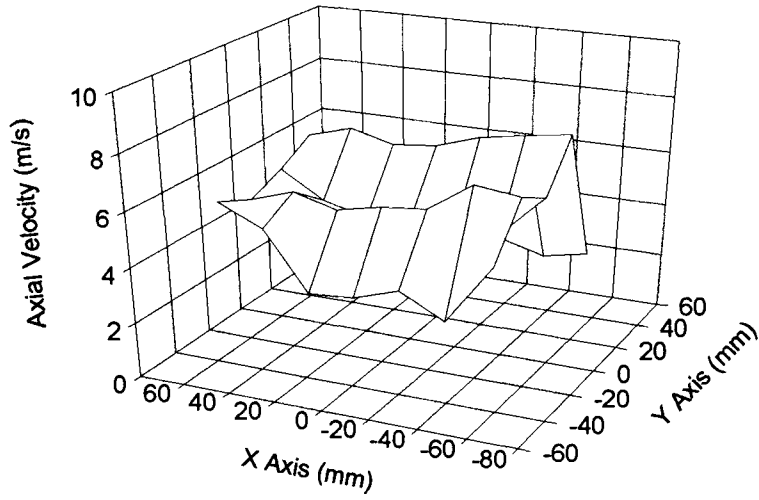


Fig. 4.40 Axial Velocity Downstream ($0.5 \mu\text{m}$ Particles, $204 \text{ m}^3/\text{hr}$, Feb. 95)

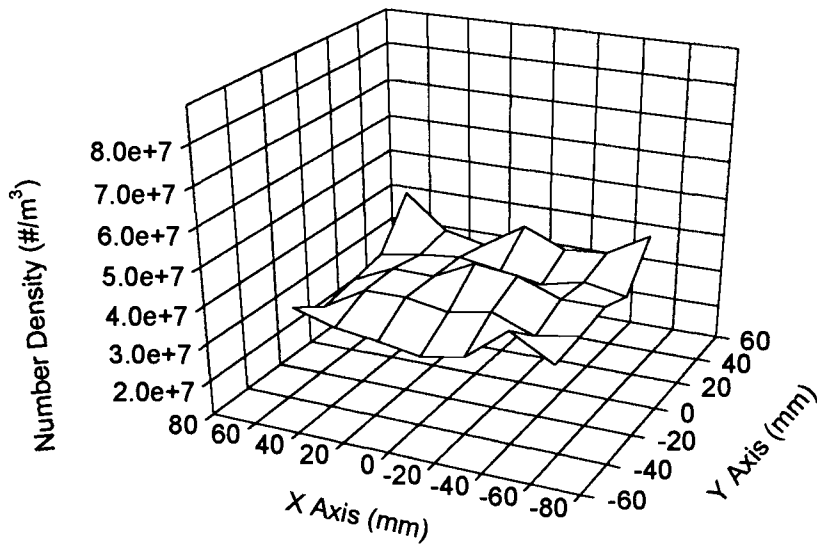


Fig. 4.41 Number Density Downstream ($0.5 \mu\text{m}$ Particles, $204 \text{ m}^3/\text{hr}$, Feb. 95)

number density profile in Fig. 4.41 is also uniform over the filter area. The local efficiency values as plotted in Fig. 4.42 are lower than the values obtained for 0.966 μm particles at the same flow rate.

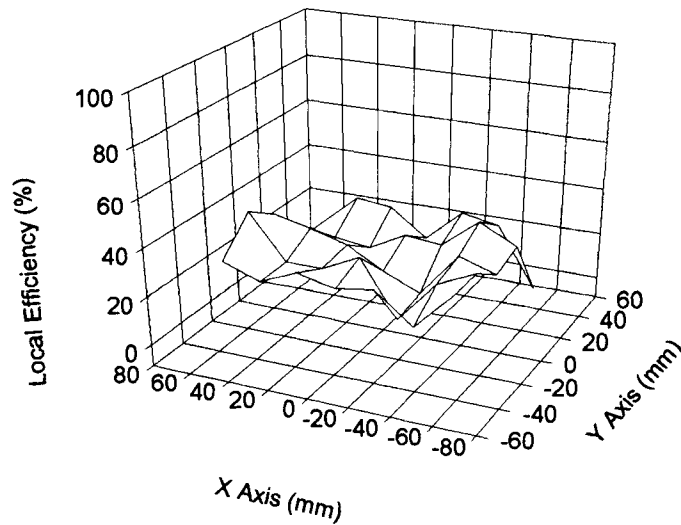


Fig. 4.42 Local Efficiencies (0.5 μm Particles, Feb. 95)

4.6 Filtration Efficiency Modeling

With the measured upstream axial velocity values, filtration efficiencies were calculated using the program EFFMODEL.FOR (Duran, 1995). For calculating these efficiencies, the elemental areas of the measurement grid for each of the 35 points had to be modified in the program. They are tabulated in Table 4.3. All calculations are based on an effective uniform fiber diameter of 51.78 μm and a packing density of 0.345. Once

the individual elemental efficiencies were known, an overall filtration efficiency, η_6 , was obtained as a weighted average of the elemental efficiencies. Only the velocity values obtained from the new diffuser housing were used for the calculations.

Table 4.3 Elemental Areas Covered by the Measurement Points

Measurement Points	Area covered (mm ²)
1, 7, 29, and 35	1512.09
2 to 6 and 30 to 34	604.84
8, 14, 15, 21, 22, and 28	907.26
9 to 13, 16 to 20, and 23 to 27	362.9

The various assumptions used in the filtration efficiency computations, as given by Duran (1995) are:

1. Non-perfect particle adhesion and retention
2. Re-entrainment effects of particles are neglected
3. Diffusive filtration mechanisms are negligible
4. Uniform particle concentration at filter inlet
5. Aerosol particles are monodisperse at the given particle diameter
6. Filter packing density, c , is uniform throughout the filter media
7. Uniform air velocity distribution through the elemental filter media
8. Uniform fiber diameter throughout the filter media

9. Filter media is clean

The elemental efficiencies for 0.966 μm particles for the velocity values obtained at 204 m^3/hr flow rate are shown in the Fig. 4.43. The elemental efficiency variations are similar to the axial velocity variations over the filter face (refer to Fig. 4.4). The efficiencies are in the range of 17.7% to 34.3%, and the overall efficiency is 26.3%. These efficiency values are lower as compared to the measured efficiency values which range from a low of 23.6% to a high of 74.5% with an average efficiency of 58.9%. Both the measured and calculated overall efficiencies are plotted as a function of flow rate in Fig. 4.44. Again the calculated overall efficiencies are lower as compared to the measured values.

Since the calculated efficiencies are a strong function of packing density 'c', and the fiber diameter, an analysis was made on the effect of these factors on the efficiency with all the other parameters remaining same. The packing density used in these calculations was 0.345 as suggested and used by Duran (1995). Similar calculations using an arbitrary packing density of 0.49 increased the efficiency values almost at par with the measured values. Figure 4.45 gives the efficiency values obtained with a packing density of 0.49. The integrated overall efficiency for $c = 0.49$ was 57.1% whereas the measured overall efficiency at 204 m^3/hr was 59.6%.

Similarly some guess values for the fiber diameter and the packing density were used in the program to evaluate the overall efficiencies at different flow rates to understand their effects better. The results are tabulated in Table 4.4. From the table, one

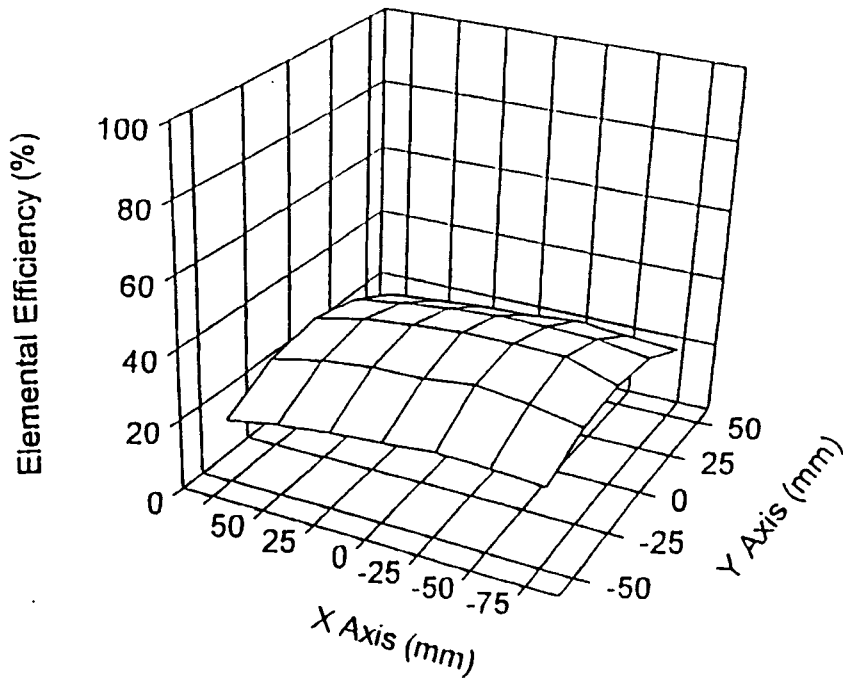


Fig. 4.43 Elemental Efficiencies over the Filter (Diffuser, 204 m³/hr, 0.966 μm Particles, Duran's Model with $c = 0.345$, $D_f = 51.78 \mu\text{m}$, and Velocities from Fig. 4.27)

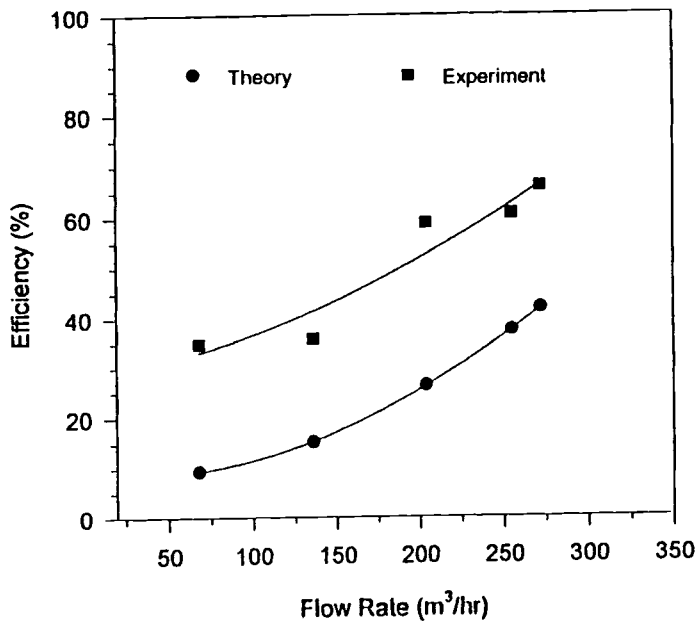


Fig. 4.44 Comparison of Measured and Calculated Overall Efficiencies as a Function of Flow Rate

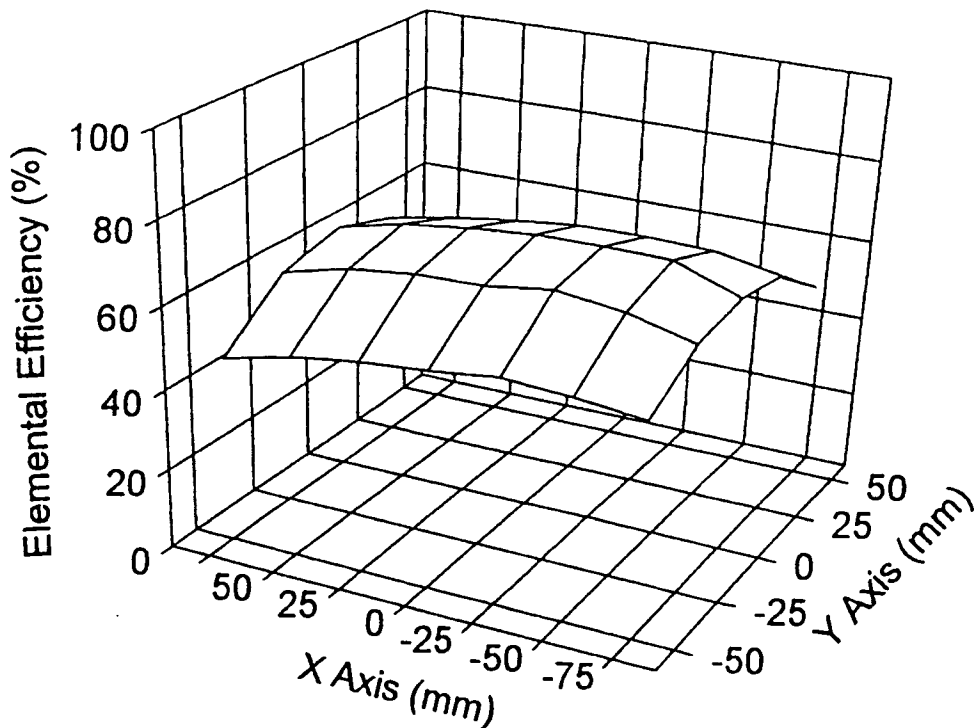


Fig. 4.45 Elemental Efficiencies over the Filter (Diffuser, 204 m³/hr, 0.966 μm Particles, Duran's Model with $c = 0.49$, $D_f = 51.78 \mu\text{m}$, and Velocities from Fig. 4.27)

can see that the overall efficiency increases as the fiber diameter decreases. Increasing the packing density results in an increase in the efficiency. For 5.3 μm particles, with $c = 0.345$, the overall efficiency for 68 m³/hr is 99.96%. For higher flow rates, it reaches and remains at 100%. Thus using a higher packing density would give very high unrealistic efficiency values for larger [than 1 μm] particles. From the microscopic photographs of the filter media (Section 2.4) the maximum diameter of the fibers appears to be approximately 40 μm. So, I think it is better to use 40 μm as the fiber diameter as used by Sabnis (1993).

Table 4.4 Overall Efficiency for Different Values of Packing Density and Fiber Dia.

Packing Density	Fiber Diameter (μm)	Overall Efficiency at 204 m^3/hr for 0.966 μm Particles (%)
0.49	51.78	57.1
0.49	38	89.9
0.345	38	51.6
0.4	40	61.1
0.39	40	58.2

4.7 Stokes Number Analysis

It is customary to compare the filtration performances in terms of Stokes number which involves the particle diameter, fiber diameter and the flow velocity which are three of the most important variables affecting the filtration process. The simple inertial impaction and interception theory predicts the filtration process with respect to the Stokes number as shown in Fig. 4.46. The results of section 4.5 for 0.966 μm and 0.5 μm particles and the previous results of 5.3 μm particles of section 4.3.2 are compared in terms of Stokes number. The average velocity through the filter and the integrated overall efficiencies along with the corresponding Stokes and Reynolds numbers are listed in Table 4.5.

Figure 4.46 shows the comparison between the exact solution given by Flagan and Seinfeld (1988) and the Sabnis' model as given by Eq. 2.18. It also includes three isolated collision efficiencies, the inertial impaction efficiency model given by Landahl and

Herrmann (1949), the isolated collision efficiency due to interception and inertial impaction derived by Suneja and Lee (1974), and combined inertial impaction and interception model developed by Ptak and Jaroszczyk (1990). A detailed discussion of these models can be found elsewhere (Duran, 1995, Sabnis, 1993). As mentioned earlier, the results for the three different monodisperse particle sizes are given as a function of Stokes number in Fig. 4.47. The solid line connecting the points in the graph is a third order regression fit connecting all the data points in the graph. Both of the axes in Fig. 4.47 were plotted on logarithmic scales to make the comparison easier with Fig. 4.46.

Table 4.5 Overall Filtration Parameters As a Function of Particle Diameter

Particle Diameter (μm)	Nominal Flow Rate (m/s)	Average Velocity (m/s)	Reynolds Number	Stokes Number	Overall Efficiency (%)
0.5	204	3.15	37.1	0.0463	24.5
0.966	68	1.09	24.7	0.0556	34.9
0.966	136	2.14	48.6	0.109	35.9
0.966	204	3.08	70	0.157	58.9
0.966	255	3.8	86.4	0.194	60.6
0.966	272	4.07	92.7	0.208	66
5.3	68	0.957	119	1.38	64.7
5.3	119	1.55	193	2.23	76.33
5.3	204	2.64	329	3.8	72.3
5.3	255	3.32	414	4.78	84.84

From Fig. 4.46, it would seem that for Stokes number less than 0.07, the filtration efficiency remains constant. Between Stokes numbers 0.07 and approximately 0.1, there is a steep increase in filtration efficiency. Compared to this, the experimental results in Fig. 4.47 show a relatively steep increase in the range of 0.05 to 0.12. There are not enough data points to follow the behavior below a Stokes number of 0.05. Maybe the curve would go flat at less than this value of Stokes number. The maximum efficiency value for 5.3 μm particles reaches only 0.85 at a Stokes number of 4.78, whereas the theory predicts an efficiency of up to approximately 0.9 for a Stokes number of 0.5. Also shown in Fig. 4.47 is a second set of theoretical efficiencies calculated with different packing density and fiber diameter values. The values were selected by making the fiber diameter equal to 40 μm , and then adjusting the packing density to make the theoretical overall efficiency equal to the experimental overall efficiency at 204 m^3/hr .

Figure 4.48 shows the comparison of the measured and the calculated efficiencies as a function of Stokes number on a linear scale. The experimental curve shows a similar trend as the theoretical one, giving slightly higher efficiencies at lower Stokes numbers. The theoretical curve was obtained by using the axial velocity values for 0.5 μm , 0.966 μm and 5.3 μm particles. The deviation could be explained by the fact that the theory assumes perfect adhesion of the particles, no re-entrainment, a uniform fiber diameter throughout the filter media, and a uniform filter packing density. These factors for an actual filter could cause significant changes in the general trend as well as in the absolute filtration efficiency levels. Also some of the parameters such as the packing density and

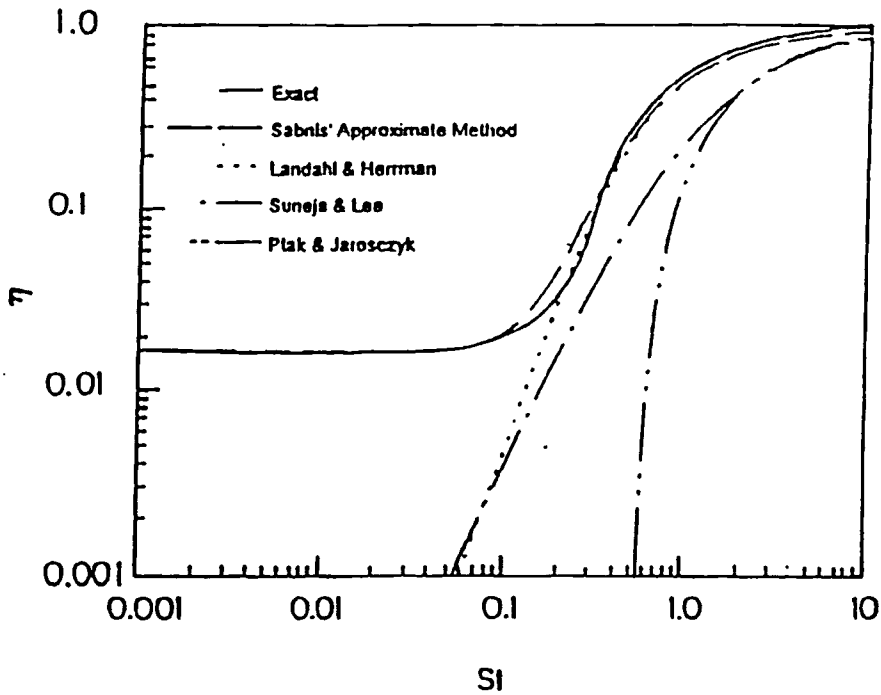


Fig. 4.46 Comparison of Sabnis' Model to Flagan and Seinfeld's Exact Solution and Other Isolated Collision Efficiency Models (Duran, 1995)

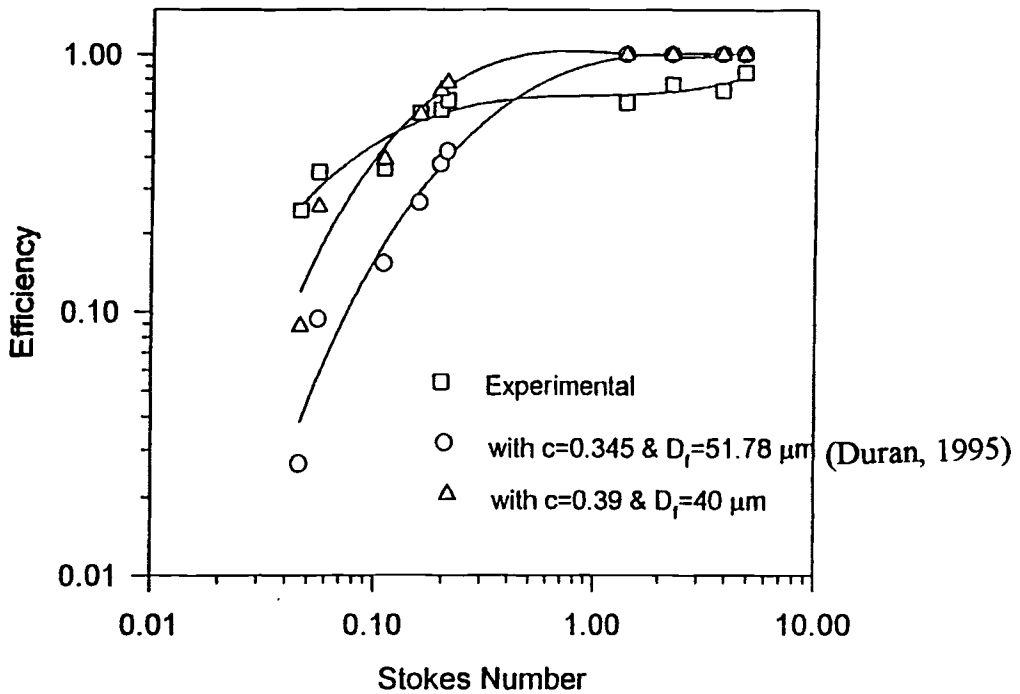


Fig. 4.47 Measured Filtration Efficiencies as a Function of Stokes Number

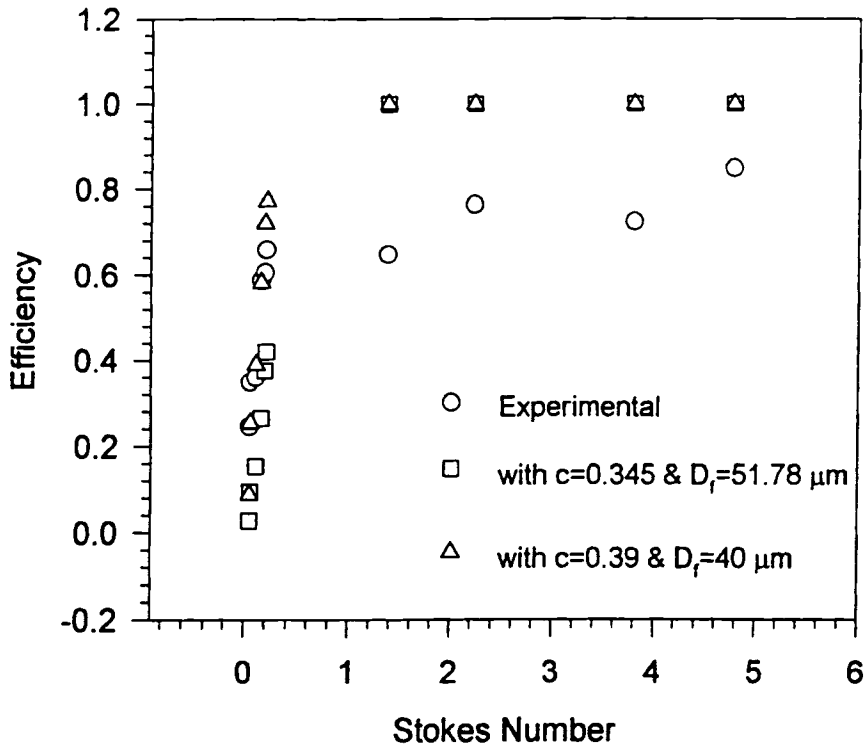


Fig. 4.48 Comparison of Measured Overall Efficiencies with Theoretical Model

the fiber diameter used in the present modeling may not be the accurate values for this filter as discussed in the previous section. The values used in the second set of results in Fig. 4.47 make a better comparison for lower particle diameters.

4.8 Data Reproducibility Measurements

Several types of experiments were carried out to check for the data repeatability. One type of experiment consists of taking number density measurements repeatedly at nine different points upstream of the filter. The grid of measurement points is shown in Fig. 4.49. The parameters such as laser power, number of signals, PSL dilution ratio, DSA parameters, variables set in the atomizer, and flow rate were the same for all of the tests. Four sets of measurements were taken each on two consecutive days. A time gap of 10 minutes was left between the sets of measurements. Each set of nine measurements took approximately 10 to 15 minutes. Thus the whole test took about 90 minutes each day.

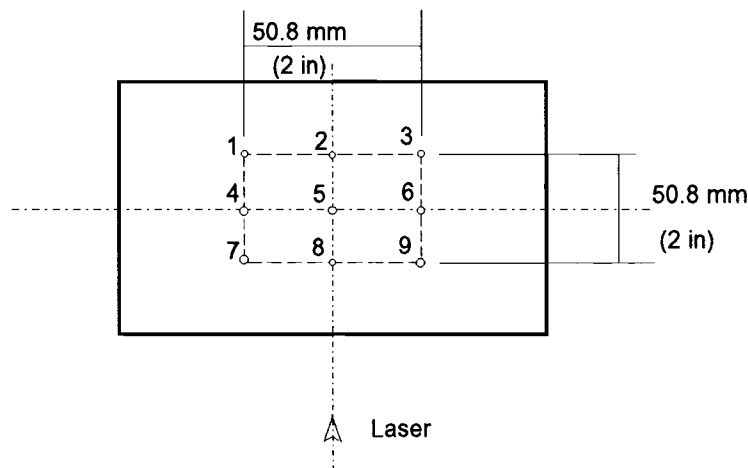


Fig. 4.49 Measurement Grid for Repeatability Tests

Figure 4.50 shows the two-dimensional plot of number densities at the various points across the measurement grid. It is not exactly known why the number density values at points 2 and 3 are much higher than the rest of the points. These measurements

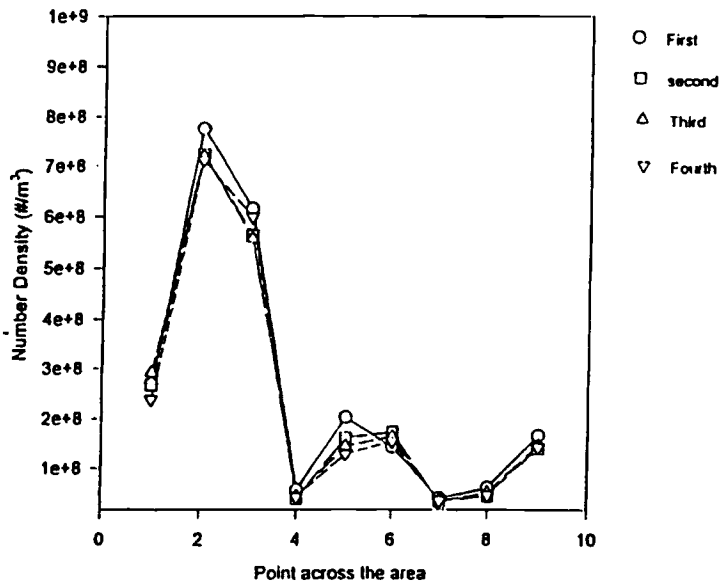


Fig. 4.50 Data Repeatability Upstream of Filter at Nine Locations in a Grid (10-1-94)

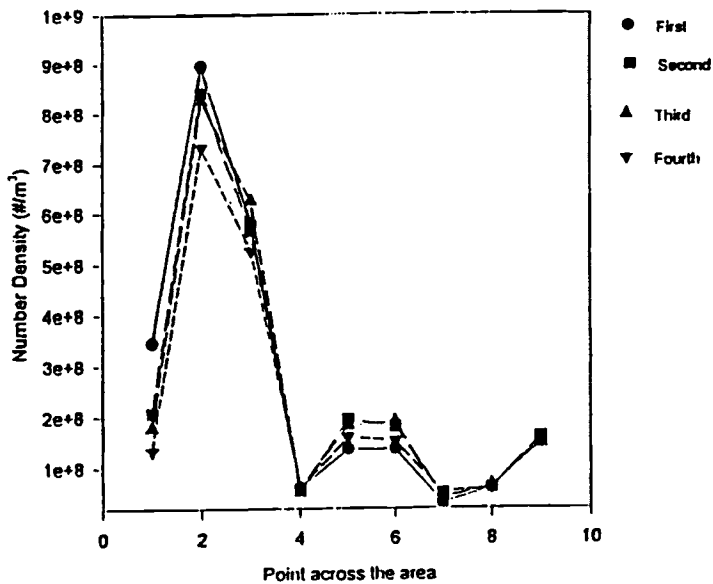


Fig. 4.51 Data Repeatability Upstream of Filter at Nine Locations in a Grid (10-2-94)

were taken in October of 1994 with the same experimental setup used for the earlier efficiency tests discussed in sections 4.2 and 4.3. Figure 4.51 shows the results of the second day with the same filter and parameters. There seems to be a good agreement between all the sets.

Figure 4.52 shows the repeatability of the number density measurements at one location with time without any filter. The measurements were taken at the center of the housing at 204 m³/hr with 0.966 μm particles. The dilution ratio was the same as that for the small angle diffuser housing with 5 ml of PSL solution added to 1000 ml of distilled water. Each of the 40 sets of data took approximately 45 minutes with a five minute interval between the sets. Tests were done at three different laser power settings. The atomizer was set at a pressure setting of 25 psi with all the six jets working. It seems that there is an alternating up and down swing in the number density with time. This might be due to the atomizer not atomizing at a constant rate. The variation above and below the average at 0.4 W laser power is +11% and -8% and at 0.6 W it is +10.2% and -11.8%. At a laser power of 0.8 W the variation is +11.6% and -9.5%.

Figure 4.53 shows one reading at each laser power setting from 0.2 W to 1.4 W with 0.2 W increment. This was done to find out at what power setting the number density measurements reach an upper limit. It would seem that at and above 1 W, the readings are almost constant. It is not advisable to run the LDV with a high power setting because it may be detrimental to the fiber optic cables which carry the laser beams to the transceiver. Hence it is advisable to run either at 0.8 W or 1W at the maximum. Efforts were made to conduct some more of these repeatability tests to reduce the aforementioned ±10% variation so that the parameters which control the stability of the atomizer output

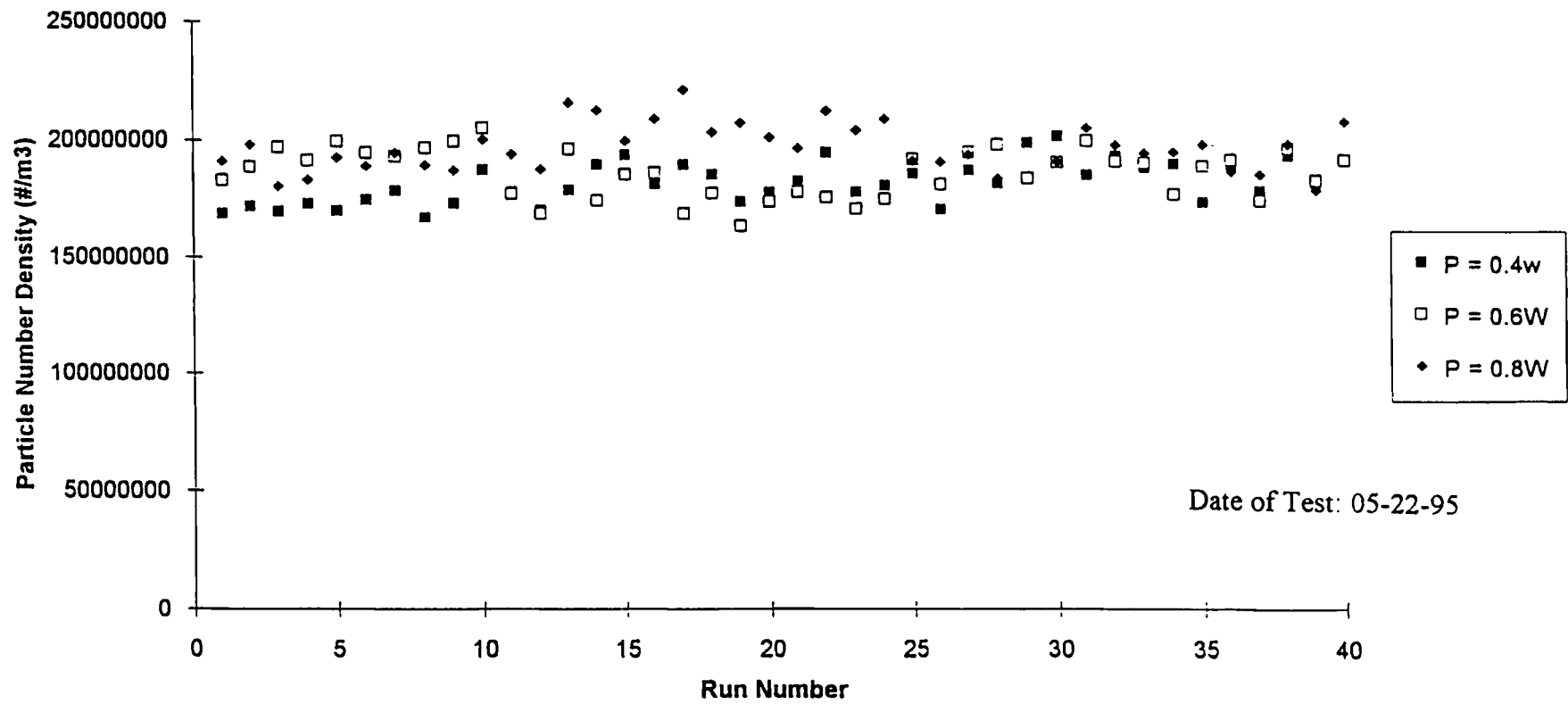


Fig. 4.52 Data Repeatability with Time at Center of the Housing Without Filter

and the laser power could be well understood. Then concrete guidelines could be suggested for placing more confidence on future test results.

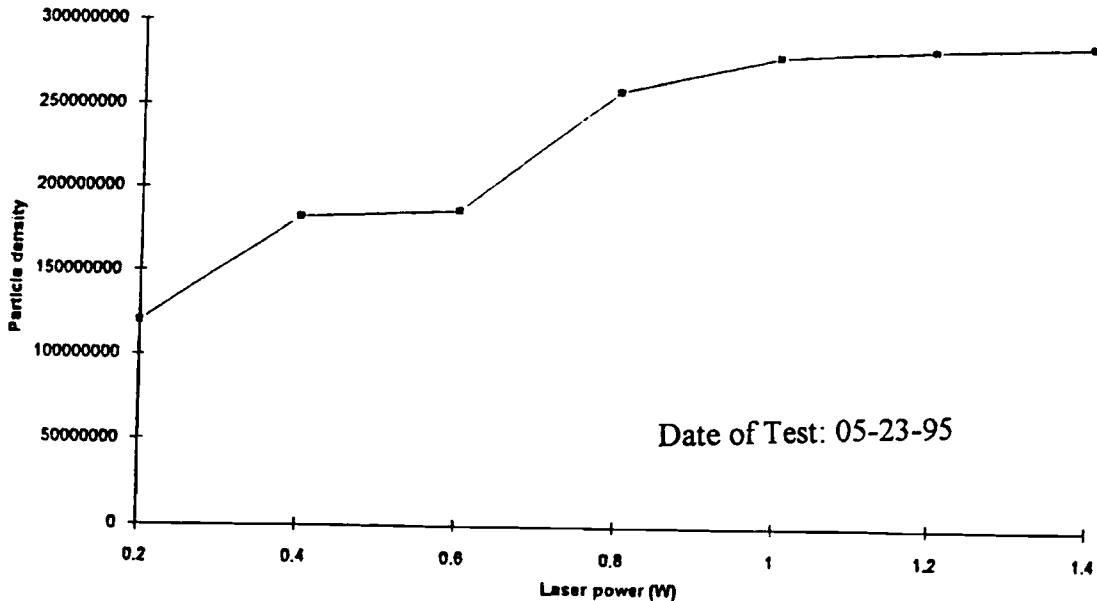


Fig. 4.53 Dependence of Number Density on Laser Power

Nevertheless I believe that the latest results of section 4.5 could be relied upon to have $\pm 10\%$ accuracy. This corresponds to the accuracy of the measuring technique used to get the number of particles at any location. There are other variables such as velocity of the particles, run time, and the dimensions of the probe volume which are involved in the estimation of the particle number density. Each of the three variables would have a separate value for the accuracy of measurement. Because of the inherent capabilities of the LDV system, the combined accuracy of measurement of the above three variables

should be less than 1%. Therefore the above estimate of $\pm 10\%$ accuracy applies to the particle number density at any location. The problem arises when the upstream number density falls in the upper region of variation (+10%) while the downstream number density falls in the lower region (-10%), then the local efficiency might well be off by up to 14%.

4.9 Flow Visualization

Flow visualization techniques provide a quick overall perspective of the flow field. They also can be used to analyze a particular phenomena in a complex flow field as that inside the filter test housings. The qualitative insight gained from flow visualization can be of much help in redesigning the flow housings. The main purpose for which the technique was used here was to investigate the cause of the recirculating flow in the bottom housing of the new setup. The two probable causes we thought of for the recirculating flow were: (1) there was leakage through the flange joint between the top and bottom housings, and (2) the rubber sealing underneath the filter caused locally recirculating flows close to the filter affecting the measurements in that region. Both water droplets atomized by room humidifiers and smoke produced by smoke generator were used in flow visualizations. Still photographs and video pictures of the flow visualizations were taken. Here a word of thanks is due to Dr. Chambers for his immense help in taking photographs.

A sheet of laser light was produced by focusing the main multi-line laser beam through a cylindrical lens. The laser comes out of the lens as a sheet of light which can be arranged to be in either horizontal or vertical orientation. Flow visualization was initially

carried out with the smoke generator described in Appendix E, to gain an overall perspective of the flow in both the top and the bottom housings using axial and transverse laser sheet lighting. The problem appears to be that the smoke gets mixed very fast into the flow due to the turbulent nature of the flow and spreads throughout the housing within a short time after introducing the smoke. To overcome this, the smoke was intermittently introduced into the flow by opening the valve instantly and closing it instantly after a period of 2-3 seconds. Although some flow patterns could be seen by the naked eye, nothing could be effectively recorded on a still photograph.

Water particles were introduced into the housing by atomizing the water with two room humidifiers. When the water particles traveled through the laser sheet, the light was reflected by the water droplets giving flow patterns in the plane of the laser sheet. Figure 4.54 shows a photograph of the setup for the flow visualization using the water mist. The mist was introduced from the top while the blower maintained the flow through the bottom housing. One can see the laser sheet lighting (low laser power) across the filter, covering both the top and bottom housings.

The flow field in the top housing just above the filter looking in the short side of the filter is shown in Fig. 4.55. The flow taking place in the downward direction was well behaved without any swirl or separation. This would aid in a uniform use of the entire area of the filter. Figure 4.56 shows the flow pattern downstream of the filter just after exiting the filter. The flow is separated and recirculating near the left edge of the filter more than that at the right edge. To the naked eye, it appeared that the separation was due to the rubber seals underneath the filter. Though the rubber seals were of the same

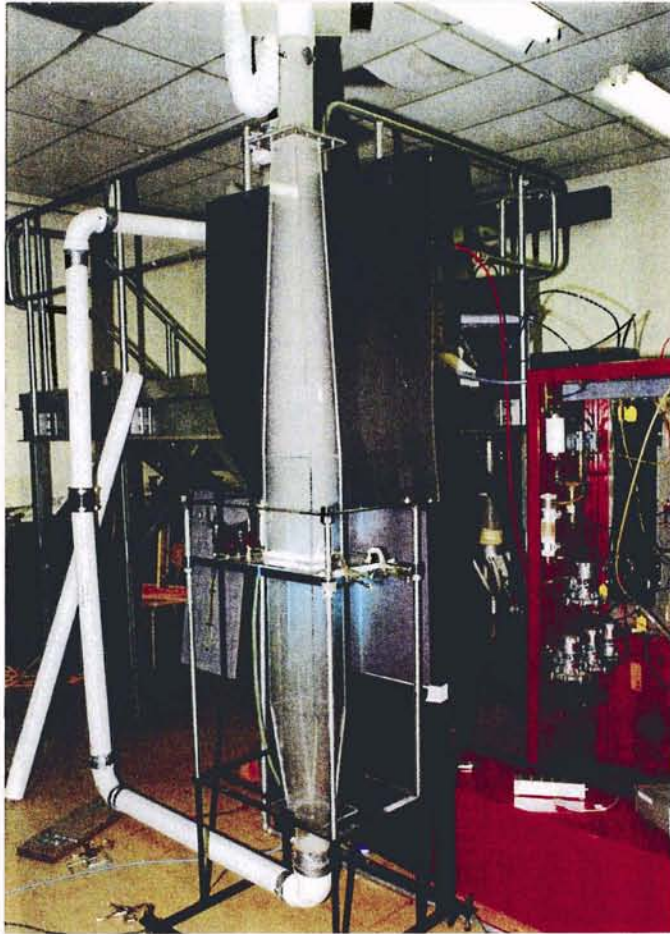


Fig. 4.54 Setup for Flow Visualization Using Water Mist



Fig. 4.55 Flow Visualization Using Water Mist Upstream of the Filter

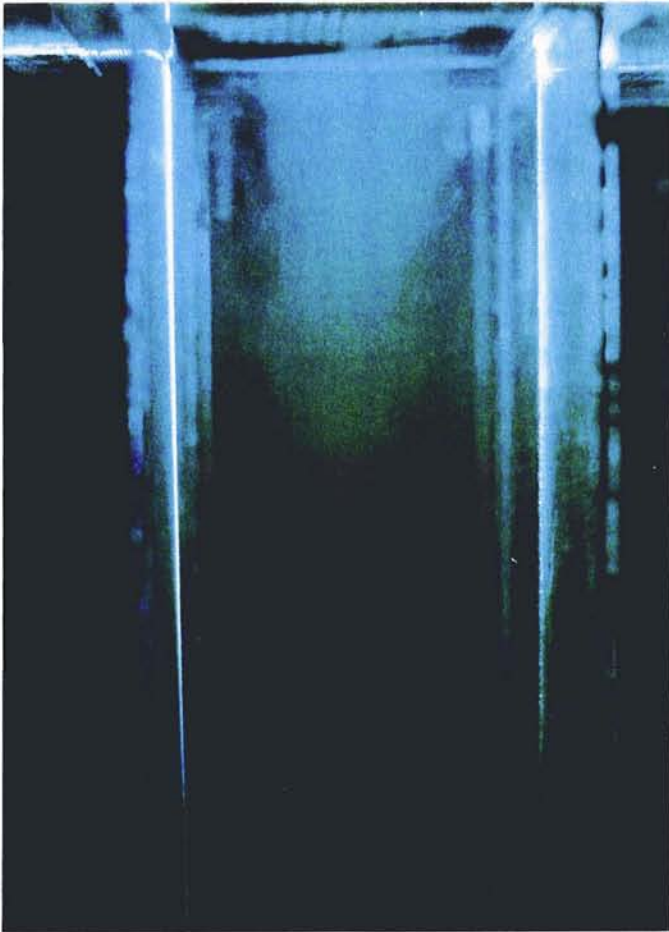


Fig. 4.56 Flow Visualization Using Water Mist Near the Filter Exit

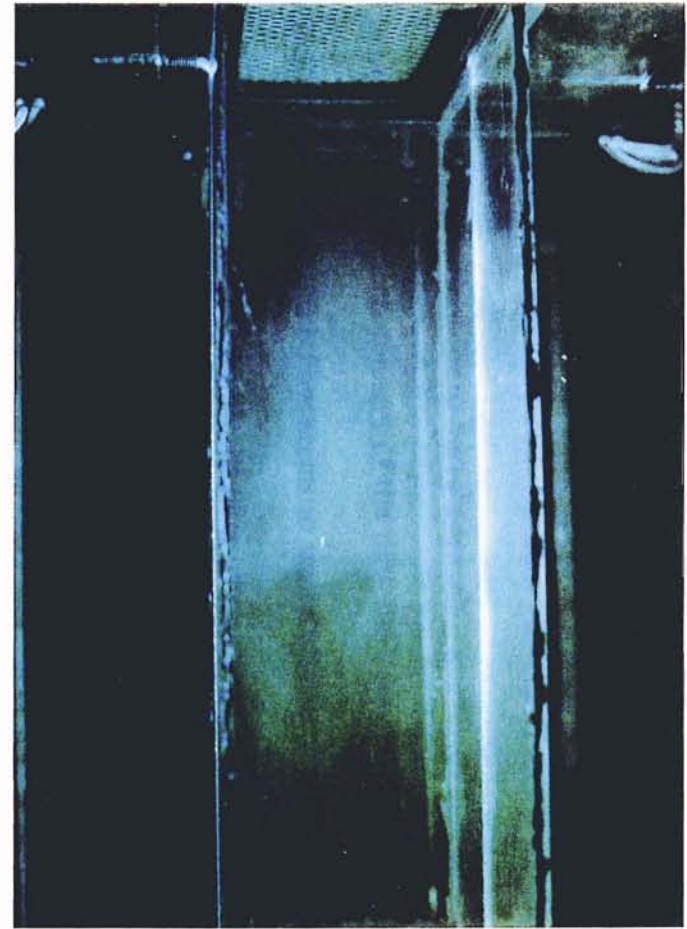


Fig. 4.57 Flow Visualization Using Water Mist Far from the Filter

thickness on all of the edges, the recirculation was predominant only on the left side (front side of the housing near the transceiver). Even providing two extra clamps on that side of the filter to arrest any leakage did not change the flow pattern. Hence it was thought that the recirculating flow was mainly due to the rubber seals.

Figure 4.57 shows a photograph of the flow field downstream of the filter at a distance from the filter exit. The flow seems to reattach to the walls and become fairly uniform after about 203 mm (8 in) below the filter where this photograph was taken. The present downstream measurement plane was situated at about 50.8 mm away from the exit of the filter. It might be better to take downstream particle number density measurements in the future, in a plane very close to the filter to avoid the effects of recirculation and swirling flows downstream of the filter.

CHAPTER V

SUMMARY AND RECOMMENDATIONS

5.1 Summary of Results

The following is a summary of the results obtained from the present study:

1. The flow field inside the small angle diffuser housing is more like a developed duct flow and presents a more uniform flow field to the filter than does the SAE J726 housing. It is important to use a large enough mixing chamber to provide for thorough mixing of the aerosol before it enters the housing. The manner in which the flow is entering the housing affects the flow pattern presented to the filter. Any side entry could cause skewed velocity profiles.
2. The shape of the bottom housing plays an important role as the top housing does in developing the velocity and number density profiles. Any reduction in the cross-sectional area of the housing should be gradual so as not to present sudden obstruction to the flow. There should not be any sudden change in the flow direction as is the case in the downstream portion of the SAE J726 housing. These tend to produce swirling and recirculating flow fields.

3. The recirculating zones can be completely avoided by proper designing of the housings, and proper sealing of the flange joints between the housings. There were certain instances where these could not be completely avoided, as in the case of some of the filters where the bottom rubber seal was so large as to create recirculating zones.
4. Generally care should be taken to avoid taking LDV number density measurements in the recirculating zones. This resulted in unrealistic number density values downstream of the filter, leading to negative local efficiencies, as found for the 5.3 μm particles.
5. For most of the tests, the downstream velocity profile was also uniform except at some corners of the housing.
6. There is a strong dependence of filtration efficiency on the fluid velocity. In an overall context, the higher the velocity of the flow through the filter, the higher the efficiency. But for some of the tests, the local efficiencies were lower along the center line of the filter (along the $Y = 0.0$ axis) where the axial velocities were the maximum.
7. Filtration efficiencies are higher for larger particles irrespective of the flow rate or the velocity of flow. For example the overall efficiency for 5.3 μm particles at the lowest flow rate of 68 m^3/hr was higher than the overall efficiency for 0.966 μm particles at the highest flow rate of 272 m^3/hr . The overall efficiencies for 5.3 μm particles are lower than predicted by theory. This may be due to the large number of negative local efficiencies obtained for the 5.3 μm particles. Moreover the overall

efficiencies are less sensitive to the flow rate as compared to those for the 0.966 μm particles.

8. Both the local and the overall efficiencies for the particle sizes 0.5 μm and 0.966 μm are higher than the efficiencies predicted by the theory. But the measured efficiencies for the 5.3 μm particles are lower than the theoretical ones. The packing density 'c' and the fiber diameter has a strong influence on the theoretical models. Increasing the packing density from 0.345 to 0.49 increased the theoretical overall efficiency for the 0.966 μm particles to that of the measured value. But at the same time, the theoretical overall efficiency for 5.3 μm particles was 100% even with a packing density of 0.345.
9. Comparing the performances of the two housings used, the overall efficiencies for the SAE J726 housing are higher than the ones for the small angle diffuser housing for any given flow rate. Though I do not believe all of the results from the SAE housing, they definitely give some trends as to the effect of the housing and the filter on filtration performance. While the axial velocities range from 2.3 to 3.7 m/s for the small angle diffuser at a flow rate of 204 m^3/hr , they range from 0.6 m/s at one end of the filter along the long axis to 6.3 m/s at the center of the filter for the SAE housing. Along the extreme small axis, ($Y = 50.8 \text{ mm}$), the local efficiencies are as high as 80%. The local efficiency profiles are more uniform for the diffuser housing as compared to the SAE housing.
10. Stokes number analysis of the results shows that the measured and the theoretical overall efficiencies lie within a close band, using the present packing density and the

fiber diameter values of 0.345 and 51.78 μm , respectively.

11. Calculated local efficiency profile based on the theory generally follows the bell shaped velocity profile. Local efficiencies are lower for lower axial velocities, especially at the edges of the filter.
12. From the flow visualization tests, it seems that the recirculation zones in the bottom housing are not due to the leaks but due to the rubber seal underneath the filter. Also there are no visible recirculating flow or separating flow upstream of the filter, and the flow seems to be well behaved.
13. With the typical dilution ratio of 5 ml of 10% solution to 1000 ml of water for the 0.966 μm particles, the atomizer was run at 50 psi pressure setting and 40 to 60 litres/min of air dilution with 6 jets. With these settings, the atomization rate of the atomizer at a flow rate of 204 m^3/hr for the 0.966 μm particles varied from approximately 80 to 100 ml/hr. Then the average input particle number density was computed to be between 1.67×10^8 and $2.45 \times 10^8 \text{ m}^{-3}$. The measured number density values were within this range for most of the upstream locations, especially with the diffuser housing.

5.2 Recommendations for Future Work

As mentioned in Chapter III, there were many shortfalls in the manner in which the tests were conducted. A definite improvement in the reliability of the results was obtained by overcoming many of the shortfalls. Nevertheless the present study has given an

understanding of the way in which the LDV can be used for filtration efficiency measurement. Some of the directions the future research work might take are listed as follows:

1. More experiments with the SAE J726 housing using 0.5 μm , 0.966 μm , and 5.3 μm particles should be conducted. At this point, measurements can be made very close to the filter in the SAE housing, because the old plexiglass wall in the front has been replaced with a glass wall. It is important to ascertain whether resorting to the small angle diffuser and getting more uniform velocity profile improves the accuracy of filter test results and actually improves filtration.
2. More tests with 0.5 μm and 5.3 μm particles in the small angle diffuser housing could be done by using the 19.05 mm by 19.05 mm (0.75 in x 0.75 in) grid so as to avoid any negative local efficiencies.
3. The present dilution ratio used with 0.966 μm particles at 500 ppm gives upstream number density values of the order of 10^8 . Since the LDV can easily detect concentrations up to 10^7 , it is suggested that a dilution ratio of 2.5 ml of PSL solution to 1000 ml of water be tried. But at the same time, it should be realized that, due to good filtration efficiencies, the particle concentration downstream might become less than 10^7 making it difficult for LDV measurements.
4. The flange of the small angle diffuser housing is made of a 6.35 mm (0.25 in) thick plexiglass sheet which does not give enough stability in clamping the filter down, and it actually bends upwards in the center when clamping pressure is applied from the sides. Hence modifications could be made to the diffuser housing to make the flange

stronger by making it out of a 9.525 mm (3/8 in) or 12.7 mm (1/2 in) thick plexiglass sheet. Another possibility is to add a metal strip of about one inch width all around the flange both up and down.

5. More atomizer stability tests and data repeatability tests should be conducted before embarking on further tests with actual filter. Repeatability tests should be done for some of the important DSA parameters such as low pass filter, sampling rate, burst filter, and envelope filter with all of the other variables remaining the same.
6. More tests could be conducted with different sized particles such as 2.0 μm , and 10 μm at different flow rates. Particularly flow rates lower than 68 m^3/hr (40 cfm) should be used to avoid some re-entrainment effects for larger particle sizes. When using larger particles, it is recommended that a new filter be used each time.
7. Since actual dust is used in SAE tests, tests could be performed with cut dust with size ranges of 0-5 μm , 5-10 μm , 10-20 μm , and 20+ μm particles.
8. Efficiency measurements should be performed for filters loaded with dust in several steps like 1", 2", 5" 8", and at the final pressure drop of 10" of H_2O . Pressure drop should also be monitored during these tests to evaluate the effect of dust loading on pressure drop and efficiency.
9. The results of the tests conducted with these housings can not be used to deduce the actual performance of the filter in its installed condition in an automobile. Hence efforts should be made to test the filters using the LDV, in housings more closely resembling the actual housing used in the automobile.

REFERENCES

Aerometrics (1992), Doppler Signal Analyzer for Phase Doppler Particle Applications User's Manual, Sunnyvale, CA, draft 2.

American Society for Testing and Materials (1989), "ASTM F 1215-89, Standard Test Method for Determining the Initial Efficiency of a Flatsheet Filter Medium in an Airflow Using Latex Spheres," Annual Book of ASTM Standards, Vol. 14.02.

Baczewski, K. and Jaroszczyk, T. (1981), "Laboratory and Service Testing of Air Filters," Filtech Conference, London, 1981, pp. 197-202.

Broussard, J. M. (1991), "Purolator Products, Inc. SAE J726 Air Test Stand Instruction Manual and Test Procedure," Purolator Products, Inc.

Buchhave, P., Delhay, J. M., Durst, F., George, W. K., Refslund, K. and Whitelaw, J. H. (1975), "Introduction," Proceedings of the LDA-Symposium, Copenhagen, pp. 9-17.

Davies, C. N. (1973), Air Filtration, Academic Press, New York.

Davis, W. T. (1994), "Air Filtration Efficiency Testing," *TAPPI Journal*, Vol. 77, No. 2, Feb. 94, pp. 221-226.

Duran, R. (1995), "Improvement of Flow Uniformity and Modelling of Filtration Efficiencies for Automotive Air Filter Test Housings," MS Thesis, Oklahoma State University, School of Mechanical and Aerospace Engineering, Stillwater, OK.

Durst, F., and Eliasson, B. (1975), "Properties of Laser-Doppler Signals and Their Exploitation for Particle Size Measurements," Proceedings of the LDA-Symposium, Copenhagen, pp. 457-477.

Emi, H., Wang, C. and Tien, C. (1982), "Transient Behavior of Aerosol Filtration in Model Filters," *AIChE Journal*, Vol. 28, No. 3, May, 1982, pp. 397-405.

Flagan, R. C., and Seinfeld, J. H. (1988), Fundamentals of Air Pollution Engineering, Prentice Hall Eaglewood, NJ.

George, Jr., W. K. (1975), "Limitations to Measuring Accuracy Inherent in the Laser Doppler Signal," Proceedings of the LDA-Symposium, Copenhagen, pp. 20-63.

Gillespie, T. (1955), "The Role of Electric Forces in the Filtration of Aerosols by Fiber Filters," *Journal of Colloid Science*, Vol. 10, pp. 299-314.

Gould, R. D. and Loseka, K. W. (1993), "A Comparison of Four Velocity Bias Correction Techniques in Laser Doppler Velocimetry," *Journal of Fluids Engineering*, Vol. 112, pp. 508-514.

Graden, L. (1987), "Influence of Electrostatic Interactions and Slip Effect on Aerosol Filtration Efficiency in Fiber Filters," *Industrial Engineering Chemical Research*, Vol. 26, pp. 306-311.

Haldhani, M. K. (1993), "Particle Number Density Distribution and Its Time History for an Automotive Air Filter," MS Thesis, Oklahoma State University, School of Mechanical and Aerospace Engineering, Stillwater, Oklahoma.

Jaroszczuk, T., and Wake, J. (1991), "Critical Aerosol Velocity in Nonwoven Filtration," TAPPI Proceedings, Nonwoven Conference, pp. 125-135.

Jaroszczuk, T., Wake, J., and Connor, M. J. (1993a), "Automotive Engine Air Filter Media Performance," The Filtration Society, Filtech Conference, Karlsruhe, Germany.

Jaroszczuk, T., Wake, J., and Connor, M. J. (1993b), "Factors Affecting the Performance of Engine Air Filters," American Society of Mechanical Engineers, Energy Sources Technology Conference and Exhibition, Houston, Texas.

Jaroszczuk, T., Hoops, R. H., and Kreikebaur, G. (1987), "Measurement of Engine Air Filter Efficiency Using a Continuous Aerosol Monitoring System," SAE Technical Paper 872268, Truck and Bus Meeting and Exposition, Dearborn, Michigan, Nov. 1987.

Landahl, H. D., and Herrmann, R. G. (1949), "Sampling of Liquid Aerosols by Wires, Cylinders, Slides, and the Efficiency of Impaction by the Droplet," *Journal of Colloid Science*, pp. 103-136.

Lee, K. W., and Liu, B. Y. H. (1982), "Theoretical Study of Aerosol Filtration by Fibrous Filters," *Aerosol Science and Technology*, Vol. 1, Elsevier Science Publishing Co., Amsterdam, pp. 147-161.

Liang, F. (1994), "Particle Counting and Sizing with LDV for Automotive Air Filters," Ph.D. Qualifying Exam Report, School of Mechanical and Aerospace Engineering, Oklahoma State University, Stillwater, Oklahoma.

Liang, F., Natarajan, B., Tian, Y., and Dougherty, R. L. (1995), "Local Efficiency Measurements Applicable to Both Automotive Engine and Cabin Filtration," *Particulate Science and Technology*, Taylor and Francis Publishers, Vol. 12, No. 4, Oct.-Dec. 1994, pp. 333-350.

Liu, B. Y. H., and Pui, D. Y. H. (1974), "Electrical Neutralization of Aerosols," *Journal of Aerosol Science*, Vol. 5, pp. 465-472

Melling, A., and Whitelaw, J. H. (1975), "Optical and Flow Aspects of Particles," Proceedings of the LDA-Symposium, Copenhagen, pp. 382-402.

Natarajan, B., Liang, F., Williams, J., and Dougherty, R. L. (1995), "Local Efficiency Measurements of Pleated Panel Air Filter Used in Automotive Engines," AIAA/ASME Oklahoma Symposium XV, Oklahoma State University, Stillwater, OK., Feb. 1995.

Newman, R. A. (1994), "Uniformity of Airflow in Automotive Air Filter Test Housings and Its Effects on the Efficiency of Fibrous Filters," MS Thesis, Oklahoma State University, School of Mechanical and Aerospace Engineering, Stillwater, Oklahoma.

Ptak, T., and Jaroszyk, T. (1990), "Theoretical-Experimental Aerosol Filtration Model for Fibrous Filters at Intermediate Reynolds Numbers," Proceedings of the Fifth World Filtration Congress, France, pp. 566-572.

Raabe, O. G. (1968), "The Dilution of Monodisperse Suspensions for Aerosolization," *American Industrial Hygiene Association Journal*, Sept. - Oct. 1968.

Rodman, C. A., and Lessmann, R. C. (1988), "Automotive Nonwoven Filter Media: Their Constructions and Filter Mechanisms," *Tappi Journal*, Apr. 1988, pp. 161-168.

Ruck, B., and Pavlovski, B. (1993), "Particle-Induced Limits of Accuracy in Laser Doppler Anemometry," *Particle and Particle System Characterization*, Vol. 10, No. 3, pp. 129-137.

Sabnis, R. D. (1993), "Effects of Non-Uniform Air Flow Through Filters on Filtration Efficiency," MS Thesis, Oklahoma State University, School of Mechanical and Aerospace Engineering, Stillwater, Oklahoma.

Sabnis, R. D., Cai, Q., and Chambers, F. W. (1994a), "Flow Distribution Effects Upon Air Filter Performance Measurements," Society of Automotive Engineers, Climate Control and Automotive Cabin Air Filtration (SP-1040), SAE Paper 940317, Detroit, MI.

Sabnis, R. D., Cai, Q., and Chambers, F. W. (1994b), "Diagnosis of the Flow Fields in a Housing for Automotive Air Filter Performance Testing," American Institute of Aeronautics and Astronautics, 32nd Aerospace Sciences Meeting & Exhibit, Reno, NV, AIAA 94-0117.

Society of Automotive Engineers (1987), "SAE J726 Air Cleaner Test Code - SAE Recommended Practice," SAE, Inc., Warrendale, PA.

Suneja, S. K., and Lee, C. H. (1974), "Aerosol Filtration by Fibrous Filters at Intermediate Reynolds Number," *Atmospheric Environment*, Vol. 8, pp. 1081-1094.

Tedjojuwono, K., Asakura, T., and Kawase, Y. (1984), "Measurement of Particle Density Using the Variable-Fringe-Spacing Laser Doppler Velocimeter," *Applied Optics*, Vol. 23(15), pp. 2554-2558.

Tian, Y. (1995), "TSTEP - Three Dimensional Traverse Software," OCAST Applied Research Project, Oklahoma State University, Stillwater, Oklahoma.

Wang, Y. (1990), "Effect of Component Layout and Geometry for Surface Mounted Electronic Components: A Smoke Flow Visualization Study," MS Thesis, Oklahoma State University, School of Mechanical and Aerospace Engineering, Stillwater, OK.

Whitby, K. T., Lundgren, D. A., and Peterson, C. M. (1965), "Homogeneous Aerosol Generators" *International Journal of Air and Water Pollution*, Vol. 9, pp. 263-277.

APPENDIXES

APPENDIX A

EQUIPMENT LIST

1. 4 Watt Argon ion laser: Coherent, Innova 70-A, P/S 92K-1758
2. Remote control for the laser: Coherent, I-70, 92411171
3. Fiber drive: Aerometrics, Inc., FBD1240, 026
4. Bragg cell: IntraAction, Inc., ME-40H,3247
5. Photomultiplier tubes: Aerometrics, Inc., RCM2200L, 029
6. Doppler signal analyzer: Aerometrics, Inc., DSA3220, 044
7. Computer and monitor: Impression 3, IBM compatible 80486 DX2, 66 MHz
8. Computer for traverse system: Gateway 2000, IBM compatible, 80486 DX2, 33 Mhz
9. Laser transceiver: Aerometrics, Inc., XRV1212, 001
10. Three Stepper Motors (Sanyo Denki, Type: 103-850-11)
11. Oscilloscope: Hewlett Packard, 54501A
12. Plexiglass test housings: both SAE J726 and new small angle diffuser housing
13. Test filter: Purolator, Inc., A13192 (formerly AF3192)
14. TSI mass flow sensor: TSI, 2018, 30644
15. Atomizer: TSI model 9306, six-jet atomizer

16. SAE J726 air stand, Purolator Products, Inc.
17. Rival compact heater, model T114
18. CMD-40 Stepper Motor Drives
19. 24 v DC - 6 A Power Supply (Acme Electronics)
20. Connector 3 for Digital Output (PCLD-780)
21. Ultrasonic Humidifier: Pollenex, SH55R
22. Smoke Generator with its Variacs
23. Polaroid Microcam (Microscope Camera)

APPENDIX - B

DSA PARAMETERS

Figure B.1 shows the variable setup page from the DSA software that needed most of the parameter adjustments.

```

IMM Velocity Setup ***** Date: 15 MAY 1993 11 Time: 15:34:10 M:
: ***** Ch1 ***** Ch2 ***** :
:: A] High Voltage ( V)3      800      3      800      3      :
:: B] Freq Shift (MHz)3      40        3      40        3      :
:: C] DC Offset (mV)3       5.0      3      -16.2     3      :
:: D] Mixer Freq (MHz)3     40        3      40        3      :
:: E] Low Pass (MHz)3       5.000   3      5.000   3      :
:: F] Burst Filter 3      40 MHz BP  3      40 MHz BP  3      :
:: G] Threshold (mV)3     15.0      3      13.0     3      :
:: H] Envel Filter 3       1 uS      3      1 uS     3      :
: *****X*****X*****X*****X*****X*****X*****X*****X*****X*****X***** :
:: I] Peak Detection 3      On        3      On        3      :
:: J] % After Peak 3       50        3      50        3      :
:: K] # Of Samples 3      128       3      128       3      :
:: L] Samp. Rate 3     20.000 MHz 3     20.000 MHz 3      :
:: M] Min S/N Ratio 3     0.30       3     0.30       3      :
: *****X*****X*****X*****X*****X*****X*****X*****X*****X*****X***** :
:: N] Enabled 3      On        3      On        3      :
:: Range (m/s)3    -14.2 - 14.2  3    -13.5 - 13.5  3    - :
:: O] Vel Minimum (m/s)3 -10.00   3    -10.00   3      :
:: P] Vel Maximum (m/s)3 10.00    3     10.00    3      :
:: Meas. Range (m/s)3 -10.0 - 10.0  3 -10.0 - 10.0  3    - :
: *****X*****X*****X*****X*****X*****X*****X*****X*****X*****X***** :
Use or Press Character to Select                               Mns                                DAV
    
```

Fig. B.1 Variable Setup Page from DSA Software

1. **High Voltage:** The variable 'high voltage' was used to set the photomultiplier tube (PMT) operating voltage. Its range is from 200 to 800 volts. The present maximum setting of 800 volts was used for all of these experiments.
2. **Frequency Shift:** The variable 'frequency shift' was fixed at the frequency of the Bragg cell at 40 MHz. This entry lets the software know what frequency shift is being used, so that the effect of frequency shift in the velocity determination could be accounted.
3. **DC Offset:** This variable had to be constantly monitored and adjusted to bring the background level of the 'RAW' signal observed on the oscilloscope to a value just above the ground (0 volts). This setting is important when using 'peak detection' (item I in Fig. B-1). Its value could be adjusted by using the [+] or [-] key from the keyboard.
4. **Mixer Frequency:** The 'mixer frequency' determines the amount by which the signal from the PMT is reduced before it is processed. Typically, it was set at the Bragg cell shift frequency at 40 MHz. Its value could range from 40 to 200 MHz.
5. **Low Pass Filter:** The 'Low pass' entry was used to set the low pass filter of the DSA which limits the high frequency noise band and removes the upper side of the mixed signal that was obtained from the mixer. The low pass filter values were selected using [+] or [-] key and have values of 5, 20, 50, and 80 MHz.
6. **Burst Filter:** The burst filter is used to remove high frequency noise before the signal reaches the burst detector. There are five settings that may be used; a 10 MHz low pass filter, a 40 MHz bandpass filter, a 50 MHz low pass filter, a mixer

out, and an all pass setting. The 40 MHz bandpass setting is suitable for velocities in the range of ± 15 m/s, with Doppler frequencies less than 5 MHz.

7. **Threshold:** This entry corresponds to the amplitude at which the burst detector will trigger. Rough guidelines are that with the burst filter set at 40 MHz band, the threshold may be between 5 and 30 mv.
8. **Envelope Filter:** The envelope filter smoothes the burst signal, removing the high frequency noise. The range of values are 0, 100 ns, 330 ns, 1 μ s, and 3.3 μ s. Typically 3.3 μ s was used for our experiments.
9. **Peak Detection:** The largest amplitude of a burst signal is sought with the peak detector. It can help to make the signal-to-noise-ratio of the sampled signal large by centering the sampled signal at the peak. It can be either 'ON' or 'OFF'. It was set at 'ON' for our experiments.
10. **Percentage after Peak:** With the peak detection 'ON', this gives the % of the sampled signal taken after the peak. A setting of 50% works fine for our settings..
11. **Number of Samples:** The range is from 1 to 512. The DSA manual suggests a value of 128 for our settings. The same was used for our experiments.
12. **Sample Rate:** The sample rate must be set so that aliasing is avoided, and the record length must be shorter than the length of a burst. The [+] or [-] keys was used to increase the sample rate from 78.125 KHz to 160 MHz by a factor of two with each key stroke. Mostly either 20 or 40 MHz was used for these tests.
13. **Min. S/N Ratio:** The actual value used for these experiments was 0.3 as recommended by the DSA manual.

14. **Velocity Range:** The possible velocity range that can be measured with the selected parameters is displayed on this line. Range was from -57 to +57 m/s. Since for our flow setup, the maximum velocity in either direction would not go more than 10 m/s, a range of ± 14 m/s was used.

Due to the recent upgrades in the DSA system by the Aerometrics, Inc. in July of 1995, the parameters such as Threshold, Peak Detection, and DC Offset have changed dramatically and must be re-evaluated.

APPENDIX C

VERTICAL TRAVERSE

As mentioned in Chapter III, initially a manual vertical traverse was fabricated to move the transceiver between upstream and downstream planes. Though vertical positioning tables were commercially available, none of them were exactly suitable for our purpose. The maximum length of vertical travel had to be more than 18 inches for our purpose, whereas most of the commercial tables had a maximum of 12 inches travel only. Hence a vertical traverse was designed to meet our needs, based on the model M3-80618 of LINTECH positioning systems (Texonics, Inc.).

A sketch of the traverse is shown in Fig. C-1. The traverse was bolted down on top of the horizontal traverse table. The traverse had a pedestal on which the transceiver was mounted. The pedestal could be moved up or down by rotating the lead screw. The pitch of the lead screw was 4 mm. A handle was attached to the top of the lead screw to facilitate manual movement of the pedestal. All of the experimental results presented herein were obtained with this setup. The primary concern with this setup was that, this would take 1 to 2 minutes for moving the transceiver between planes. Hence, only after finishing all the 35 grid point measurements in one plane, the transceiver could be moved to the other plane. Due to this time lag between the corresponding X and Y grid points on

the top and bottom planes, it might not be a true reflection of local efficiency at that point. Hence, it was decided to automate this movement, so that the transceiver could be moved between top and bottom planes for individual X and Y location grid points.

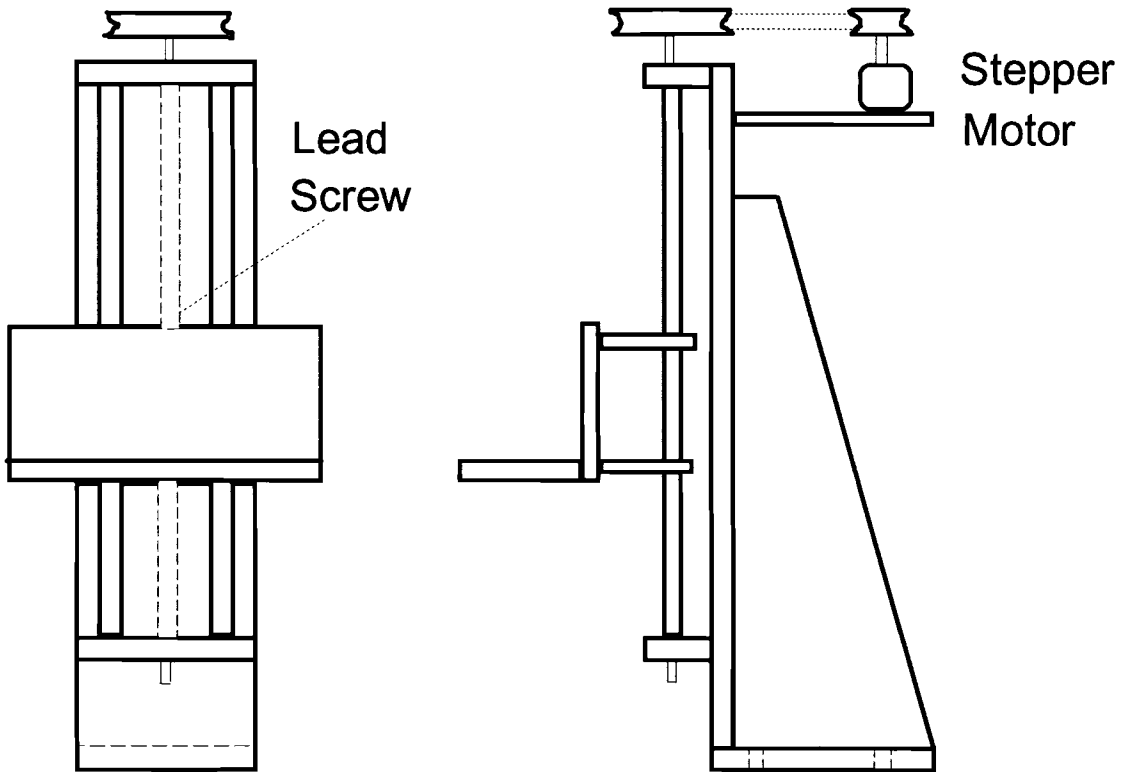


Fig. C-1 The Vertical Traverse

The vertical traverse was automated using computer controlled stepper motors. A stepper motor provided torque in discrete steps and it was easily controllable through a computer program. Each stepper motor had a range of operating torque limits, one for

static torque, and another for dynamic torque. The torque required to rotate the lead screw of the vertical traverse must be well within the dynamic torque range. A piece of thread was wound on the lead screw and with the help of a spring balance, the approximate torque required to rotate the lead screw was determined as 125 oz.-in. Then with a factor of safety of 3, the stepper motor must be capable of providing 375 oz.-in. static torque. Each stepper motor needed a stepper motor drive, which in turn was controlled by a computer through a data acquisition card. A compatible power supply source, a digital input-output connector and a compatible data acquisition board were also needed. The X-Y traverse automation was done by Haldhani (1993). Bi-polar stepper motors with 1.8° revolution per step were used by him. Since two sets of stepper motors and compatible drives and supply were already available, it was decided to use the same kind of stepper motor for this purpose.

It was difficult to mount the stepper motor directly on top of the traverse. Hence it was decided to use 'V' belt drive to connect the motor to the lead screw even though it might result in loss of some accuracy. The existing power supply had a maximum current output of 6 amperes. Since each of these stepper motors' current rating was 1.7 amperes, the same power supply was used for the third motor also. With a step reduction of 5:1 obtained through the pulley system, the same kind of stepper motor was able to provide the necessary torque to turn the lead screw. The V-belt pulleys were secured to the shafts by allen screws. The smaller pulley was connected to the motor shaft while, the larger pulley was connected to the lead screw at the top of the traverse. An aluminum plate was screwed on to the main pedestal of the traverse to support the motor. The motor was

secured by 4 screws to the aluminum plate. A slot was cut on the plate, to facilitate the adjustment of belt tension.

The stepper motor drives used are called “Chopper Modular Drives”, CMD. The chopper drives apply a high voltage at the beginning of each step, but prevent the current from exceeding its rated value by sensing and chopping it at a predetermined value (Haldhani, 1993). The power supply source used was a 24 v DC, 6A supply from Acme Electronics. The various connections between the supply, computer, and CMD are shown in Fig. C-2.

There were 2 terminal strips on the top of the CMD (CMD-40), terminal strip 1 (TS1), and terminal strip 2 (TS2). Leads from the motor were connected to the terminals #2 - #5 on TS2. The 24 v DC power supply was connected between terminal #1 on TS2 and terminal #10 on TS1. The logic inputs required by the CMD-40 were made at TS1. A 33 K Ohm resistance was connected between terminals #7 and #8 on TS1. The 5 v DC supply required for the operation of CMD-40 was given through a LM 340 transistor (7805), from the 24 v DC supply. The base of the transistor was connected to the common ground. Terminals #2 and #3 were for the step input and direction input. The step input instructed the motor to take a single step. The direction input determined the direction of rotation of the stepper motor for each step.

As mentioned earlier, the CMD-40 drives were controlled by a computer through a data acquisition card. A data acquisition card (PCL-818), initially installed was found to be suitable for this purpose. Its primary purpose was to generate digital output signals as dictated by the software, and send them to a daughter board called the PCLD-780. The

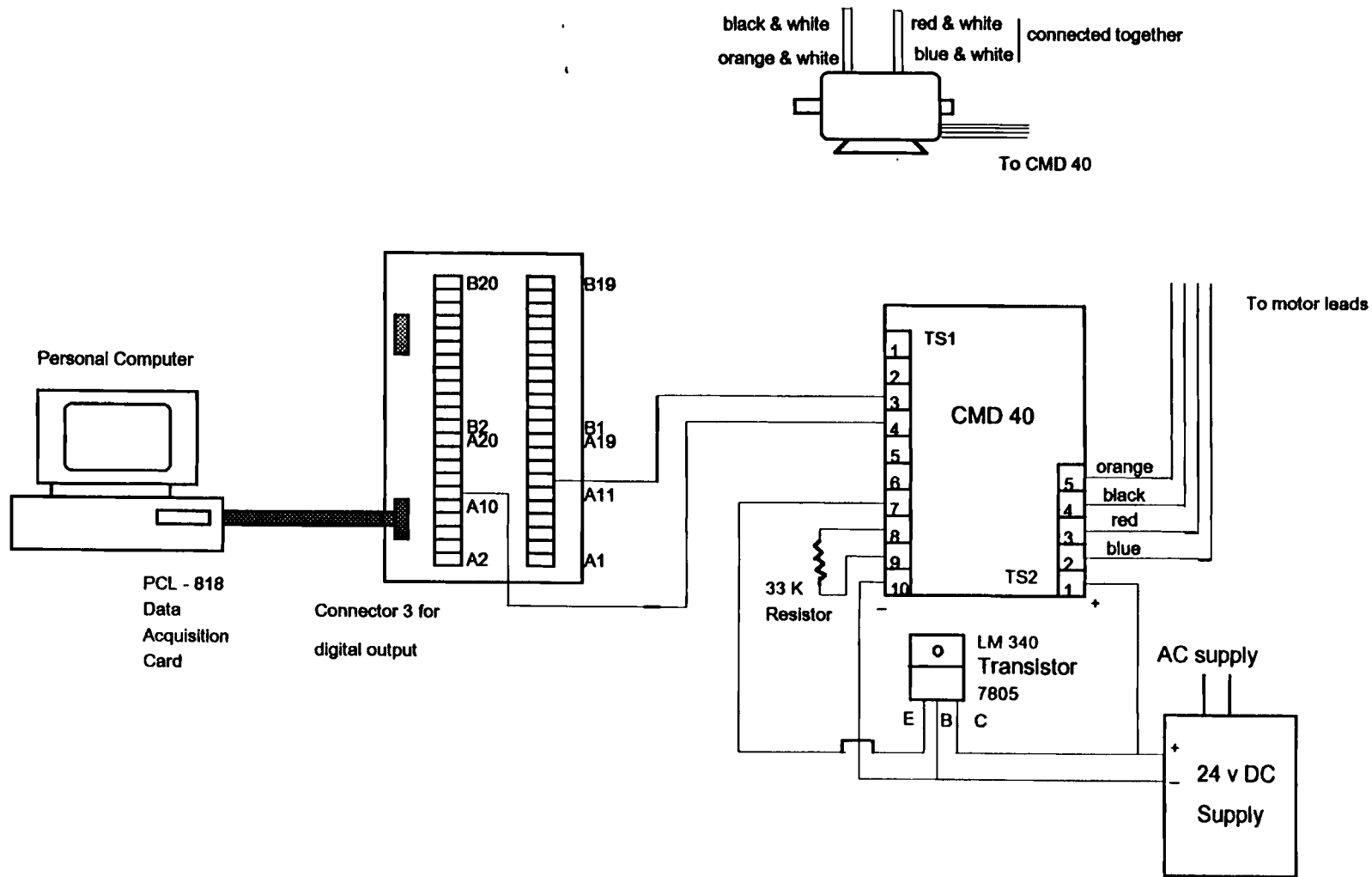


Fig. C-2 Wiring Diagram for Vertical Traverse Automation

daughter board was mainly a screw terminal board for easy digital output connections. The software was written by my colleague, Tian (1995), in Turbo C. The digital outputs for the vertical traverse motor were obtained at terminals A10 and A11 in the PCLD-780 board. These terminals were connected to terminals #3 and #4 for the step and direction inputs at the CMD-40.

Due to the 5:1 reduction in speed, the vertical traverse operated relatively slowly. This could be improved in the future by mounting a higher powered stepper motor directly on top of the traverse.

APPENDIX D

SMOKE GENERATOR

D.1 Smoke Generator Apparatus

This apparatus can be used to generate either continuous or intermittent supply of smoke to get a qualitative estimate of the flow field in wind tunnel tests. Either CO₂ or N₂ can be used as the pressurized gas to produce the smoke. The following description and procedure were adapted and modified from Wang's thesis (1990). A schematic of the apparatus is shown in Fig. D-1. It consists of a smoke chamber where the smoke is generated by electrically heating Mobil Velocity #10 oil, under pressure. A gage displays the pressure within the smoke chamber which is maintained at 20 psi. Two variacs are used to supply the necessary current, one to the smoke chamber electric heating element, and the other to the heating element of the insulation around the pipe supplying the compressed gas. There is a reservoir for oil whose filler cap has to be secured properly after filling the oil. There are five valves, two for controlling the compressed gas supply, one for controlling the smoke output, one for controlling the oil supply, and the last one

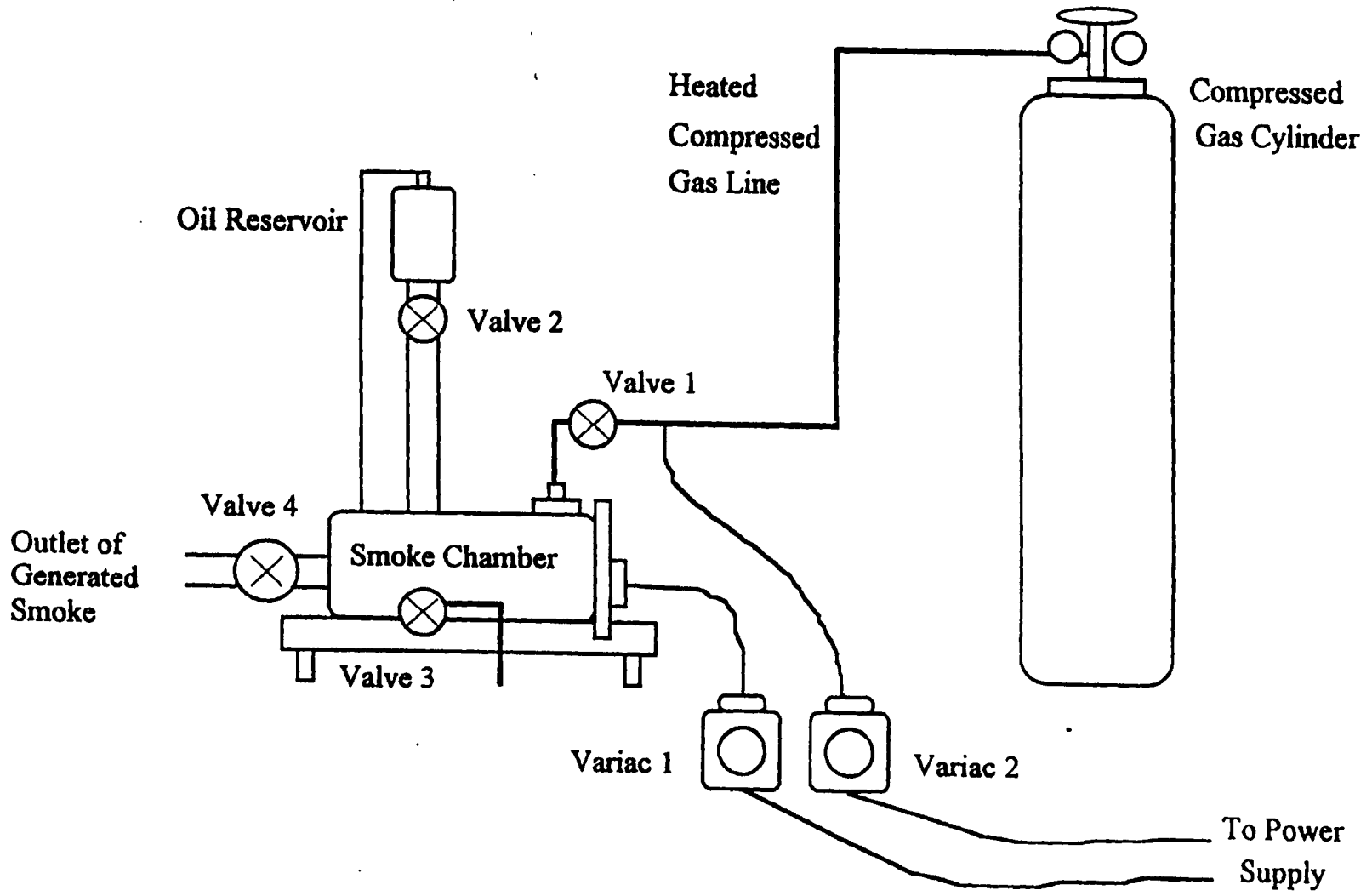


Fig. D-1 Schematic of the Smoke Generator (Wang, 1990)

for draining the oil from smoke chamber. Intermittent smoke was produced by closing and opening the valve # 4 in Fig. D-1. Both a still camera and a video recorder were used to record the flow visualizations. Laser power was maintained at 3W for these tests.

D.2 Procedure

1. Close all the five valves, fill the oil reservoir with Mobil Velocity #10 oil and secure the filler plug in place.
2. Setup the N₂ cylinder and connect the smoke generator to the cylinder. Open valves 5 and 1 to pressurize the chamber. After the chamber pressure reaches 10 psi, close valve 1.
3. Set variac # 1 for 100 volts and variac # 2 for 90 volts. Turn on both variacs. Let the system heat up for 20 minutes.
4. After preheating for 20 minutes, open valve 1 until the chamber pressure reads 20 psi.
5. Open valve 2 about quarter of a turn and let the system heat up for another 5 minutes.
6. Connect the flexible hose from the smoke generator to the filter test housing after making sure that there is no collected oil in the hose.
7. Adjust the laser beam to the desired power; produce the laser sheet with the help of a prism; and focus it on the right spot.
8. Open valve 4. Smoke should be coming out. Adjust valves 1 and 4 for a stable

density smoke. If the output quantity is not sufficient, close valve 4 for a minute and open it again. For intermittent smoke, open and close valve 4 whenever necessary. But do not keep valve 4 closed for a long time.

9. When the test is over, allow the system to cool down. Close all valves and drain any oil left in the chamber with valve 3.

APPENDIX E

OTHER RESULTS

Presented in the following pages are some of the other results with the diffuser housing from the tests conducted in both Summer of 94 and Spring of 95. Mainly three-dimensional figures of upstream and downstream axial velocities, and number densities along with the three-dimensional plots of local efficiencies are given. Results of tests using both the 0.966 μm particles and 5.3 μm particles are presented.

Presented in Figs. E-1 through E-20 are the results of the tests conducted using the 0.966 μm particles using the diffuser housing in the month of July, 1994. The results are given for the flow rates of 68 m^3/hr , 170 m^3/hr , 204 m^3/hr , and 255 m^3/hr . All of the upstream axial velocity profiles are of the same type with the velocity values increasing with increasing flow rates. All of the downstream axial velocity profiles have negative velocity values along the long edges of the filter, because most of these measurement points are either exactly under the rubber seal underneath the filter or adjacent to it. Surprisingly, not all of the local efficiencies along these edges are negative. Only at one or two points wherever the downstream particle number density profile has a peak, resulted in negative or very low local efficiencies. These results are in general, similar to the

results given in the main text of this thesis (Figs. 4.11 through 4.17). Once again note that these measurements were taken with a grid size of 25.4 mm x 25.4 mm (1 in x 1 in).

Given in Figs. E-21 through E-35 are the results of the tests with the diffuser housing using 5.3 μm particles at the flow rates of 68 m^3/hr , 119 m^3/hr , and 255 m^3/hr . Again one can see the similar patterns in both the velocity and number density profiles for these 5.3 μm particles. Figures E-36 through E-55 give the results of the test runs conducted with the modified setup using the diffuser housing as explained in section 4.5. The flow rates presented herein are 68 m^3/hr , 136 m^3/hr , 255 m^3/hr , and 272 m^3/hr . The axial velocity profiles are more uniform and their values are directly proportional to the flow rates.

But the upstream number density values are inversely proportional to the flow rates, meaning the higher the flow rate, the lower is the range of number density values. For example, the upstream number densities are in the range of 1.0×10^9 to 2.0×10^9 for 68 m^3/hr flow rate, whereas they are in the range of 1.8×10^8 to 3.4×10^8 for the flow rate of 255 m^3/hr . This is true even with the results of 0.966 μm particles presented earlier. But this effect is not as pronounced for the 5.3 μm particles. This might be explained by the fact that at the lower flow rates, the flow was comprised almost entirely of the atomized aerosol with a very small quantity of outside air being sucked by the blower. Whereas at high flow rates, the blower drew in a greater amount of makeup air which ultimately got mixed with the atomized aerosol, reducing the particle concentration in the flow. There were no negative local efficiencies for any of the flow rates.

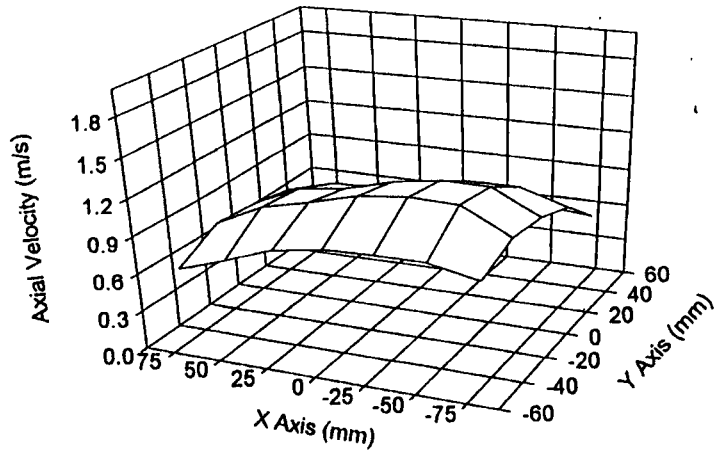


Fig. E-1 Axial Velocity Upstream (Diffuser, $68 \text{ m}^3/\text{hr}$, $0.966 \text{ }\mu\text{m}$ Particles, July 94)

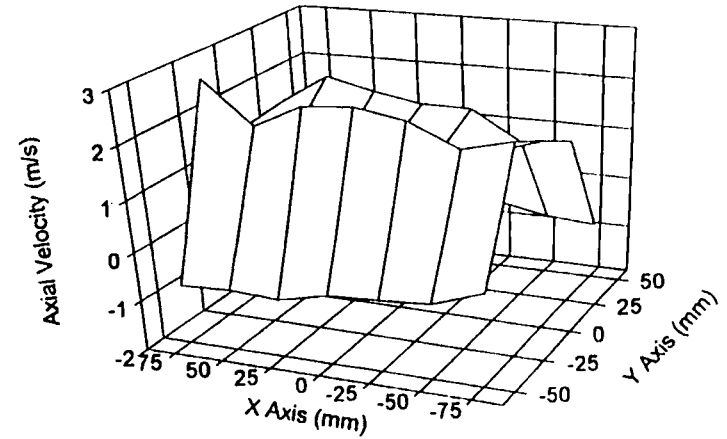


Fig. E-3 Axial Velocity Downstream (Diffuser, $68 \text{ m}^3/\text{hr}$, $0.966 \text{ }\mu\text{m}$ Particles, July 94)

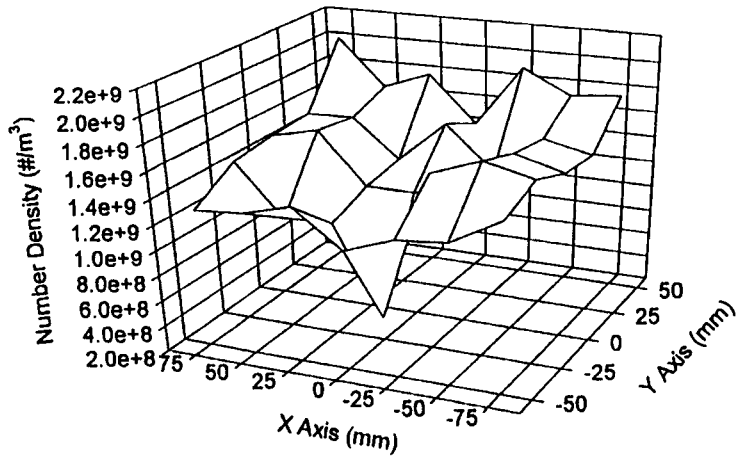


Fig. E-2 Number Density Upstream (Diffuser, $68 \text{ m}^3/\text{hr}$, $0.966 \text{ }\mu\text{m}$ Particles, July 94)

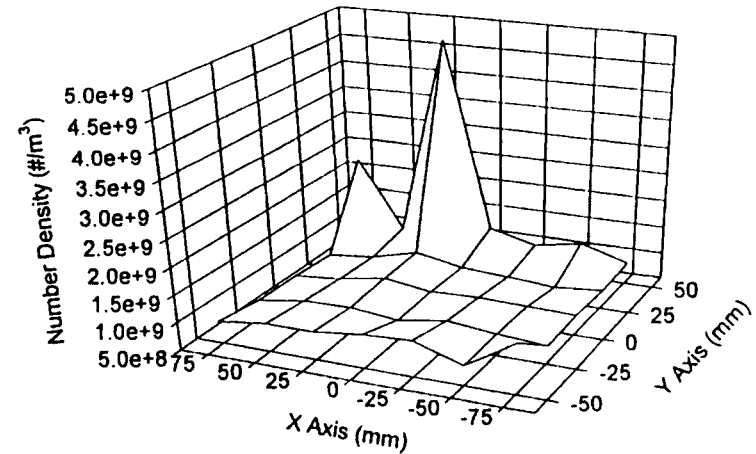


Fig. E-4 Number Density Downstream (Diffuser, $68 \text{ m}^3/\text{hr}$, $0.966 \text{ }\mu\text{m}$ Particles, July 94)

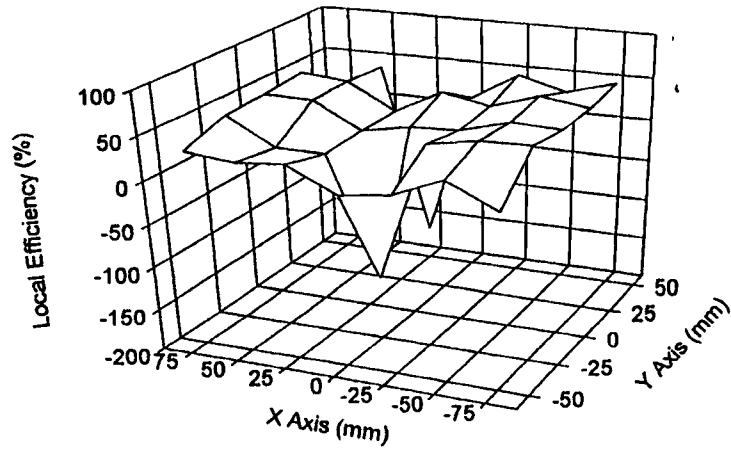


Fig. E-5 Local Efficiencies over Filter Face (Diffuser, 68 m³/hr, 0.966 μm Particles, July 94)

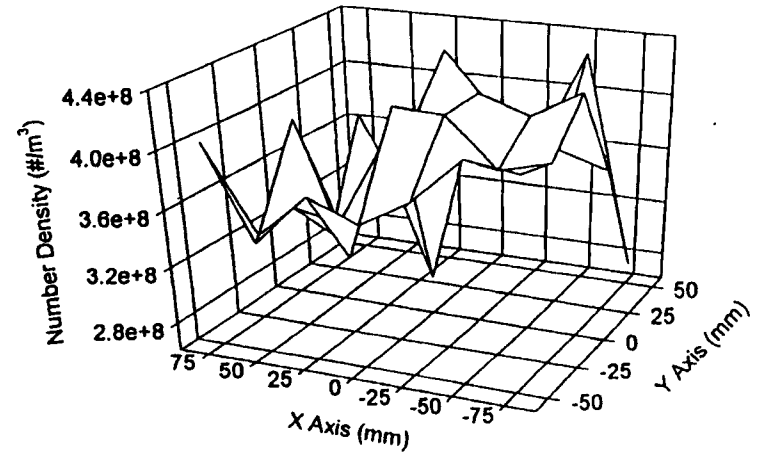


Fig. E-7 Number Density Upstream (Diffuser, 170 m³/hr, 0.966 μm Particles, July 94)

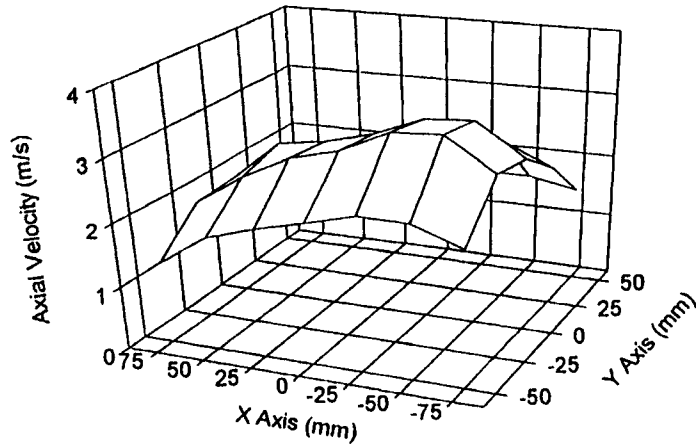


Fig. E-6 Axial Velocity Upstream (Diffuser, 170 m³/hr, 0.966 μm Particles, July, 94, July 94)

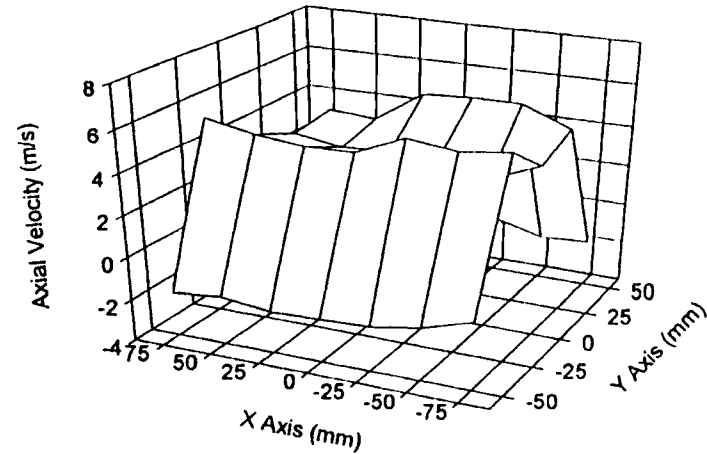


Fig. E-8 Axial Velocity Downstream (Diffuser, 170 m³/hr, 0.966 μm Particles, July 94)

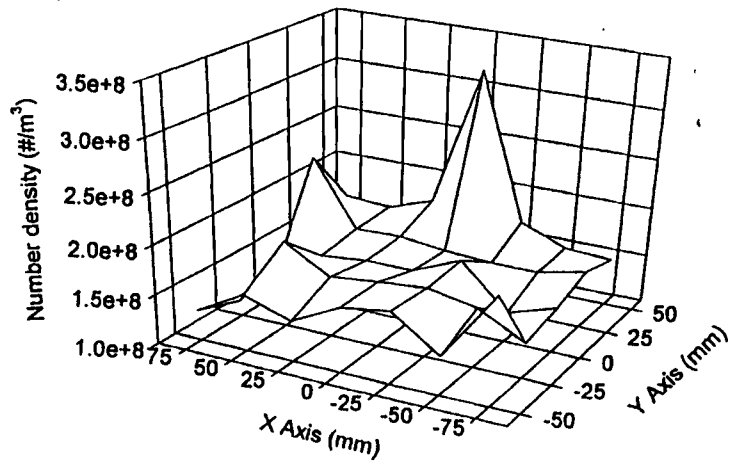


Fig. E-9 Number Density Downstream (Diffuser, 170m³/hr, 0.966 μ m Particles, July 94)

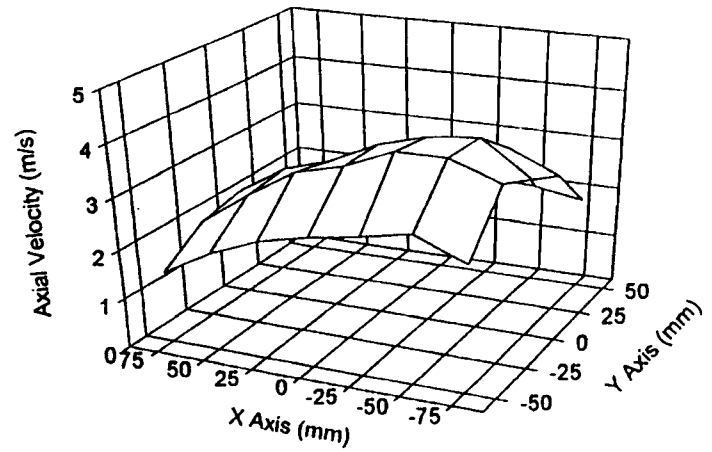


Fig. E-11 Axial Velocity Upstream (Diffuser, 204 m³/hr, 0.966 μ m Particles, July 94)

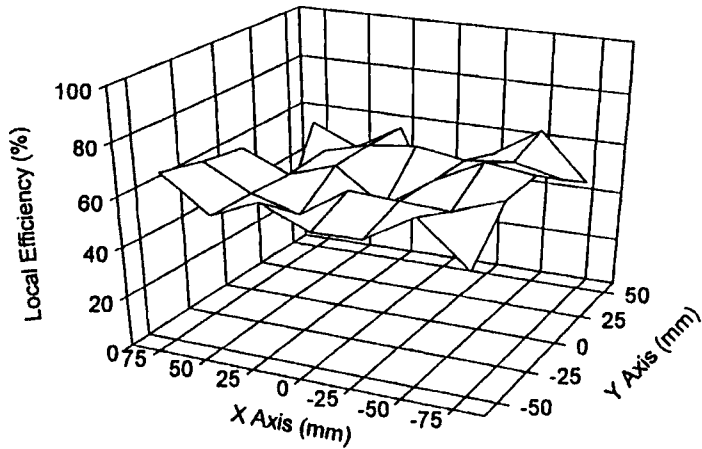


Fig. E-10 Local Efficiencies over Filter Face (Diffuser, 170 m³/hr, 0.966 μ m Particles, July 94)

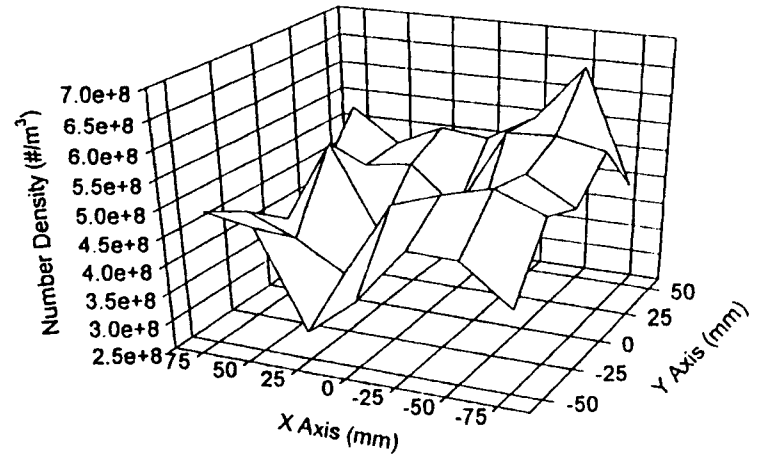


Fig. E-12 Number Density Upstream (Diffuser, 204 m³/hr, 0.966 μ m Particles, July 94)

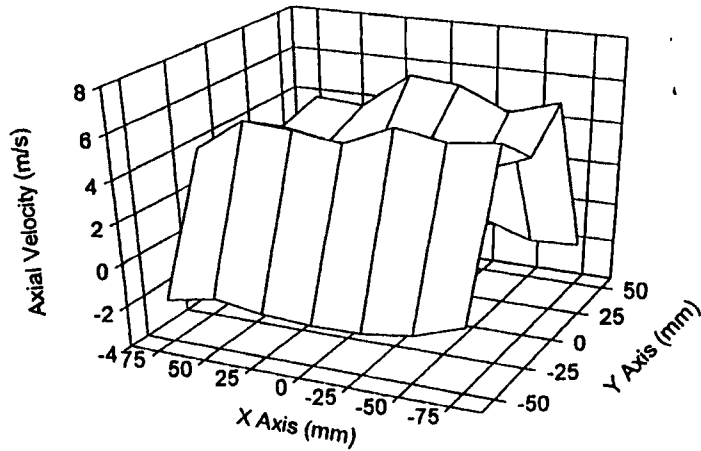


Fig. E-13 Axial Velocity Downstream (Diffuser, 204 m³/hr, 0.966 μm Particles, July 94)

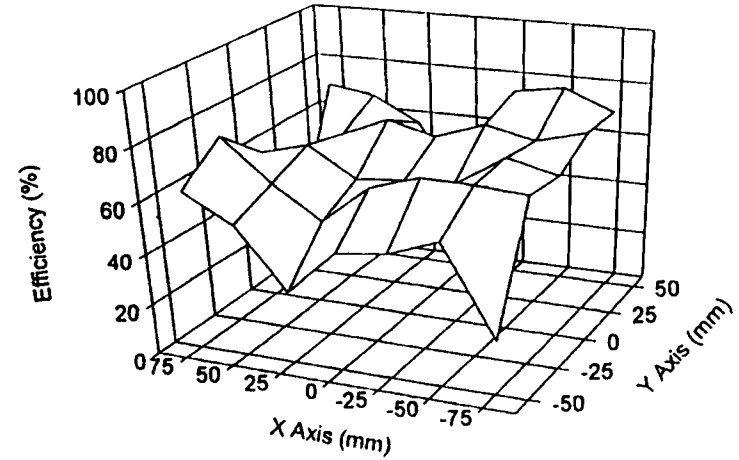


Fig. E-15 Local Efficiencies over Filter Face (Diffuser, 204 m³/hr, 0.966 μm Particles, July 94)

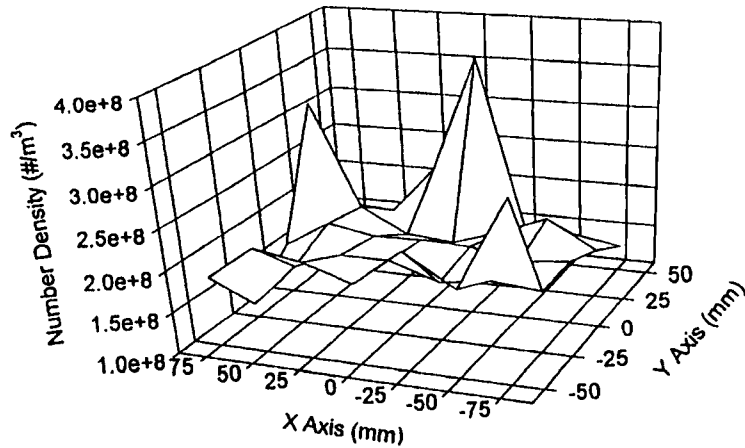


Fig. E-14 Number Density Downstream (Diffuser, 204 m³/hr, 0.966 μm Particles, July 94)

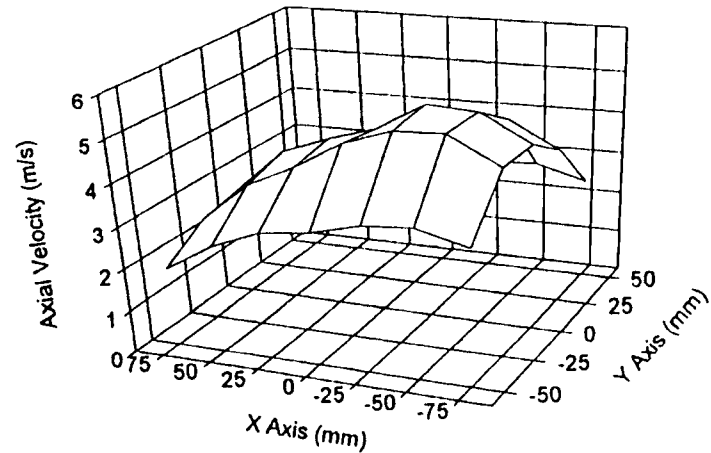


Fig. E-16 Axial Velocity Upstream (Diffuser, 255 m³/hr, 0.966 μm Particles, July 94)

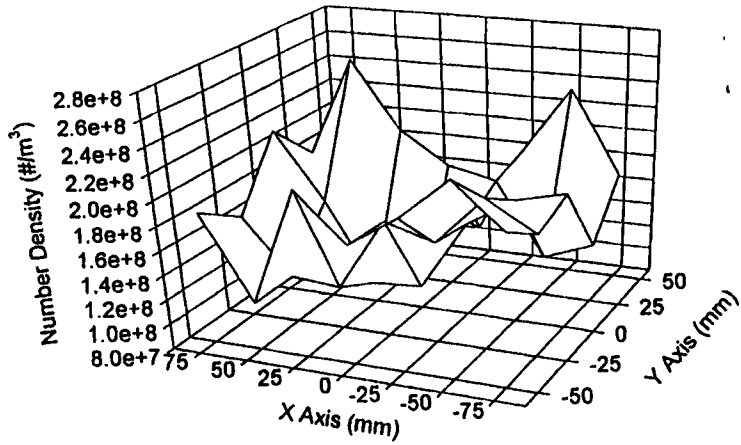


Fig. E-17 Number Density Upstream (Diffuser, 255 m³/hr, 0.966 µm Particles, July 94)

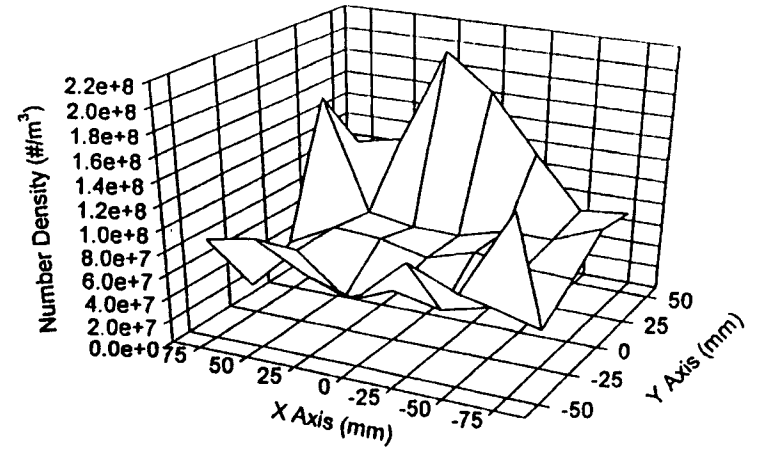


Fig. E-19 Number Density Downstream (Diffuser, 255 m³/hr, 0.966 µm Particles, July 94)

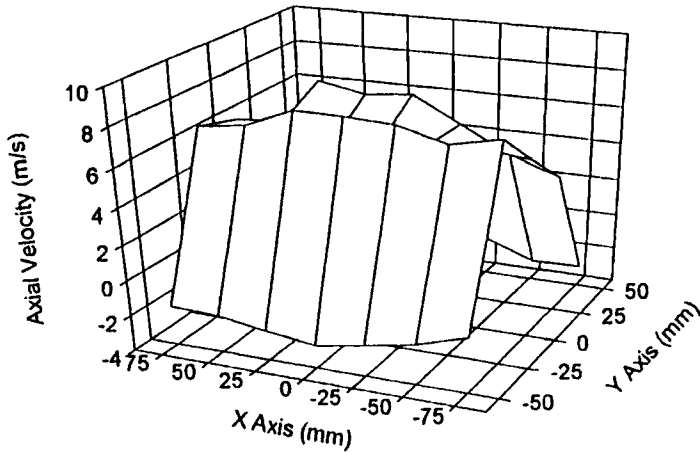


Fig. E-18 Axial Velocity Downstream (Diffuser, 255 m³/hr, 0.966 µm Particles, July 94)

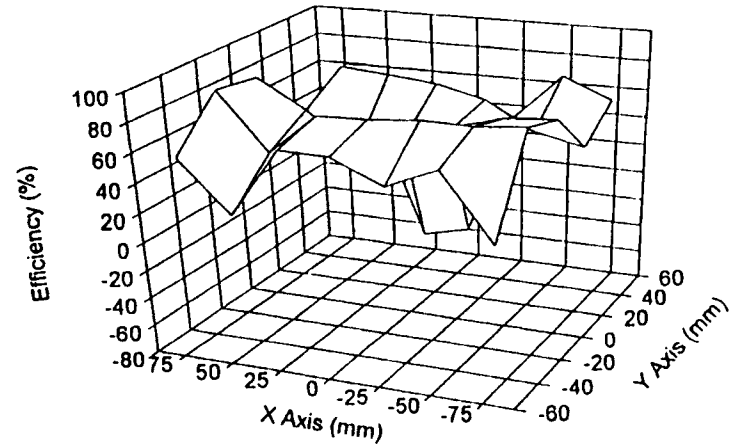


Fig. E-20 Local Efficiencies over Filter Face (Diffuser, 255 m³/hr, 0.966 µm Particles, July 94)

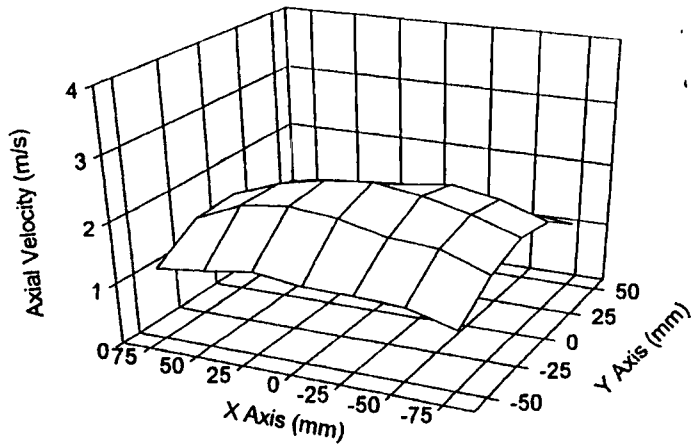


Fig. E-21 Axial Velocity Upstream (Diffuser, 68 m³/hr, 5.3 μm Particles, July 94)

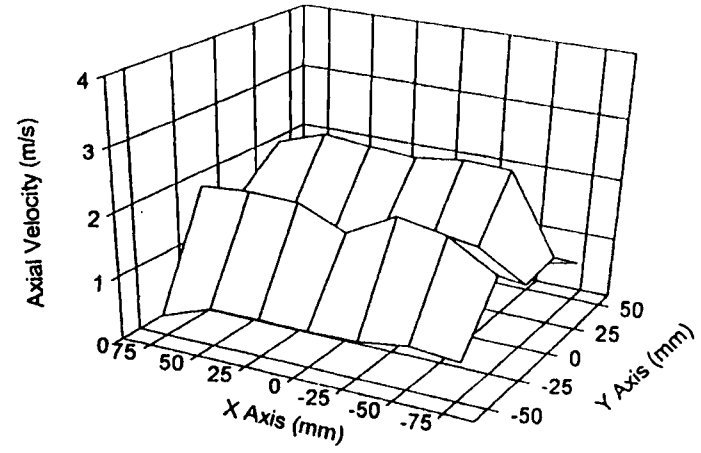


Fig. E-23 Axial Velocity Downstream (Diffuser, 68 m³/hr, 5.3 μm Particles, July 94)

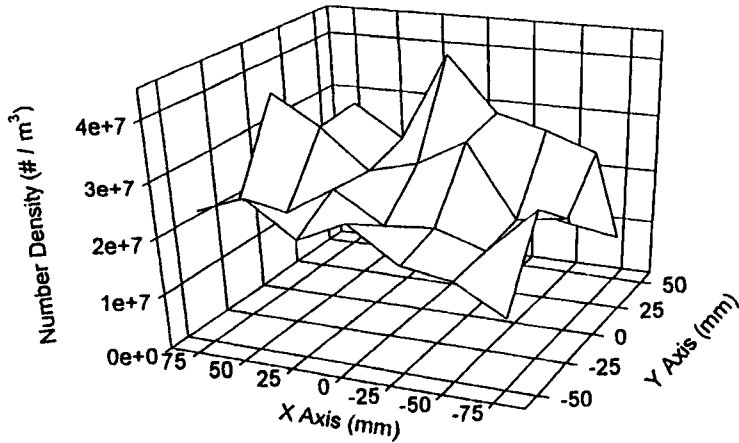


Fig. E-22 Number Density Upstream (Diffuser, 68 m³/hr, 5.3 μm Particles, July 94)

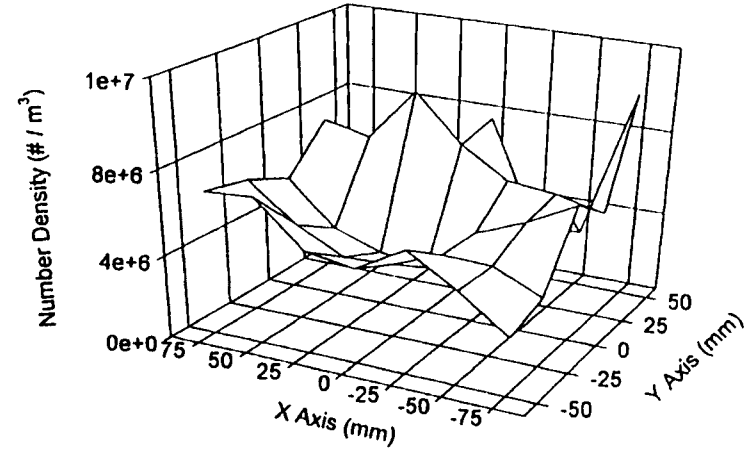


Fig. E-24 Number Density Downstream (Diffuser, 68m³/hr, 5.3 μm Particles, July 94)

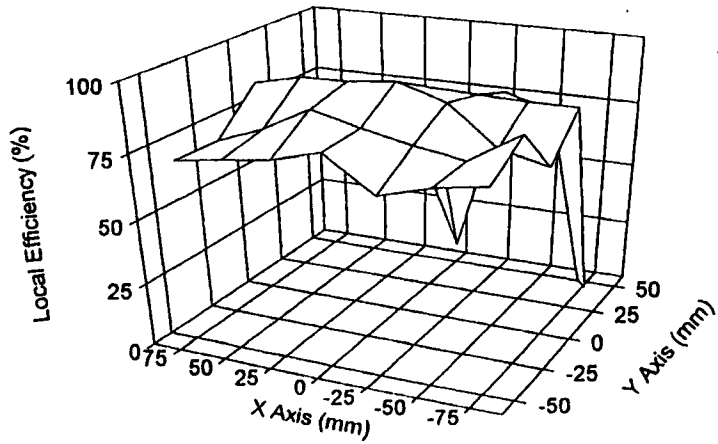


Fig. E-25 Local Efficiencies over Filter Face (Diffuser, 68 m³/hr, 5.3 μm Particles, July 94)

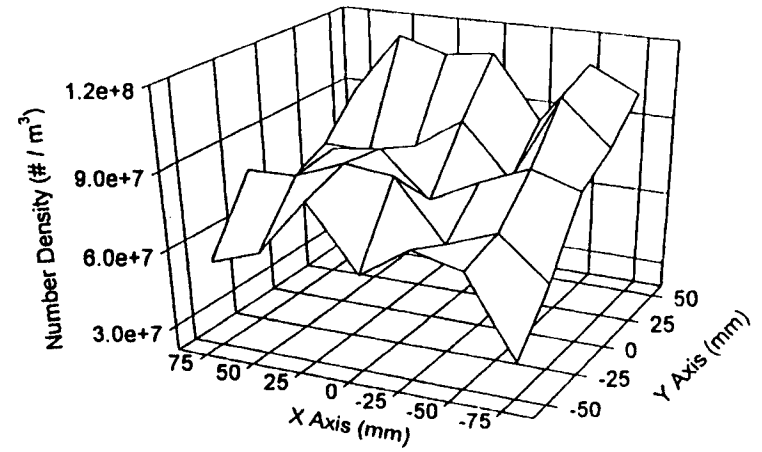


Fig. E-27 Number Density Upstream (Diffuser, 119 m³/hr, 5.3 μm Particles, July 94)

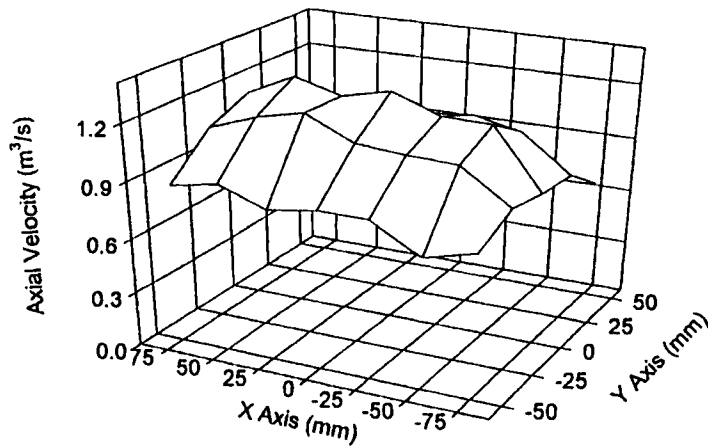


Fig. E-26 Axial Velocity Upstream (Diffuser, 119 m³/hr, 5.3 μm Particles, July 94, July 94)

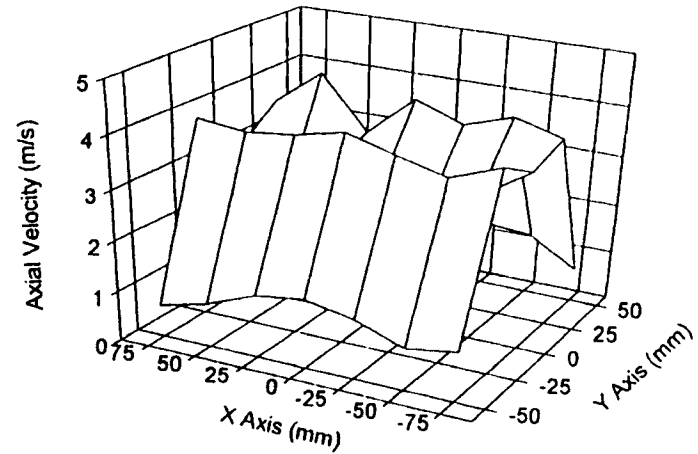


Fig. E-28 Axial Velocity Downstream (Diffuser, 119 m³/hr, 5.3 μm Particles, July 94)

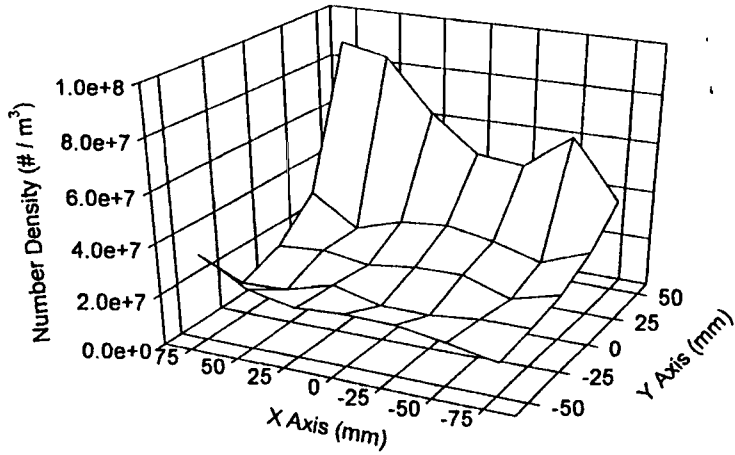


Fig. E-29 Number Density Downstream (Diffuser, 119m³/hr, 5.3 μm Particles, July 94)

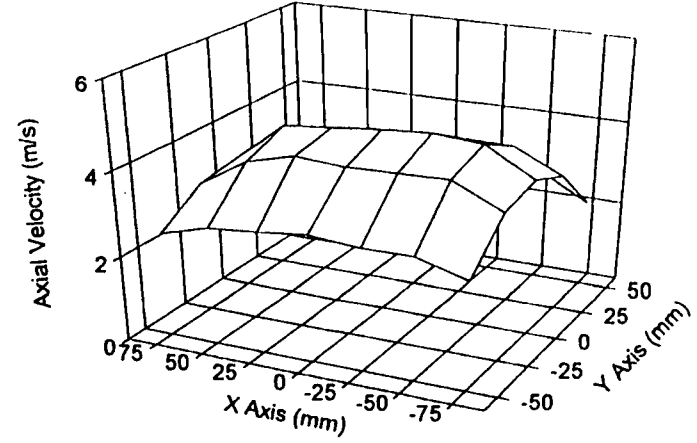


Fig. E-31 Axial Velocity Upstream (Diffuser, 255 m³/hr, 5.3 μm Particles, July 94)

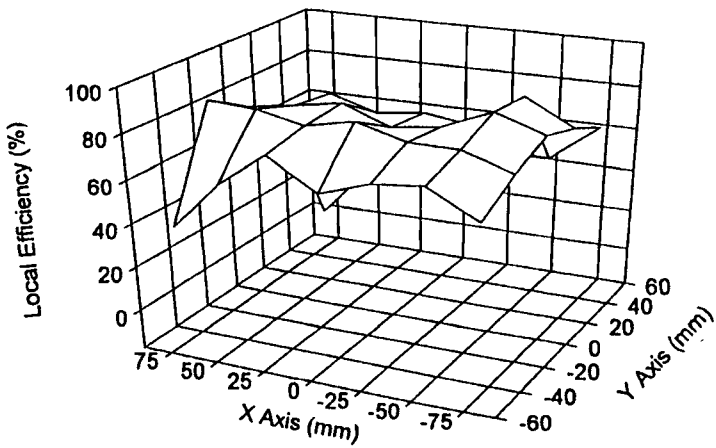


Fig. E-30 Local Efficiencies over Filter Face (Diffuser, 119 m³/hr, 5.3 μm Particles, July 94)

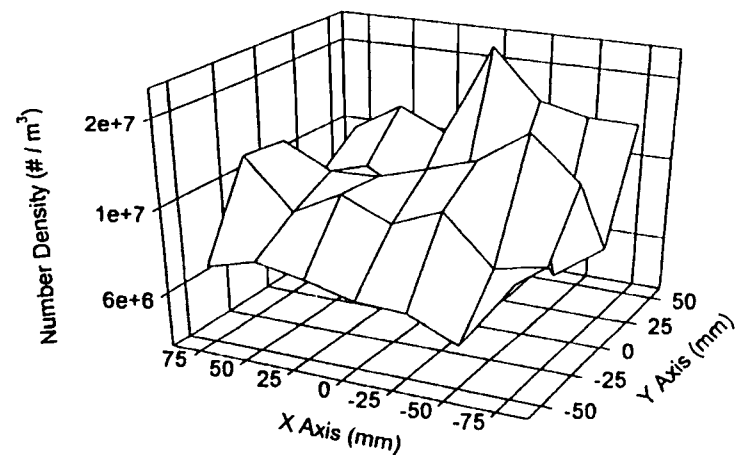


Fig. E-32 Number Density Upstream (Diffuser, 255 m³/hr, 5.3 μm Particles, July 94)

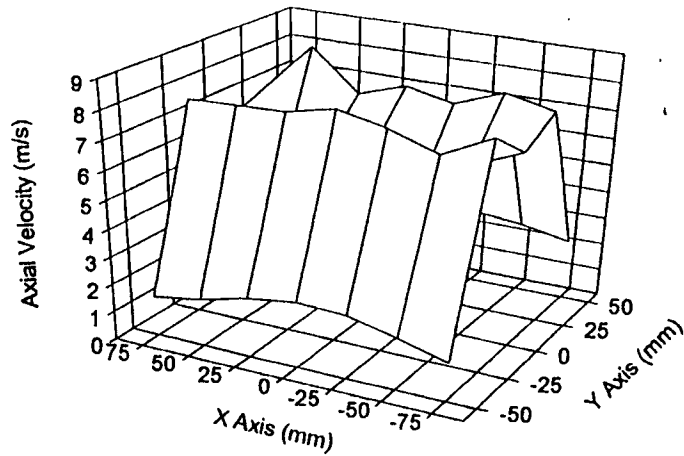


Fig. E-33 Axial Velocity Downstream (Diffuser, 255 m³/hr, 5.3 μm Particles, July 94)

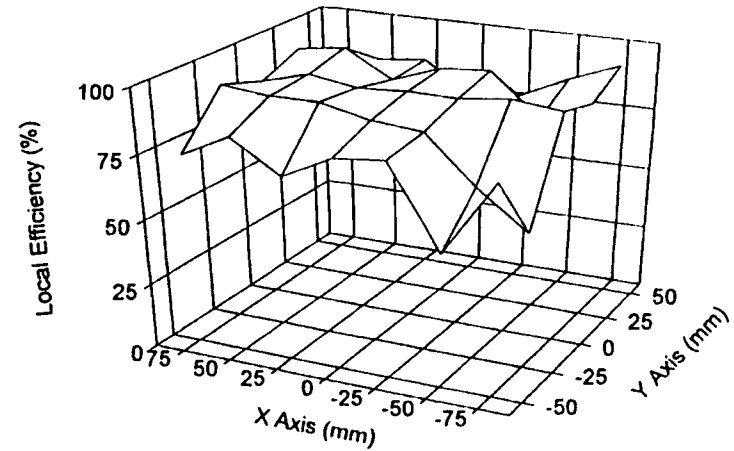


Fig. E-35 Local Efficiencies over Filter Face (Diffuser, 255 m³/hr, 5.3 μm Particles, July 94)

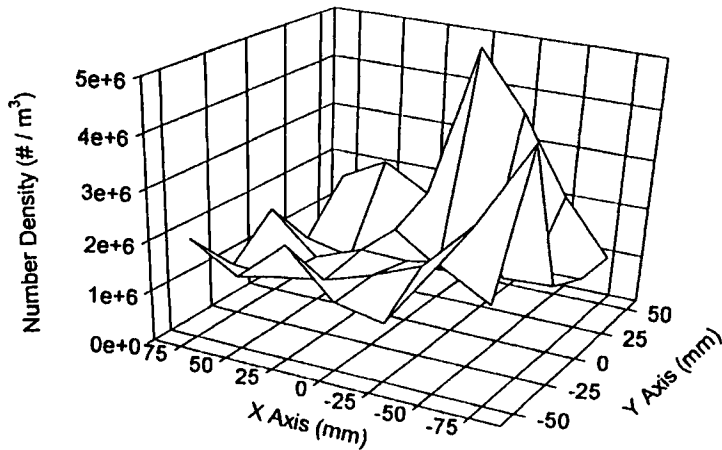


Fig. E-34 Number Density Downstream (Diffuser, 204 m³/hr, 5.3 μm Particles, July 94)

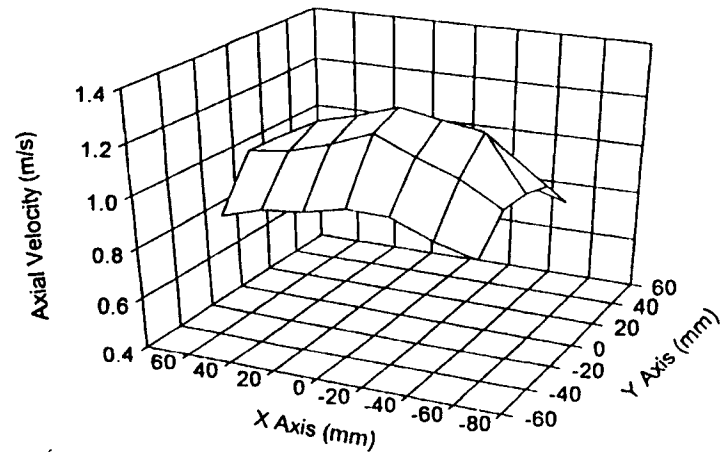


Fig. E-36 Axial Velocity Upstream (Diffuser, 68 m³/hr, 0.966 μm Particles, Feb. 95)

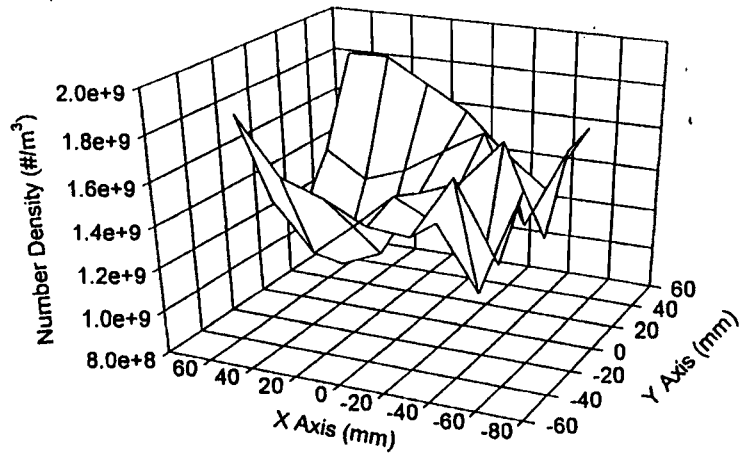


Fig. E-37 Number Density Upstream (Diffuser, 68 m³/hr, 0.966 μm Particles, Feb. 95)

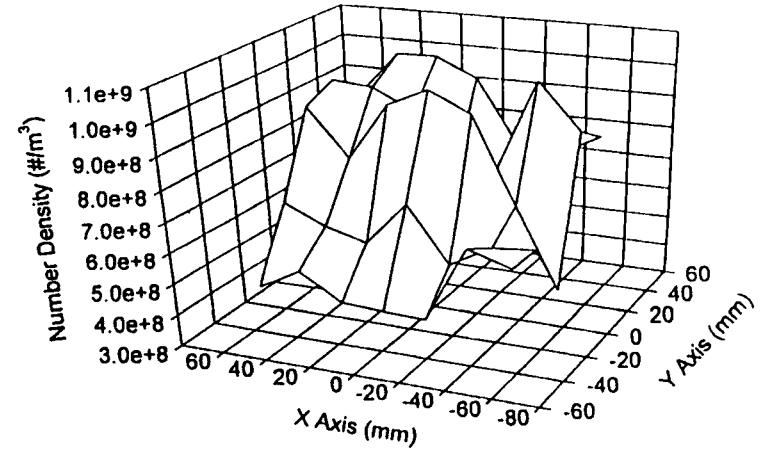


Fig. E-39 Number Density Downstream (Diffuser, 68m³/hr, 0.966 μm Particles, Feb. 95)

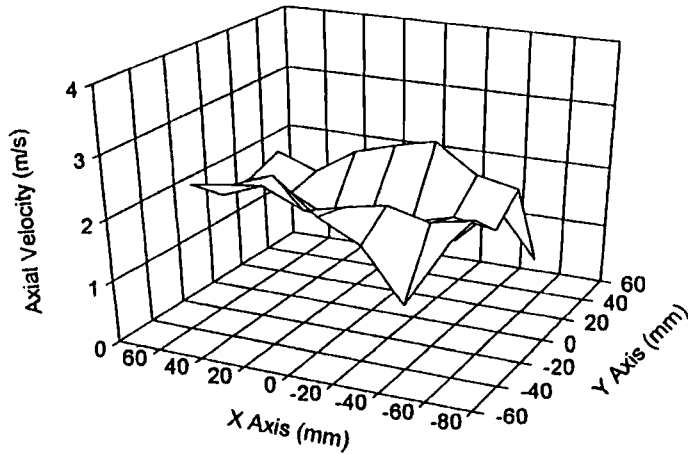


Fig. E-38 Axial Velocity Downstream (Diffuser, 68 m³/hr, 0.966 μm Particles, Feb. 95)

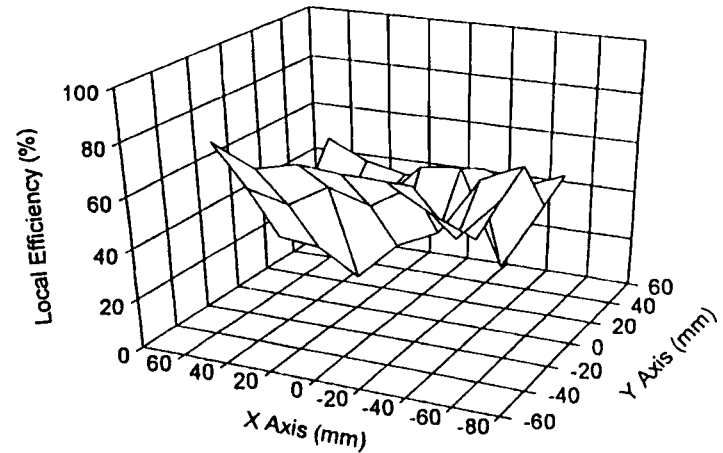


Fig. E-40 Local Efficiencies over Filter Face (Diffuser, 68 m³/hr, 0.966 μm Particles, Feb. 95)

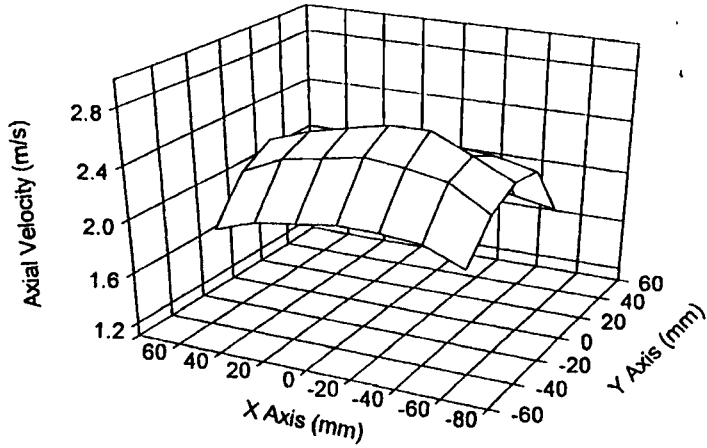


Fig. E-41 Axial Velocity Upstream (Diffuser, $136 \text{ m}^3/\text{hr}$, $0.966 \text{ }\mu\text{m}$ Particles, Feb. 95)

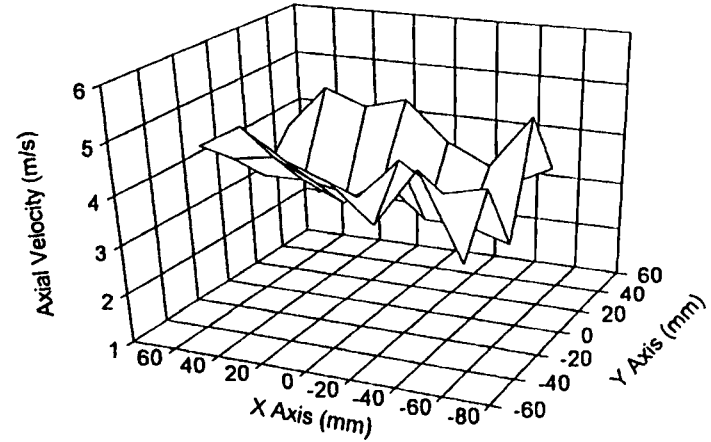


Fig. E-43 Axial Velocity Downstream (Diffuser, $136 \text{ m}^3/\text{hr}$, $0.966 \text{ }\mu\text{m}$ Particles, Feb. 95)

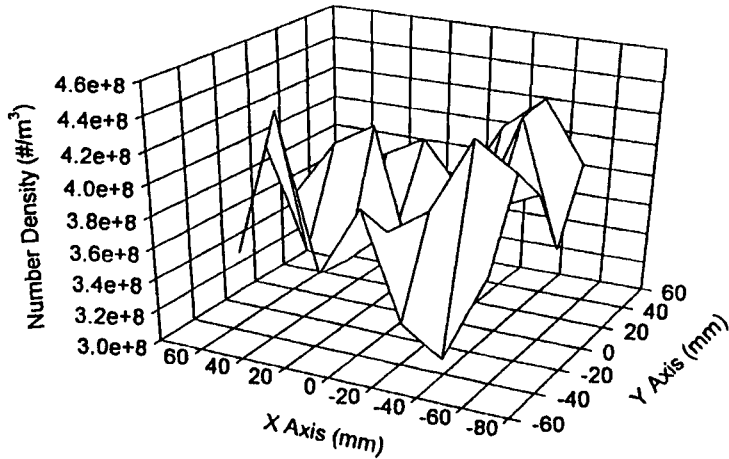


Fig. E-42 Number Density Upstream (Diffuser, $136 \text{ m}^3/\text{hr}$, $0.966 \text{ }\mu\text{m}$ Particles, Feb. 95)

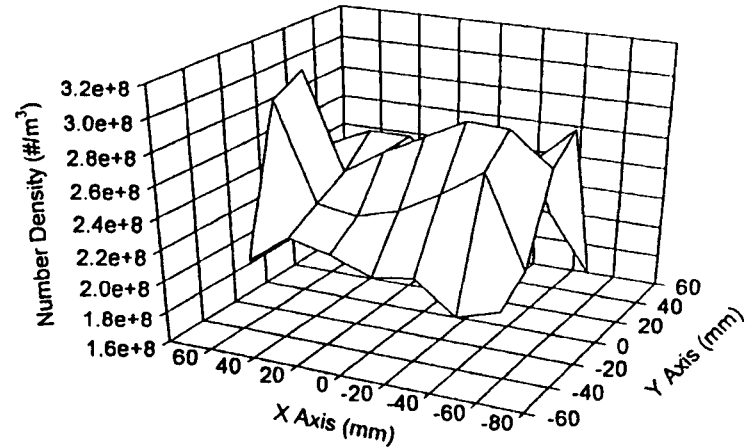


Fig. E-44 Number Density Downstream (Diffuser, $136 \text{ m}^3/\text{hr}$, $0.966 \text{ }\mu\text{m}$ Particles, Feb. 95)

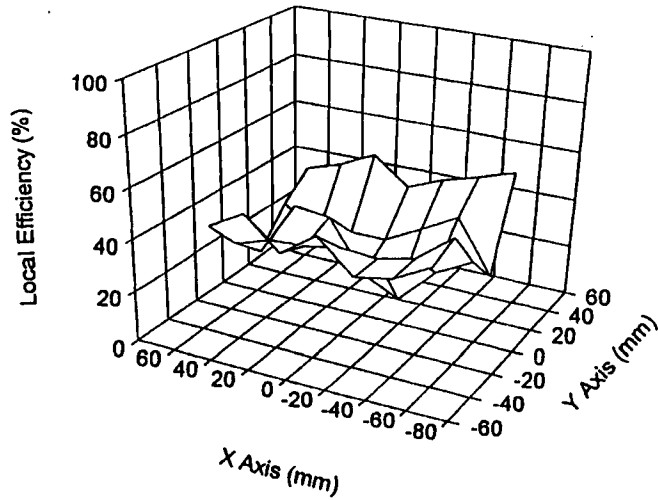


Fig. E-45 Local Efficiencies over Filter Face (Diffuser, 136 m³/hr, 0.966 μ m Particles, Feb. 95)

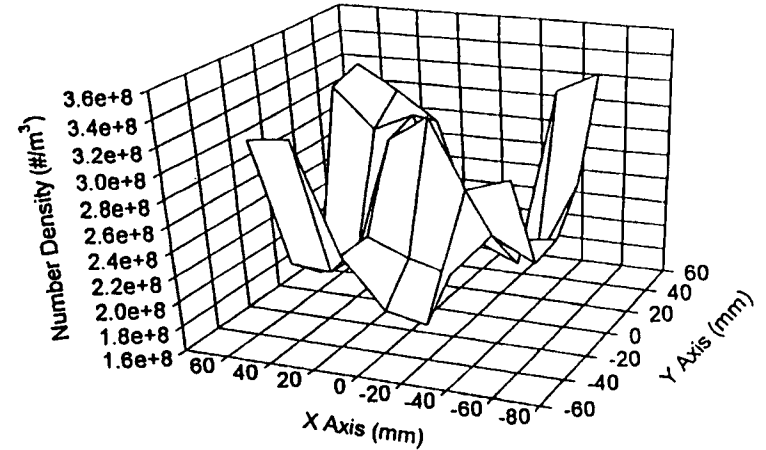


Fig. E-47 Number Density Upstream (Diffuser, 255 m³/hr, 0.966 μ m Particles, Feb. 95)

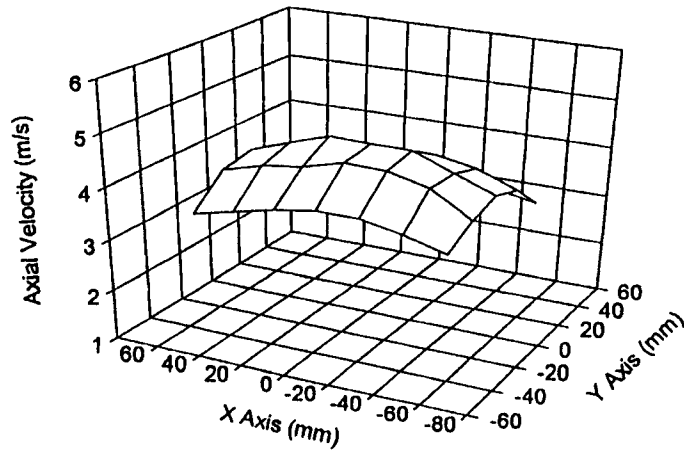


Fig. E-46 Axial Velocity Upstream (Diffuser, 255 m³/hr, 0.966 μ m Particles, Feb. 95)

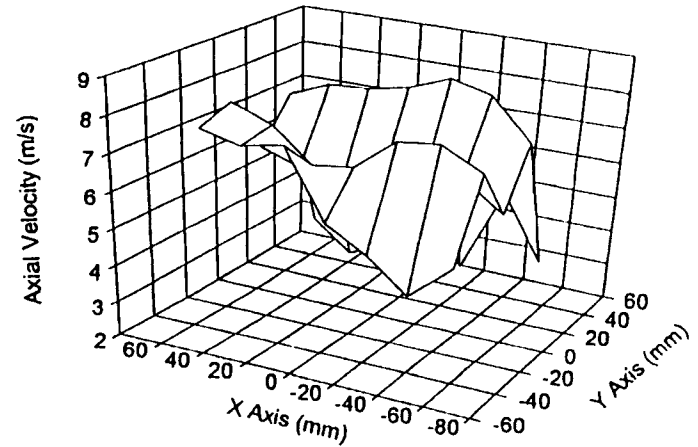


Fig. E-48 Axial Velocity Downstream (Diffuser, 255 m³/hr, 0.966 μ m Particles, Feb. 95)

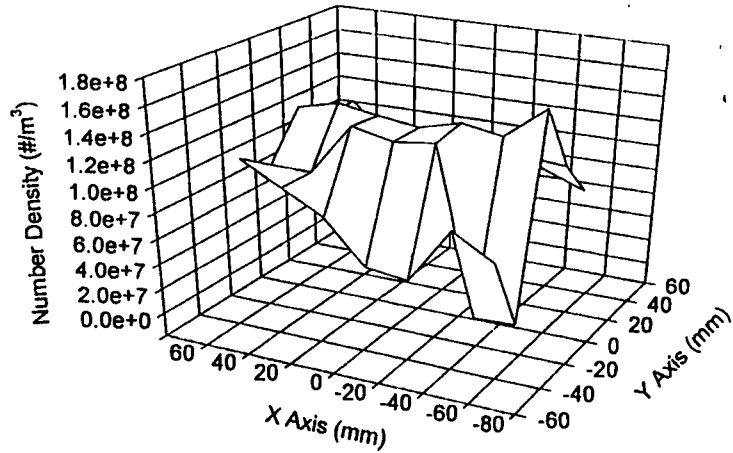


Fig. E-49 Number Density Downstream (Diffuser, 255 m³/hr, 0.966 μm Particles, Feb. 95)

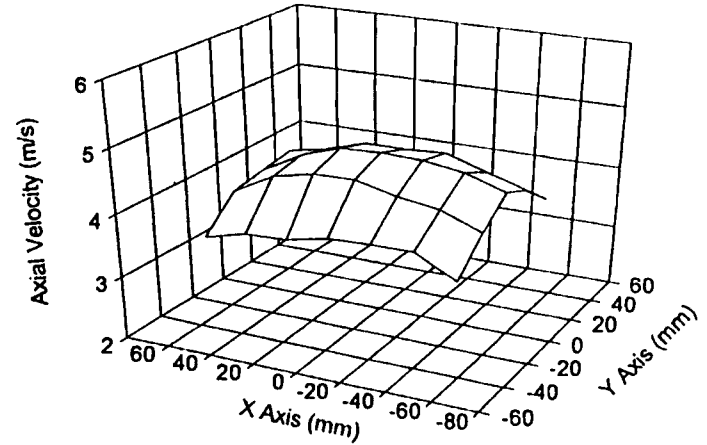


Fig. E-51 Axial Velocity Upstream (Diffuser, 272 m³/hr, 0.966 μm Particles, Feb. 95)

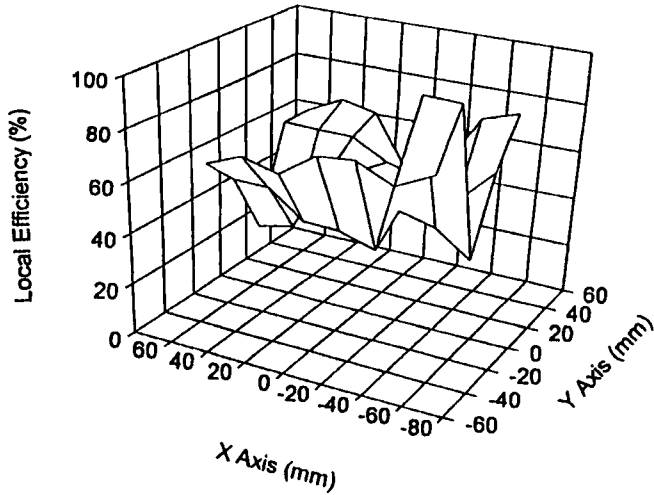


Fig. E-50 Local Efficiencies over Filter Face (Diffuser, 255 m³/hr, 0.966 μm Particles, Feb. 95)

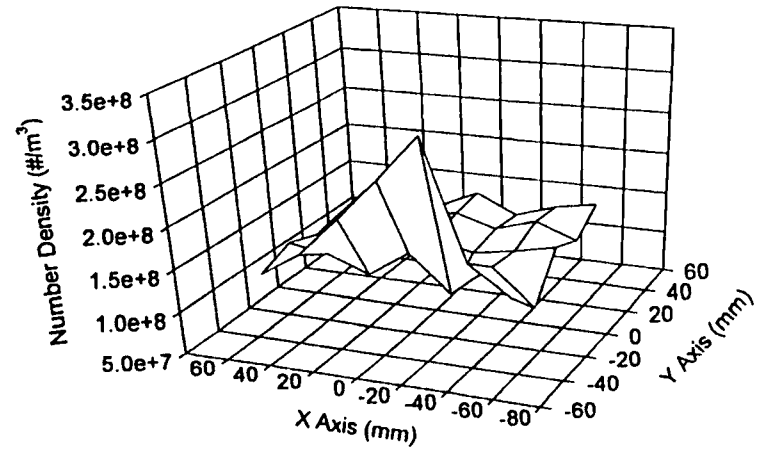


Fig. E-52 Number Density Upstream (Diffuser, 272 m³/hr, 0.966 μm Particles, Feb. 95)

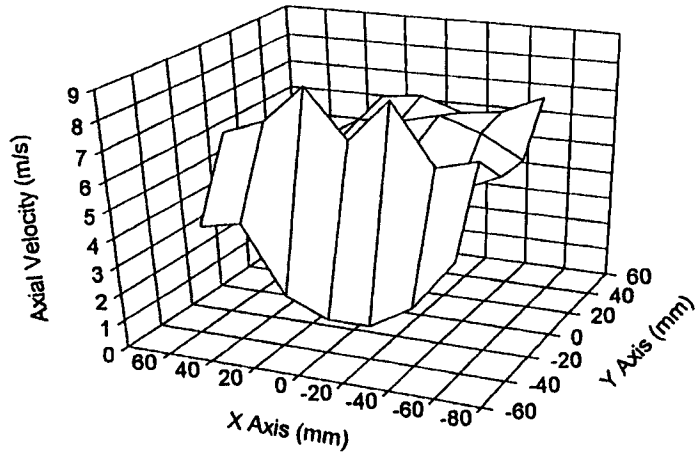


Fig. E-53 Axial Velocity Downstream (Diffuser, 272 m³/hr, 0.966 μm Particles, Feb. 95)

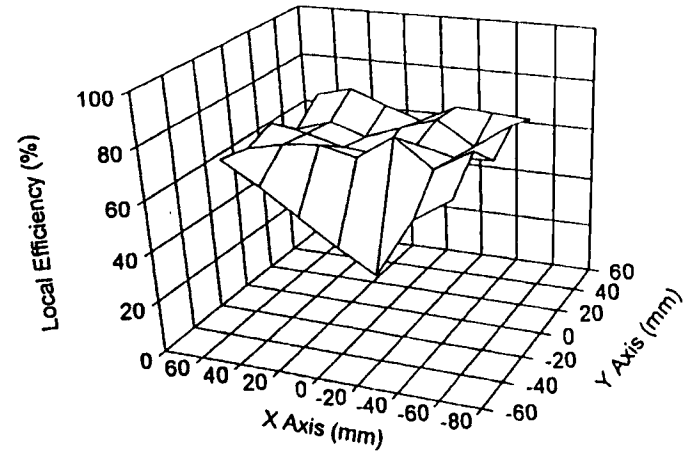


Fig. E-55 Local Efficiencies over Filter Face (Diffuser, 272 m³/hr, 0.966 μm Particles, Feb. 95)

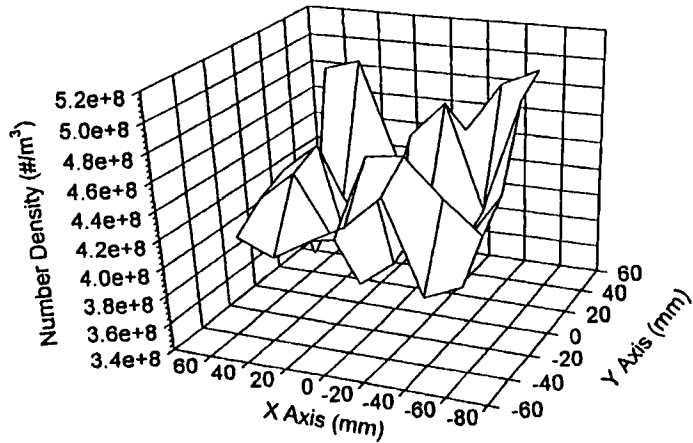


Fig. E-54 Number Density Downstream (Diffuser, 272 m³/hr, 0.966 μm Particles, Feb. 95)

VITA

Balasubramanian Natarajan

Candidate for the Degree of

Master of Science

Thesis: LOCAL EFFICIENCY MEASUREMENTS OF AUTOMOTIVE AIR FILTERS
USING LASER DOPPLER VELOCIMETRY

Major Field: Mechanical Engineering

Biographical:

Personal Data: Born in Erode, Tamilnadu, India, on July 28, 1966, the son of Natarajan and Bragannayaki Natarajan.

Education: Graduated from Seshasayee Institute of Technology, Trichirappalli, Tamilnadu in May 1984 with a Diploma in Mechanical Engineering; received Bachelor of Engineering degree in Mechanical Engineering from the Institution of Engineers (India), Calcutta, India in December 1990. Completed the requirements for the Master of Science Degree with a major in Mechanical Engineering at Oklahoma State University in December 1995.

Experience: Employed by Oklahoma State University from March 1994 to August 1995 as a graduate research assistant and as a graduate teaching assistant during Spring 1994; employed by South Central Railways, India from January 1991 to June 1993 as a maintenance engineer; employed by Sakthi Sugars Private Limited, Erode, Tamilnadu from November 1984 to August 1986.

Professional Membership: Professional Engineering Intern in the state of Oklahoma, Associate member of Institution of Engineers (India), Student member of the American Society of Mechanical Engineers, and the American Society of Heating, Refrigeration, and Air-Conditioning Engineers.